



UNIVERSIDAD NACIONAL AUTÓNOMA DE MÉXICO

Programa de Doctorado en Ciencias Biomédicas

Instituto de Investigaciones Biomédicas

Cambios diarios en la permeabilidad de la barrera hemato-hipotalámica: su papel en la regulación metabólica y hormonal.

TESIS

Que para optar por el grado de:

Doctora en Ciencias Biomédicas

Presenta

Beatriz Rodríguez Cortés

Tutor Principal

Dr. Ruud Marinus Buijs

Instituto de Investigaciones Biomédicas, Ciudad Universitaria.

Comité tutor:

Dra. Lorena Aguilar Arnal

Instituto de Investigaciones Biomédicas, Ciudad Universitaria.

Dr. Daniel Reyes Haro

Instituto de Neurobiología, Campus Juriquilla

Ciudad Universitaria, Ciudad de México; enero, 2023



Universidad Nacional
Autónoma de México

Dirección General de Bibliotecas de la UNAM

Biblioteca Central



UNAM – Dirección General de Bibliotecas
Tesis Digitales
Restricciones de uso

DERECHOS RESERVADOS ©
PROHIBIDA SU REPRODUCCIÓN TOTAL O PARCIAL

Todo el material contenido en esta tesis esta protegido por la Ley Federal del Derecho de Autor (LFDA) de los Estados Unidos Mexicanos (México).

El uso de imágenes, fragmentos de videos, y demás material que sea objeto de protección de los derechos de autor, será exclusivamente para fines educativos e informativos y deberá citar la fuente donde la obtuvo mencionando el autor o autores. Cualquier uso distinto como el lucro, reproducción, edición o modificación, será perseguido y sancionado por el respectivo titular de los Derechos de Autor.

A mi Haza, a mis hermanas y hermanos,
a Margarita, Volland, Tichy, Tery, Ari,
a Milagros, a Stanislaw Lem, a Ruud, a la montaña y
a mis queridos amigos Buni, Leo, Sergio, Roberto,
Edgar, Rafa.

Nada es pequeño, en efecto; cualquiera que esté sujeto a las penetraciones profundas de la naturaleza lo sabe. Aunque no sea dada satisfacción alguna a la filosofía, no más que circunscribir la causa y limitar el efecto, el contemplador cae en éxtasis en razón de que todas estas descomposiciones de fuerza terminan en la unidad.

El álgebra se aplica a las nubes; la irradiación del astro aprovecha a la rosa; ningún pensador se atrevería a decir que el perfume del espino blanco resulta inútil a las constelaciones. ¿Quién puede calcular el trayecto de una molécula? ¿Qué sabemos nosotros si las creaciones de los mundos no están determinadas por las caídas de granos de arena? ¿Quién conoce los flujos y reflujos de lo infinitamente grande y de lo infinitamente pequeño, el resonar de las causas en los principios del ser, y los aludes de la Creación? Un insecto importa; lo pequeño es grande, lo grande es pequeño; todo está en equilibrio en la necesidad; terrible visión para el espíritu.

Hay entre los seres y las cosas relaciones de prodigio; en este inagotable conjunto, de sol a pulgón, no hay desprecio; tienen necesidad unos de otros. La luz no se lleva al firmamento los perfumes terrestres sin saber lo que hace de ellos; la noche hace distribuciones de esencia estelar entre las flores dormidas. Todos los pájaros que vuelan tienen en la pata el hilo del infinito. La germinación se complica con la aparición de un meteoro y con el picotazo de la golondrina rompiendo el huevo, y se ocupa simultáneamente del nacimiento de un gusano y del advenimiento de Sócrates.

[...]

Un moho es una pléyade de flores; una nebulosa es un hormiguero de estrellas. Igual promiscuidad, y más inaudita aún, de las cosas de la inteligencia y de los hechos de la sustancia.

Los elementos y los principios se mezclan, se combinan, se unen, se multiplican unos por otros, hasta el punto de llevar el mundo material y el mundo moral a la misma claridad. El fenómeno está perpetuamente en repliegue sobre sí mismo. En los vastos cambios cósmicos la vida universal va y viene en cantidades desconocidas, rodando en el invisible misterio de los efluvios, empleándolo todo, no perdiendo ni un ensueño, ni un sueño, sembrando un animalillo aquí, desmenuzando un astro allí, oscilando y serpenteando, haciendo de la luz una fuerza, y del pensamiento un elemento, diseminado e indivisible, disolviéndolo todo, excepto ese punto geométrico, el yo; llevándolo todo al alma átomo; enredando, desde la más alta a la más baja, todas las actividades en la oscuridad de un mecanismo vertiginoso, sujetando el vuelo de un insecto al movimiento de la tierra, subordinando. Máquina hecha espíritu. Engranaje enorme, cuyo primer motor es el insecto y cuya última rueda es el zodíaco.”

Les Misérables

Victor Hugo

Content

1	Nomenclature-Biological rhythms	1
2	Abstract.....	2
3	Introduction.....	3
3.1	Circadian Rhythms.....	3
3.2	Suprachiasmatic Nucleus	3
3.2.1	Cell subpopulations of the SCN	6
3.2.2	Circadian regulatory mechanisms	9
3.3	Arcuate Nucleus of the hypothalamus, a hub for metabolic regulation.....	13
3.3.1	Melanocortin system in the Arcuate Nucleus	14
3.3.2	Tanycytes; the non-neuronal cells in the ARC bridging the circulation with the hypothalamus.....	17
3.4	Non-photoc feedback to the SCN.....	21
3.4.1	Non-photoc feedback from the ARC to the SCN	21
3.5	Other sources of non-photoc feedback to the SCN	23
3.5.1	Circumventricular organs	23
3.6	Disruption of circadian physiology as a risk factor for metabolic diseases	24
4	Problem Statement and Hypothesis.....	24
5	General Objective	25
5.1	Particular objectives	25
6	Methology.....	25
6.1	Experimental model and subject details	25
6.2	Experimental protocols.....	26
6.2.1	Intrajugular cannulation.....	26
6.2.2	SCN lesioning.....	26
6.2.3	ICV cannula.....	26
6.2.4	Fasting	27
6.2.5	Permeability assays	27
6.2.6	2-NBDGlucose penetration assays.....	27
6.2.7	Intracerebroventricular injections	28
6.2.8	Immunohistochemistry and data analysis	28
6.2.9	Immunofluorescence protocol and image analysis for GLUT1/Vimentin/ CD31	29
6.2.10	Aurothioglucose staining.....	29
6.3	Quantification and statistical analysis.....	29

7 Results.....	30
7.1.1 The entry of circulating molecules into the ARC fluctuates daily	30
7.1.2 Structural changes in ME-ARC and CSF-ARC barriers correlate with permeability states.	32
7.1.3 The Suprachiasmatic nucleus mediates the opening of the ME-ARC barrier at ZT22	35
7.1.4 High tanycytic GLUT1 at ZT22 promotes glucose entrance into the ARC.....	38
7.1.5 Glucose entrance into the ARC is essential for low glycemia.....	43
8 General Discussion.....	48
9 Perspectives.....	53
10 Tanycytes targets for treatment in type 2 diabetes?.....	53
11 Aknowledgements	54
12 Bibliography.....	55

1 Nomenclature-Biological rhythms

Acrophase: point of a circadian-regulated variable with the highest values

Bathiphase: point of a circadian-regulated variable with the lowest values

Circadian time (CT): Internal/Endogenous representation of the time in constant-dark conditions associated with the light period's beginning.

Entrainment: active adjustment of the circadian cycle by Zeitgebers

Period: the time that it takes for a rhythmical variable to reach its high point. In rhythms expressed in a circadian manner, the period is close to 24h.

Phase: any value in the curve of a variable fluctuating in a circadian manner.

Zeitgeber (ZT): an external signal that resets or entrains the clock to an environmental rhythm
1. The master Zeitgeber is light.

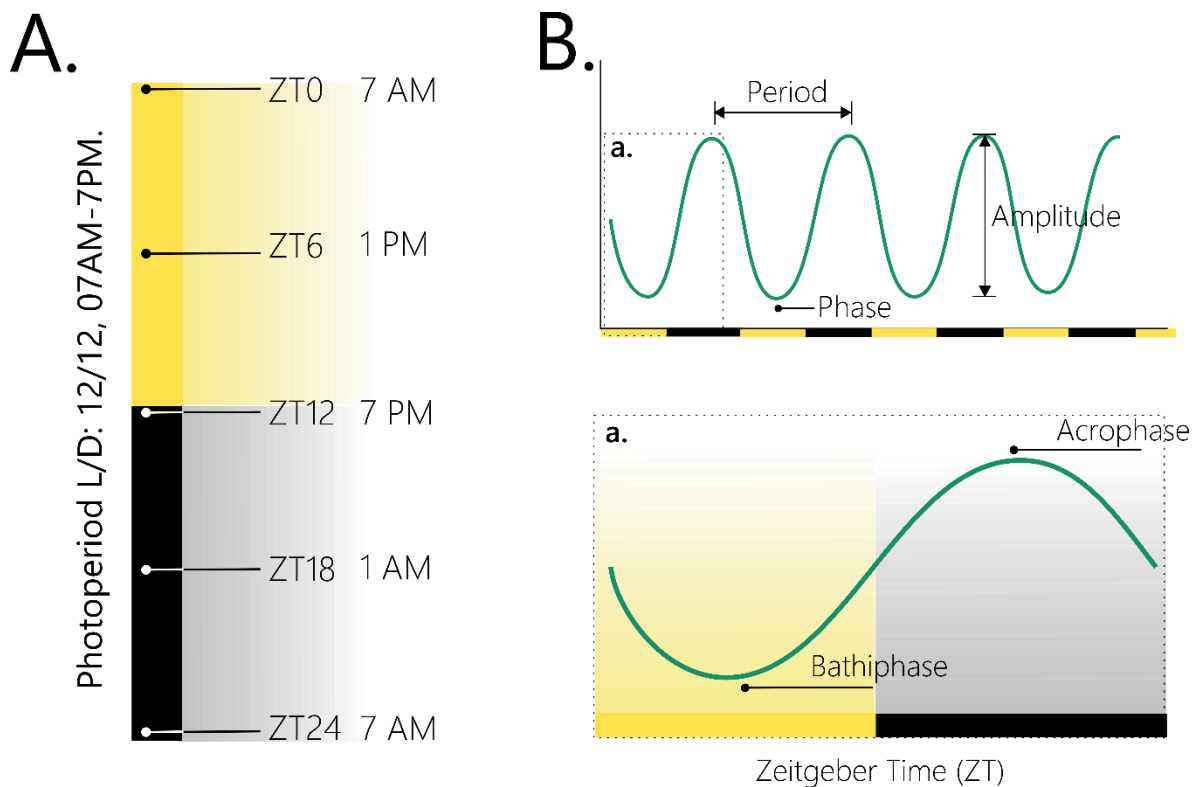


Fig. N. 1 A. Scheme depicting the nomenclature used in the typical photoperiod schedule used in the study of circadian rhythms in rodents, including this study. B Drawing of sequential values of a circadian variable. The oscillations have period, amplitude, acrophase and bathiphase. Inset a, an amplification of squared space in B, showing just one light-dark cycle.

2 Abstract

Glycemia is maintained within very narrow boundaries with less than 5% variation at a given time of the day. However, over the circadian cycle, glycemia changes with almost 50% difference. How the suprachiasmatic nucleus, the biological clock, maintains these day-night variations with such small variations remains obscure. We show that via vasopressin release at the beginning of the sleep phase, the suprachiasmatic nucleus increases the glucose transporter GLUT1 in tanycytes. Hereby GLUT1 promotes glucose entrance into the arcuate nucleus, adjusting glycemia to its lowest level. Conversely, blocking vasopressin activity or the GLUT1 transporter at the daily trough of glycemia, increases glycemia to levels usually seen at the peak of the rhythm. Thus, biological clock-controlled mechanisms promoting glucose entry into the arcuate nucleus before sleep sets the circadian low-glucose levels.

Resumen

Los valores circulates de glucosa en sangre están regulados de tal manera que éstos oscilan en un rango establecido con menos del 5% de variación a un tiempo dado. Sin embargo, a lo largo del ciclo circadiano, los valores de glicemia cambian con casi un 50% de diferencia. El mecanismo empleado por el núcleo supraquiasmático, nuestro reloj biológico, para mantener estas oscilaciones día-noche con tan poca variación no se han esclarecido. En el presente estudio mostramos que la liberación de vasopresina desde las fibras de las neuronas del supraquiasmático que inervan la pared del tercer ventrículo, al inicio de la fase de sueño, incrementa la inmunoreactividad del transportador de glucosa GLUT1 específicamente en tanicitos. En consecuencia, GLUT 1 promueve la entrada de glucosa en el núcleo arqueado, y esto a su vez disminuye los valores de glicemia a su mínimo circadiano. De igual forma, el bloqueo de la actividad del transportador de glucosa GLUT1 durante la batifase de la glicemia, incrementa los niveles de ésta a niveles usualmente observadas durante el pico de éste ritmo.

Conjuntamente, en este estudio encontramos que mecanismos controlados por el reloj biológico promueven la entrada de glucosa en el núcleo arqueado antes de la fase de sueño, estableciendo en consecuencia los niveles mínimos diarios en glicemia.

3 Introduction

3.1 Circadian Rhythms

Life on Earth surged on a massive rock that rotated on its own axis, and cycled around the sun; these cosmic cycles created cycles in the environmental conditions, such as the cycle in the luminous conditions (the Light/Dark (L/D) cycle). The multiple and diverse life forms that evolved under such conditions internalized this cosmic cycle into their behavior, physiology and genome.

Currently, we know that virtually all the physiological, behavioral and metabolism-related variables oscillate through the 24h-day exhibiting a rhythm characterized by periodic acrophases (higher values of a variable) each 24h approximately; known as circadian rhythms (*circa- diem*, about 24h long). These rhythms prepare the brain and body to perform very different, often incompatible, functions appropriate for the day or the night.

3.2 Suprachiasmatic Nucleus

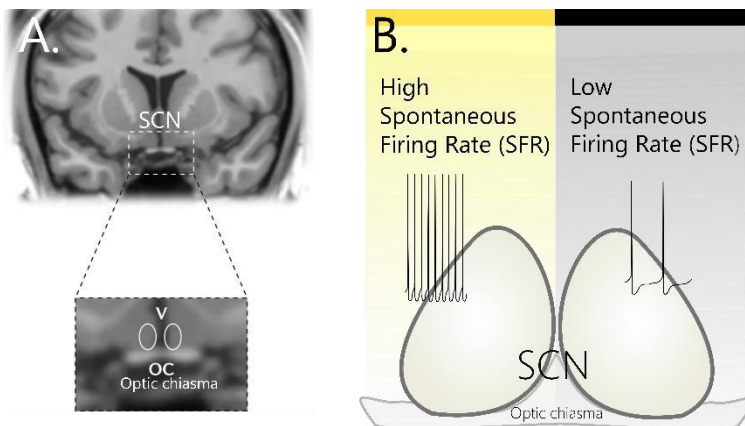


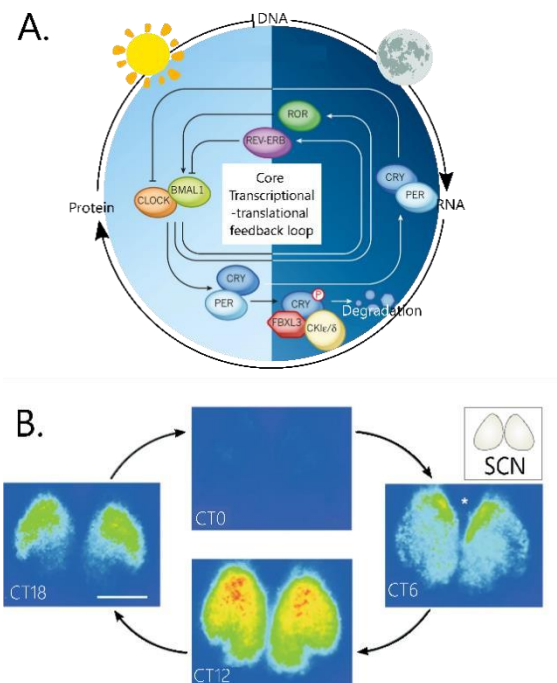
Fig. 1-1 The Suprachiasmatic nucleus of the hypothalamus is the master clock in mammals. A. The SCN is highlighted by the box on the coronal MRI scan of a human brain. The inset shows an enlarged view, with the location of the SCN outlined. The optic chiasm (OC) lies across the base of the midline third ventricle (V). B. The Suprachiasmatic nucleus of the hypothalamus (SCN) exhibits endogenous sustained circadian cycles of spontaneous action potential firing rate (SFR) without spike-frequency adaptation. Globally, the SFR is high during the light period and low during the dark phase. Importantly, these differences reflect the state of global networks; circadian regulated process executed during the dark period might depend on specific circuits active at this period. *Panel A* was taken and modified from: Hastings, M.H., Maywood, E.S. & Brancaccio, M. Generation of circadian rhythms in the suprachiasmatic nucleus. *Nat Rev Neurosci* 19, 453–469 (2018).

In vertebrates, a bilateral region in the hypothalamus, a nucleus of approximately 20,000 neurons and 60,000 glial cells clustered above the optic chiasm; the suprachiasmatic nucleus (SCN), sets the tempo to physiological variables. This nucleus is an autonomous time-keeper, expressing circadian cycles of spontaneous action-potential firing rate (SFR), both when it is isolated *in vivo* or *ex vivo*²³ (Fig. 11).

The molecular mechanism underlying clock function was described in *Drosophila* in the

early 1970s⁴, however

mammalian homologs remained elusive until 1994 with the development of an animal model bearing a dominant negative mutation of a core clock gene⁵. At genetic level, the circadian timekeeping mechanisms are constituted by self-sustained transcriptional-translational feedback loops (TTFLs), and these begin at the circadian dawn (Circadian time, CT 0) when heterodimers of circadian locomotor output cycles protein kaput (CLOCK) proteins, and brain and muscle ARNT-like 1 (BMAL1) (the positive regulators of the loop) drive the expression of the period (PER) and cryptochrome (CRY) proteins (the negative regulators)⁶. By the end of the circadian day PER-CRY complexes have accumulated in the nucleus to start to repress their own expression. Over the course of the circadian night, PER and CRY mRNA levels fall and the existing PER-CRY complexes are degraded⁶ (Fig. I-2). This degradation allows the cycle to reinitiate approximately 24-h solar hours after the previous transcriptional initiation², which happens every day, for a lifetime⁷.



FFig. ig. Iure I1- 2 Transcription-1 –translation feedback loops of core clock genes in mammals expressed both in brain and peripheral tissues. A. TTFL include opposing transcriptional activators (CLOCK–BMAL1) and repressors (PER–CRY)¹. The non-phosphorylated PER–CRY complex represses CLOCK–BMAL1; phosphorylation, in turn, results in the degradation of PER–CRY and the turnover of these repressors. In addition, CLOCK–BMAL1 induces transcription of REV-ERB and of ROR, which regulate BMAL1 expression. During the night, PER–CRY is degraded through the ubiquitylation of CRY by FBXL3. B. Images of bioluminescent signals in a coronal SCN slice from time-lapse recording of PER2 expression (scale bar 500 μm) Part

A: taken and modified from: Bass, J. Circadian topology of metabolism. Nature 491, 348–356 (2012). Part B: taken and modified from: Hastings, M.H., Maywood, E.S. & Brancaccio, M. Generation of circadian rhythms in the suprachiasmatic nucleus. Nat Rev Neurosci 19, 453–469 (2018).

An additional landmark of the molecular circadian system is the modulation of the so-called clock-controlled genes (CCG), whose transcription is regulated by the core clock genes^{8,9}. In the SCN, the entire cell physiology is synchronized to the TTFL through various gene products relevant to housekeeping and metabolic processes; these are sequentially upregulated or downregulated over circadian day and night as the levels of the core clock genes oscillate (Fig. I-2). Many of the CCG code themselves transcription factors, and so, by directing cascades of gene expression, they amplify the circadian TTFL signal and coordinate circadian programs of gene expression, ultimately guiding cell function¹⁰.

The proteins that result from the thousands of CCG expand the functions of the core clock genes, from controlling the timing in transcription/translation processes to other functions related to cellular metabolism^{11,12}.

Most known CCG encode enzymes or regulatory proteins involved in food processing and energy homeostasis. As some examples, we can find the cholesterol 7α hydroxylase (the rate-limiting enzyme in the synthesis of bile acids)^{13– 15}, some enzymes involved in the elimination of

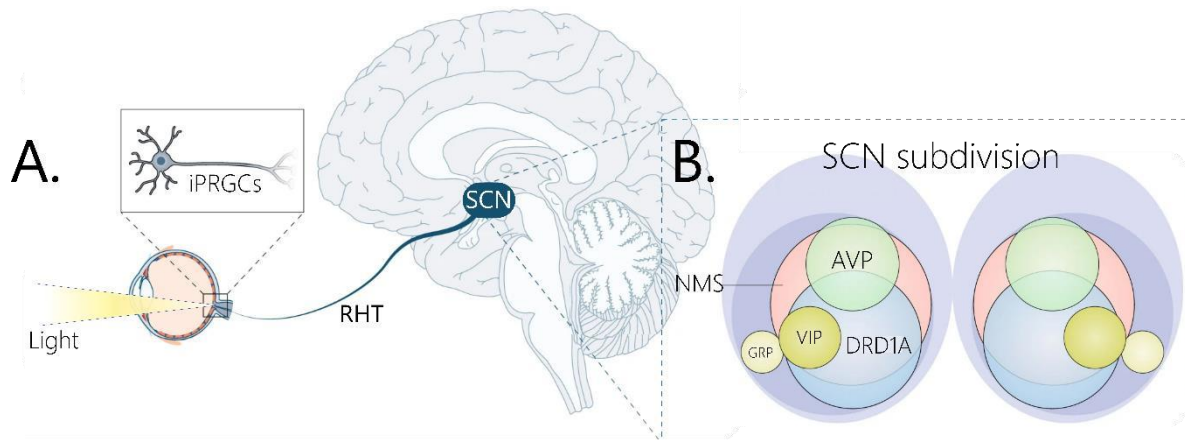
food components such as cytochrome P450¹⁶, also some key proteins involved in carbohydrate metabolism such as the Phosphoenolpyruvate carboxykinase (PEPCK), glycogen synthase, and glycogen phosphorylase¹⁷, among others.

Importantly, the TTFL program is not exclusive of SCN cells, every nucleated cell in the mammalian organism displays it in a tissue-specific manner; the TTFL in peripheral tissues is commonly known as “peripheral clocks”. In the beginning, the discovery of clock genes all over the body questioned the organization of the general circadian system. However, very soon, it was noted that the rhythm in peripheral oscillators depends on the central master clock: in animals whose SCN was ablated, the rhythms in peripheral clocks disappeared^{18,19 20}.

Despite the clear relationship between the temporal arrangement of the peripheral clocks, and the rhythms in the SCN, it remains unclear what is the actual relevance of the TTFL in peripheral tissues for the organization of *circadian* physiology. This dilemma is illustrated by the liver and the rhythm in glycemia. Here, the SCN through sympathetic afferents to the liver sets the circadian acrophase in glycemia^{21,22}, and removing the sympathetic innervation ablates the glycemia rhythm regardless of intact hepatic clock gene oscillations. This would imply that clock genes in the liver are dispensable for the circadian increase in glucose, and that these genes very likely serve more for other cellular functions than for circadian rhythmicity²³.

As almost all peripheral tissues express robust TTFL, so it happens in other brain nuclei apart from the SCN^{24–27}, in this sense why is the SCN the master clock, and why does not any other brain nucleus has the capacity to generate sustained rhythms? The answer probably lies in the intrinsic organization of the SCN cells to sustain its circadian cycle of TTFL indefinitely, even when isolated *in vitro*. In contrast, the circadian programs of other parts of the brain, and peripheral tissues damp after a few days in culture, as cell clocks lose amplitude and phase coherence⁷. Additionally, in comparison with other brain regions, what is remarkable about the SCN neuronal network is that it can sustain determined SFR for long intervals (up to 6h) without spike-frequency adaptation²⁸.

Since the neurons of the SCN can track one of the most massive time signals that exist: day/night (light-dark) cycle. The SCN entrainment is mediated by direct retinal innervation from the retino-hypothalamic tract (RHT) that evokes firing rate of the clock neurons at the daytime. The RHT originates from intrinsically photoreceptive retinal ganglion cells (iPRGCs)²⁹ that express the invertebrate-like photopigment melanopsin³⁰ (Fig. I-3). This tract provides non-imageforming visual information directly into the SCN, enough to entrain the neurons to the light/dark cycle.



▲ Fig. I-3 SCN transduces and internalize the luminous signal through the retinohypothalamic tract to then provide this signal to the multiple neuronal subpopulations residing here. A. In the input pathway to the SCN, light is received by the intrinsically photosensitive retinal ganglion cells (ipRGCs) expressing melanopsin, which sends electric signals to the SCN through the retinohypothalamic tract (RHT). B. Cartoon illustrating the highly overlapping neuronal subpopulations in the SCN: neuromedin S (NMS), arginine vasopressin (AVP), vasoactive intestinal peptide (VIP), gastrin-releasing peptide (GRP) and D1 dopamine receptor (DRD1A) cells. Taken and modified from: Ruan, W., Yuan, X. & Eltzschig, H.K. Circadian rhythm as a therapeutic target. *Nat Rev Drug Discov* 20, 287–307 (2021).

SCN neurons produce various neuropeptides and neurotransmitters, whose functions and expression patterns are changed based on locations in the SCN^{31,32}. For example, gammaaminobutyric acid (GABA) is the most common neurotransmitter in the SCN and is expressed

in many the SCN neurons^{33,34}. Although GABA is a well-known inhibitory neurotransmitter in the nervous system, it has both excitatory and inhibitory activity in the SCN.

3.2.1 Cell subpopulations of the SCN

Besides GABA, the SCN neurons also co-express a wide range of neuropeptides and neuropeptide receptors allowing receiving input from extra-SCN afferent pathways, and intraSCN networks⁷. The neuropeptidergic identity of cells was used at the beginning to subdivide the SCN anatomically into two regions: the ventral core and the dorsal shell. However, evidence showing that the complexity of the SCN circuit topology is much finer-grained than a simple core-shell dichotomy is slowly eliminating this antiquate classification³⁵.

What is typically known as the core of the SCN consist mainly of the retinorecipient part, delineated by vasoactive intestinal polypeptide (VIP) and gastrin releasing peptide (GRP) expressing neurons. On the other hand, the shell region consists of neurons expressing arginine vasopressin (AVP), nevertheless the anatomical boundaries of the shell region has been challenged by evidence showing that the AVP population continues to areas around the canonical SCN space³⁶ (Fig. I-3B).

VIP is released by the retinorecipient cells and acts on the VIPR2 (also known as VPAC2), located on the so-called shell neurons. The loss of VIP, or its receptor VPAC2 results in arrhythmic behavior in mice held in constant darkness, the loss of circadian responses to light, and impaired synchrony and amplitude of cellular TTFRL rhythms^{37–39}. Indicating that VIP likely transduces the light signals to the rest of the neuronal network.

Contrastingly, the loss of AVP signaling does not ablate SFR oscillations, however in the absence of AVPR1a and AVPR1b receptors, mice phase shift more rapidly to resetting light/dark schedules, indicating that might AVP have a central role in spreading the integrated circadian period but it is secondary in the establishment of the SFR period of the SCN internal network.

Importantly, the complexity of the SCN circuit topology is much finer-grained than a simple core-shell dichotomy³⁵. For instance, bioluminescent and fluorescent probes have shown stereotypically organized waves of cellular activation traversing the SCN as cells progress through their circadian program, showing differentially phased, spatially discrete clusters⁴¹(Fig. I-2B). To get a better appreciation of SCN circuit topology and the associated neurochemical and genetic specialization, SCN-enriched genes are being identified, and single-cell transcriptional profiling has revealed potential subnetworks based on distinct signaling modules.

One of the most complete classifications of the SCN cell subtypes, through single-cell RNAsequencing, identified seven non-neuronal cell types and five neuron subtypes (Fig. I-4). The five SCN neuron subtypes can be defined by specific combination of expressed genes as 1) *Avp*⁺/*Neuromedin S* (*Nms*)⁺, 2) *Grp*⁺/*Vip*⁺, 3) *Vip*⁺/*Nms*⁺, 4) *Cholecystokinin* (*Cck*)⁺/*(Complement C1q-like protein 3)* *C1ql3*⁺, and 5) *Cck*⁺/*Brain-Derived Neurotrophic Factor* (*Bdnf*)⁺ (Fig. I- 4B). In particular, *Avp*⁺/*Nms*⁺, *Vip*⁺/*Nms*⁺ and *Cck*⁺/*C1ql3*⁺ subtypes show robust circadian gene expression in the SCN, whereas *Grp*⁺/*Vip*⁺ and *Cck*⁺/*Bdnf*⁺ subtypes show weak circadian gene expression⁴² (Fig. I- 4B).

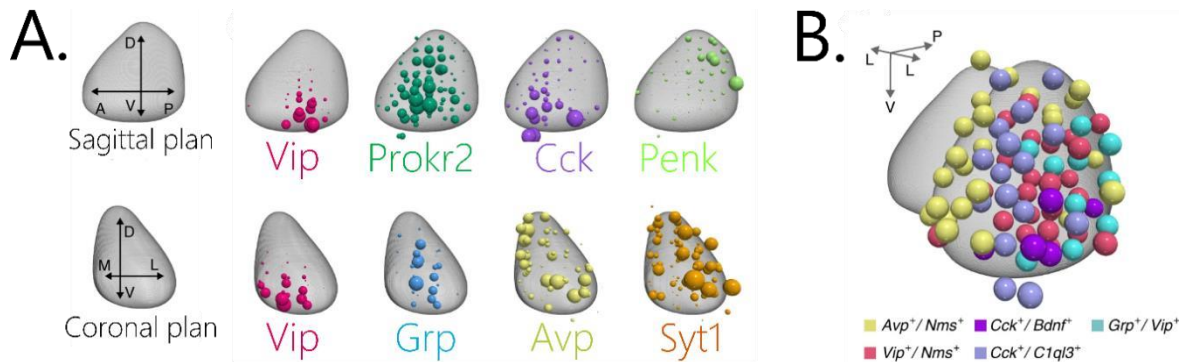


Fig. I-4 *Suprachiasmatic nucleus cell subtypes revealed through single-cell RNA-sequencing. A. The 3D gene expression patterns of selected genes obtained from RNA-seq performed in Ref. 42. The diameter of the sphere is proportional to the normalized gene expression level. B. Inferred spatial locations of five SCN neuron subtypes by non-negative linear regression. Taken and modified from: Wen, S., Ma, D., Zhao, M. et al. Spatiotemporal singlecell analysis of gene expression in the mouse suprachiasmatic nucleus. Nat Neurosci 23, 456–467 (2020).*

Additionally, some of the SCN neurons also express other neuropeptides that, despite being more spread non-clustered populations, had been proposed as key regulators of particular SCN circuit outputs. For instance, the neuropeptide prokineticin 2 (PROK2)-expressing neurons.

The loss of PROK2 or its receptor (PROK2R) in mice abolishes the peak of activity at the start of circadian night, even with the SCN TTFL unaffected^{43,44}. Thus, PROK2R may gate the function of other SCN output neurons and/or act on local hypothalamic targets of SCN and its absence breaks the link between a specific SCN evening signal and locomotor control⁴⁵. Also, as discussed above, these results question again the real functionality of the Clock genes, since an animal with the molecular clock oscillating normally, has no rhythm in locomotion.

Another example of a neuronal subpopulation whose signal is used by the SCN to direct key outputs is the AVP⁺ population. The transcriptional machinery of the core clockwork regulates the rhythmic expression of AVP in the SCN shell, but not in other AVP-producing neurons^{46,47}. We will review SCN-AVP mechanisms in more detail in subchapter 3.2.2.1.1 SCN target areas influenced by Arginine-Vasopressin.

SCN neurons expressing neuromedin-S (NMS) meet the criteria for pacemakers: silencing synaptic transmission in NMS-expressing neurons by reversible overexpression of tetanus toxin was accompanied by reversible cellular desynchrony in the SCN and loss of circadian behavioral rhythms. However, given that NMS⁺ neurons are nearly 40% of SCN neurons extending across the core and shell regions, and that the NMS⁺ cells can also co-express: AVP, VIP, and the D1 subtype of the dopamine receptor (DRD1A) raises the question which subpopulation of NMS neurons are the minimum necessary for pacemaking?

Among other non-clustered neuronal population in the SCN, the DRD1a-expressing cells have been suggested as at least part of the pacemaker. The optogenetic control of the firing rate of the DRD1A cells is sufficient to entrain circadian behavioral rhythms in mice⁴⁸. Coincidentally, manipulations of DRD1A-expressing neurons always resulted in the behavioral phenotype *in vivo* matching the SCN rhythm *ex vivo*³. However, we have again a similar dilemma as with the NMS⁺ neurons: the DRD1A represent about 60% of cells in the SCN, including most VIP-expressing cells and approximately 60% of AVP-expressing cells⁴⁹. Then, which subpopulation would be the real circadian driver?

For long time the study of SCN networks, has centered the attention on neurons, neglecting other cell populations disregarding these cells outnumber for much the neurons. Systematic single-cell RNA-sequencing revealed the presence of seven non-neuronal clustered cell types in the SCN: astrocytes, endothelial cells, ependymal cells, microglia, NG2 cells, oligodendrocytes, and tanycytes. However, until now there are no clear answers regarding the functionality of each cell-type.

SCN is densely populated by glia in an estimated ratio of approximately 3:1 neurons to glia⁷. Astroglial cells, similar to neurons, show circadian [Ca²⁺]_i oscillations but these are antiphase to neuronal oscillations, peaking during the circadian night when neurons are inactive⁵⁰. Additionally, the SCN astrocytes exhibit circadian changes in morphology⁵¹⁻⁵³, and for example, mouse cortical astrocytes contain TTFL clocks⁵⁴ that can entrain the TTFL of cortical neurons. Coincidentally, the global deletion of *Bmal1* from mouse astrocytes perturbs the profile of behavioral rhythms and dysregulates PER2 and VIP expression in the SCN⁵⁵.

In 2017, Brancaccio and collaborators convincingly showed how the neurons of the SCN constitute only one “half” of the master clock, the one metabolically active during circadian daytime, while the astrocytes are active during circadian nighttime, when they suppress the activity of SCN neurons by regulating extracellular glutamate levels⁵⁶. Surprisingly, somatic genetic reprogramming of intracellular clocks in SCN astrocytes was enough to remodel circadian behavioral rhythms in adult mice. This is contrasting with studies where the intact astrocytic clock was not necessary for circadian behavior insofar as deletion of *Bmal1* from astrocytes did not compromise rest–activity or SCN gene expression rhythms; rather, it simply lengthened their period by about 30 min⁵⁷.

3.2.2 Circadian regulatory mechanisms

As the principal pacemaker, the SCN influences the subordinate cellular clocks across the body conveying them circadian and photic information, either directly through innervation of target hypothalamic and extrahypothalamic nuclei, or indirectly through endocrine signals, the autonomic nervous system, or diffusible signals⁵⁸. The arrangement of the circadian system is conceptualized as a hierarchical arrangement of oscillators, offering numerous opportunities to control, but also for dysfunction¹.

3.2.2.1.1 Neural circuits

SCN distributes rhythm to the periphery via autonomic branches, hormonal cues and rhythmic behavior. The functioning of periphery is commonly influenced by a combination of these three control strategies, making the oscillations very robust. Anatomical studies have shown that the SCN projects to at least four different kind neuronal targets: endocrine neurons, autonomic neurons of the paraventricular nucleus of the hypothalamus (PVN), other hypothalamic structures that transmit the circadian signal to other brain regions, and areas outside the hypothalamus⁵⁹. Monosynaptic efferents of suprachiasmatic nucleus neurons terminating in nearby hypothalamic and thalamic nuclei, innervate several nuclei such as the medial preoptic nucleus (MnPO), subparaventricular zone, arcuate nucleus (ARC), dorsomedial nucleus (DMH), ventral lateral geniculate nucleus, , and as mentioned before, the PVN⁶⁰.

The way the SCN can transmit its rhythm is illustrated by how the SCN influences melatonin secretion. The synthesis of melatonin is driven directly by the SCN through a multi-synaptic neural pathway which successively includes pre-autonomic neurons of the PVN, sympathetic pre-ganglionic neurons of the intermediolateral cell column of the spinal cord (IML), and noradrenergic sympathetic neurons of the superior cervical ganglion^{61–63}. The melatonin synthesis pathway is stimulated by the release of noradrenaline from sympathetic nerve terminals within the pineal gland. The activation of β_1 -adrenergic receptors on pinealocytes causes a dramatic increase in the expression of an enzyme crucial for melatonin synthesis, this in turn induces a 50-fold increase of its enzymatic activity⁶⁴. This process induces a quick rise in the synthesis and secretion of melatonin⁶⁵.

In the next section we will focus our attention in one SCN neuronal population directing circadian outputs associated with phase transitions relevant for the present study: the arginine vasopressin expressing neurons.

3.2.2.1.1.1 SCN target areas influenced by Arginine-Vasopressin

The circadian system organized by the SCN is thought to establish different set-points for hormones and circulating metabolites, according to 1) the time of the day, and 2) emergent conditions such as fasting, sickness, or stress⁶⁶. It has been hypothesized that variations in these set-point values might have their origin in a daily modulation of key sensor structures sensitivity⁶⁷. Since vasopressin has proven to promote changes in physiology associated with phase transitions, it has been hypothesized as one of the sensitivity modulators of target hypothalamic nuclei (See Chapter 3 Problem Statement and Hypothesis).

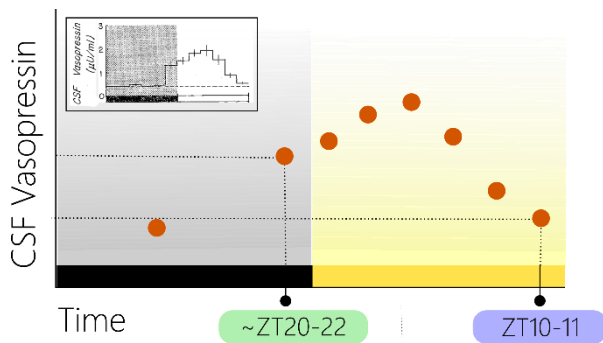


Fig. I-5 The concentration of vasopressin in the CSF fluctuates through the light/dark cycle. Cartoon based on measurements of CSF vasopressin made by Schwartz, W. J. and Reppert, S. M. in 1985 (original graph included in the upper inset). The origin of the fluctuating vasopressin has not been elucidated convincingly yet, therefore, it is not confirmed whether this neurotransmitter is indeed produced and secreted to the CSF by the SCN neurons.

Very recently SCN^{AVP} fibers projecting towards the CSF, were observed (Fig. I. 6). Once cholera toxin beta subunit (CtB) (an tracer that behaves primarily as retrograde tracer at standard doses)⁷⁵ is injected into the lateral ventricle, some SCN^{AVP} cells bearing the tracer were identified, suggesting that the SCN could sense substances into the CSF, as well³⁶. If true, this would constitute a novel mechanism by which the SCN receives non-photoc feedback.

Similar to oscillatory behavior of excitable tissues such as the heart and respiratory centers,

it is hypothesized that the SCN might also have pacemaker hub(s) embedded into its circuits, The concentration of AVP thought to be of SCN origin, fluctuates daily with a constant increases from ZT20, peaking in the morning in the CSF⁶⁸⁻⁷⁰ (Fig. I. 5) but not in the blood⁶⁸. The clear increase of this neurotransmitter towards the resting phase, raised some speculations about its role in key physiological transitions associated with this time of the day. Coincidentally, previous studies have demonstrated how AVP release from SCN neurons inhibits corticosterone secretion^{71,72}, lowers body temperature (BT)⁷³, and elicits an anticipatory surge of thirst right before the sleep period⁷⁴.

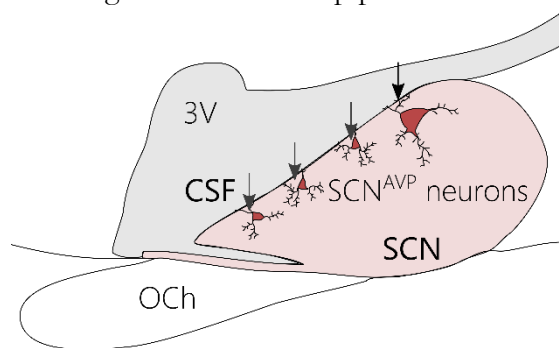


Fig. I-6 The processes of SCN^{AVP} neurons cross the epithelium of the 3V wall reaching the CSF. Cartoon illustrating the hypothetical location of SCN^{AVP} neurons in a sagittal plane. The anatomical pathway depicted here could potentially sustaining the daily fluctuation in CSF vasopressin. Cartoon adapted from: Taub A, Carbajal Y, Rima K,

Holt R, Yao Y, Hernandez AL, LeSauter J, Silver R. *Arginine 2021. Vasopressin-Containing Neurons of the Suprachiasmatic Nucleus Project to CSF. eNeuro.*

having a structured hierarchical circuit topology³. For a cellular population to be considered as a circadian driver, some basic criteria must be met at least the following criteria: 1) their electrical firing must be necessary to control circadian behavior, and 2) the cell-autonomous period of such cell cluster(s) must dictate the global period of the SCN and behavior³.

An example of vasopressin as a modulator of phase-dependent changes is appreciated in the daily decrease of the core body temperature right before the resting phase. In rats and mice, body temperature is low during the day, while high during the night; importantly, these daily differences do not depend on the locomotor activity⁷⁶, instead these are modulated by a two-branched circuit: SCN-ARC and SCN-medial preoptic area (MnPO). Here, vasopressin neurons from the SCN project to neurons in the MnPO which also receives projections from the ARC⁷⁷. Both, the release of AVP from the SCN, and α -Melanocyte stimulating hormone (α -MSH) from the ARC are rhythmic. α -MSH neurons exhibit a SCN-driven activity with their acrophase around ZT18, while SCN^{AVP} neurons are active from ZT19 towards ZT22⁷⁸. During the first part of the activity phase, the SCN-induced neuronal activity releases α -MSH in the MnPO keeping the temperature high; meanwhile the secretion of SCN AVP increases towards the end of the activity phase. In fact, the rhythms of α -MSH and AVP are to some extent overlapping, allowing a finer regulation over the MnPO. Once the SCN switches off the α -MSH neuronal activity, the concomitant increase in AVP release into the MnPO, brings the temperature abruptly down⁷⁷. It remains unclear which signal increases the temperature at the end of the sleeping period, when α -MSH neuronal activity has not yet increased.

Another crucial adjustment associated with the activity \rightarrow sleeping phase transition is an increase of thirst at this transition. An animal loses significant amounts of water while sleeping through transpiration and ventilatory function. As reviewed before, the OVLN receives SCN^{AVP} innervation which stimulates water intake right before the sleeping period. This drinking behavior is not motivated by dehydration needs; however, when this bout of water intake is not allowed the animal experiences osmolarity disturbances and light signs of dehydration later in the sleep period. The output of the SCN^{AVP}-OVLN circuit has been proposed as an anticipatory modulation that prevents dehydration and mineral imbalance during the resting period^{74,79}. It remains unexplained why the animals stop drinking while SCN^{AVP} continues and even increases in the beginning of the sleep phase. As another example, the rhythmic secretion of corticosterone right before the beginning of the activity phase depends on a variation in the sympathetic tone over the adrenal gland which is modulated by the SCN⁷¹. Animals subject to complete SCN ablation, not only lose their rhythm in corticosterone secretion; but also display increased values of this hormone comparable to acrophase levels; indicating that the SCN is responsible for both, inhibiting corticosterone and stimulating corticosterone secretion at the acrophase (around ZT11)⁷¹. Here, SCN^{AVP} neurons inhibit corticosterone secretion acting on pre-autonomic neurons in the paraventricular nucleus (PVN)⁷¹: AVP antagonist into the PVN increases corticosterone between ZT2 and ZT11; while sympathetic effect on the adrenal induces a fast release of corticosterone⁸⁰⁻⁸².

The relevance of SCN^{AVP} circuits will be further addressed in the chapter 3. Problem Statement and Hypothesis.

3.2.2.1.2 Diffusible factors

Pioneer studies whereby transplants of SCN tissue rescued circadian rhythms of locomotor activity in arrhythmic SCN-lesioned host animals⁸³, with the period of the donor animal⁸⁴, irrespective of the attachment site within the third ventricle (3V)⁸⁵; nourished the hypothesis that diffusible signals from the SCN might be enough and sufficient to entrain circadian rhythms. SCN transplants are effective even when the grafted tissue is encapsulated in a polymer plastic that blocks fiber outgrowth⁸⁶; however, SCN transplants can restore locomotor rhythmicity only, but not the secretion rhythm in hormones such as corticosterone⁸⁷.

Signals that diffuse from the SCN include paracrine outputs such as transforming growth factor alpha (TGF α)⁸⁸, prokineticin2 (PK2)^{89,90}, cardiotropin-like cytokine⁹¹, and the peptides vasoactive intestinal polypeptide (VIP), arginine vasopressin (AVP), and gastrin releasing peptide (GRP)^{40,92}.

Among all, perhaps the most popular cue is the AVP, probably because AVP shows a clear circadian fluctuation in the cerebrospinal fluid (CSF) in rodents, with higher values during the day as compared to night levels⁹³. Due to the robust circadian fluctuation, this rhythmical secretion into the CSF has commonly been assumed to originate from the SCN, nevertheless the route whereby at least part of the peptide can reach the CSF was documented only recently³⁶ and by the present study.

Recently, using immunohistochemistry, tracing experiments and cell filling techniques processes of AVP-expressing SCN neurons were shown to cross the epithelium of the third ventricular wall, reaching the CSF³⁶. Although the functionality of this SCN-CSF communication was not studied, this route of communication suggests that the SCN^{AVP} neurons can also sense molecular cues contained in the CSF as a source of negative feedback.

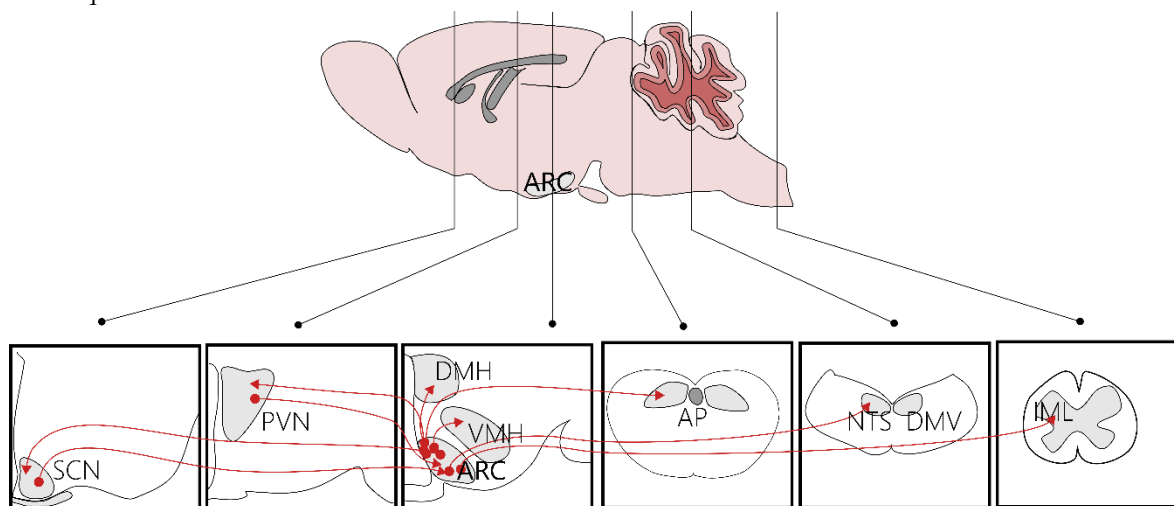
An anatomical study from the same research laboratory, using tissue clearing combined with multilabel immunostaining and light-sheet microscopy, described a new portal system between the *organum vasculum of the laminae terminalis* (OVLT) and the SCN⁹⁴. This potentially offers other routes for the SCN to communicate with key nuclei and receiving non-photic feedback from the circulation.

The OVLT is commonly known by its role in systemic osmoregulation and thermoregulation, all under circadian control⁷⁸. Some authors have speculated that this route confers slow and longterm regulation, in comparison with the neural communication that supports fast and acute signaling. It also invites to think that this kind of communication could apply to other CVOs, establishing a direct pathway to keep the clock “informed” about sudden changes in the peripheral variables. On the other hand, known reciprocal neuronal projections between SCNOVLT and SCN-Arcuate nucleus already provide a fast pathway for such communication; further studies are needed to provide functional data for this interaction.

3.3 Arcuate Nucleus of the hypothalamus, a hub for metabolic regulation.

As discussed in the last section, the SCN is not isolated from peripheral cues but is constantly receiving non-photoc feedback conveyed by other nuclei taking care of specific tasks. Here, the arcuate nucleus of the hypothalamus (ARC) plays an essential role transmitting non-photoc feedback from the periphery to the SCN^{76,96,97}.

The ARC receives information from the periphery (through its association with the Median Eminence, a circumventricular organ), and transmits this to the paraventricular nucleus (PVN) and also to nuclei directing the autonomic outflow such as the thoracic Intermediolateral column, (IML) of the spinal cord (Fig. I-7). The ARC participates in distinct regulatory circuits controlling several physiological variables including food intake, glycemia homeostasis, among others. The anatomical location of the ARC near the ME⁹⁸ has promoted the hypothesis that its neurons and other cells could sense circulating metabolism-related cues from the periphery with regulatory consequences.



For example, leptin, a cytokine/hormone produced by the fat tissue, is taken up by the ARC⁹⁹.

Fig. I-7 The ARC possesses anatomical pathways both to receive information from periphery, and transmit it to peripheral tissues. The arcuate nucleus(ARC) signals to a variety of nuclei, participating in the regulation of food intake, energy expenditure, glucose homeostasis etc. ARC neurons project to targets including the paraventricular nucleus (PVN), the ventromedial hypothalamus (VMH), dorsomedial hypothalamus (DMH), the area postrema (ap, a CVO), the nucleus of the tractus solitarius (NTS) in the brainstem. The ARC also receives input from the suprachiasmatic nucleus providing all the circuits the ARC participates in with the time signal. through its influence on pre-and autonomic nucleus (the paraventricular nucleus (PVN) and thoracic IML). The cartoon was adapted from Amado A, Cansell C, Denis RG, et al. The hypothalamic arcuate nucleus and the control of peripheral substrates. Best Pract Res Clin Endocrinol Metab. 2014 Oct.

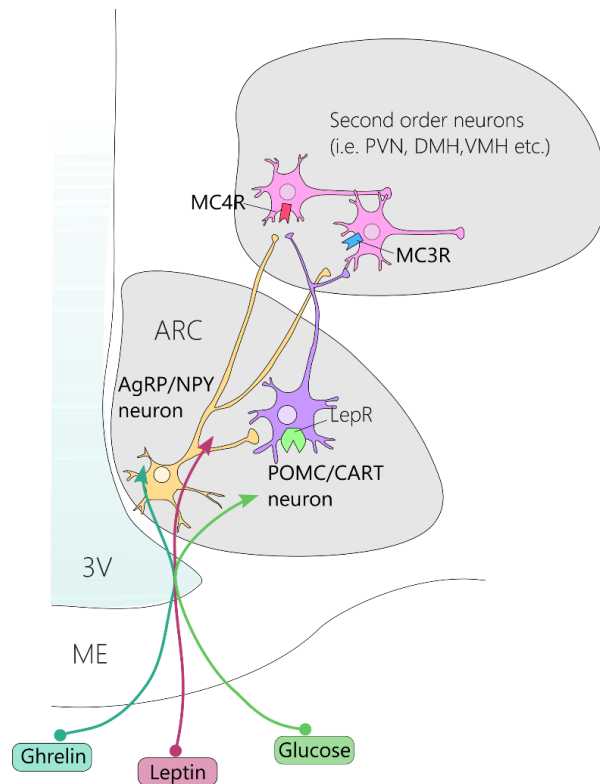
Leptin modifies the activity of two neuronal populations in the ARC: neurons expressing agouti related peptide (AgRP), and proopiomelanocortin⁺ (POMC⁺) neurons, their neuronal projections to the PVN influence pre-autonomic neurons controlling both sympathetic and parasympathetic branches of the autonomic nervous system (ANS). Using this pathway, the ARC can mediate leptin effects on heart rate and blood pressure. Leptin increases the activity of certain sympathetic branches^{96,100}, as the one innervating the liver¹⁰¹. Additionally, cocaine and amphetamine-regulated transcript (CART)⁺ neurons in the ARC project to the thoracic intermediolateral (IML) column of the spinal cord, transducing the sympathetic outflow to the periphery, also this circuit can be activated by leptin.

Besides mediating the effects of leptin, the ARC is also a cornerstone in regulating circulating corticosterone. This glucocorticoid is detected by the ARC neurons before it reaches any other brain area, thus functioning as the primary target of this hormone for the fast negative feedback of the hypothalamus-pituitary-adrenal glands axis¹⁰².

Molecularly specialized neuron subtypes support the varied functions of the ARC. As it regularly happens in practically all scientific disciplines, the study of the ARC and its functions is directed largely by the research techniques available. For instance, the study of the ARC relies for a large part on immunohistochemistry or *in situ* hybridization techniques, limiting the number of proteins or transcripts that can be visualized simultaneously. This automatically generated a bias toward two different neuronal populations: POMC⁺/CART⁺; and the AgRP⁺/NPY neurons. Together, these two neuronal populations constitute the melanocortin system of the ARC.

3.3.1 Melanocortin system in the Arcuate Nucleus

The Melanocortin system in the Arcuate Nucleus is constituted by two hypothetically antagonistic branches: 1) the orexinergic agouti-related peptide/neuropeptide Y coexpressing (AgRP/NPY) neurons, and 2) the anorexigenic pro-opiomelanocortin/cocaine-amphetamine related transcript (POMC/CART) coexpressing neurons. Both neuronal populations modulate the activity of a wideranging network of postsynaptic melanocortin 4 receptor (MC4R)-expressing neurons⁹⁸ (Fig. I-8). Importantly, the functionality of this system has clinical implications because MC4R mutations are the most common cause of monogenetic forms of obesity in humans^{103,104}.



▲ Fig. I-8 The arcuate nucleus of the hypothalamus (ARC) contains at least two populations of neurons that control energy balance the orexigenic/anabolic neurons producing neuropeptide Y and Agouti-related protein (NPY/AgRP) and the anorexic/catabolic neurons producing proopiomelanocortin (POMC) and the natural ligand for the melanocortin receptor. These first order neurons are located exquisitely close to the median eminence (ME), one of the brain's circumventricular organs that lies at the bottom of the third ventricle (3V). Together, this creates a privileged region in which macromolecules and energy-related molecules such as ghrelin, leptin and glucose target neurons in the ARC expressing key receptors. Neurons in the ARC signal to neurons in other nuclei expressing MC4R and MC3R receptors.

3.3.1.1 Agouti-Related Peptide-expressing Neurons

AgRP neurons are located in the ventromedial part of the ARC at the bottom of the third ventricle close to the ME, an ideal position to sense blood-borne metabolic signals. These neurons increase their excitability upon energy deficits and thus antagonize central MC4R signaling via the release of AgRP¹⁰⁵, ultimately stimulating food intake and reducing energy expenditure. Once the food intake is initiated, these neurons get rapidly hyperpolarized^{106,107}.

A great part of the AgRP neurons, coexpress NPY as well as GABA, and their orexigenic effect depends on NPY and GABA release^{108,109}. GABA-releasing AgRP terminals directly inhibit POMC neurons^{106,110}, while NPY is required for the acute short-term impact of AgRP neurons on feeding behavior as NPY-deficient mice fail to rapidly increase food intake upon either chemogenetic or optogenetic activation of AgRP neurons¹¹¹.

The AgRP are first-order neurons of a constellation of core forebrain nodes, forming part of extended circuits mediating feeding behavior¹¹². AgRP neurons target different brain regions, sufficient to evoke feeding independently¹¹². For instance, the optogenetic activation of the AgRP projections into the PVN is enough to induce feeding^{113,114}; additionally, the stimulation of projections to the lateral hypothalamus (LH), the anterior bed nucleus of the stria terminalis (BNST), and the paraventricular thalamus (PVT) evoke feeding as well¹¹². Congruently, the acute ablation of AgRP neurons in adult mice leads to a severe reduction in food intake and eventually to starvation^{115,116}.

Besides its role in regulating food intake, AgRP can influence substrate use by regulating glucose homeostasis. Activation of AgRP neurons leads to a rapid decrease in fat use and increases systemic glucose levels, independent of food intake¹¹⁷, simultaneously impairing systemic insulin sensitivity^{111,113}. This AgRP-neuron-dependent insulin resistance is achieved via acute impairment of insulin-stimulated glucose uptake into brown adipose tissue (BAT). Under these conditions, BAT gene expression switches towards a myogenic state, coordinating hunger states with glucose homeostasis¹¹³.

AgRP neurons can also influence pain perception depending on its origin. The activation of AgRP neurons abrogates inflammatory pain, but simultaneously, the stimulation of these neurons is mildly aversive to mice. Therefore, AgRP neurons have a major role in the prioritization of key survival needs¹¹⁸: the antinociceptive effect of hunger, and at the same time the evocation of the negative valence signals associated to hunger¹¹⁹.

Recent work revealed specific vagal afferents, ultimately controlling AgRP neuron activity in response to intestinal chemosensation and mechanosensation¹²⁰. Here, AgRP neurons are rapidly inhibited by activation of mechanoreceptors of stomach-innervating glucagon-like peptide-1 receptor (GLP1-R) neurons and intestine-innervating oxytocin (OXT) neurons. Importantly, this inhibition occurs on different time scales: activation of GLP1-R neurons leads to a rapid but transient inhibition of AgRP neurons, whereas the activation of OXT neurons results in a fast but sustained inhibition¹²⁰.

3.3.1.2 Pro-Opiomelanocortin-expressing Neurons

Pro-opiomelanocortin (POMC)⁺ neurons are mainly located in the latero-dorsal part of the ARC, and in the NTS as well. These neurons release α - and β -melanocyte-stimulating hormones due to the post-translational cleavage of POMC product and signal via MC3R and MC4R¹²¹. These neurons are activated by energy surplus and selectively inhibit food intake after prolonged periods of feeding^{122,123}. They integrate long-term adiposity signals from the hypothalamus and short-term satiety signals from the brainstem ultimately increasing energy expenditure^{124–126}.

POMC neurons are often seen as the functional opposite of the AgRP neurons, however this model is still incomplete and too simplistic¹²⁷, for example, 25% of POMC neurons coexpress AgRP¹²⁸. How POMC neuronal cells operate has remained elusive due to their high level of heterogeneity. Using an unbiased clustering analysis, Campbell and colleagues identified three main clusters of POMC neurons and two of AgRP neurons¹²⁹. Other studies found that POMC neurons could be classified 1) by the expression of glutamate or GABA^{130,131}, or 2) by the expression of Leptin, 5-HT_{2C}¹³², or GLP1 receptors since these appear as largely nonoverlapping POMC cell subtypes with a certain anatomical localization in the ARC, as well as a different regulation of feeding on acute chemogenetic activation¹³³. POMC neuronal activation can produce behavioral effects such as the promotion of feeding, just as the AgRP/NPY neurons¹³⁴. Also, cannabinoids stimulate a switch from α -melanocyte-stimulating hormone to β -endorphin release from POMC neurons and subsequently increase food intake¹³⁴, which argues against a strictly anorexigenic role of POMC neurons¹²⁷.

Additionally, rapid *in vivo* activation of AgRP/NPY neurons promotes hunger independently of POMC neuronal activity¹⁰⁶, suggesting that these supposedly antagonistic populations do not always influence appetite in an interdependent manner¹²⁷.

As evidenced by recent studies, POMC neurons also participate in anticipation of satiety as the presentation of food cues leads to their immediate activation¹³⁵. This activation is sufficient to prime the liver to the postprandial state via the melanocortin-dependent control of the sympathetic nerve activity of this organ, preparing the organism for food ingestion¹³⁶.

Recent studies show how by simply presenting food to a hungry mouse, the activity of its AgRP and POMC neurons reset: going from a pattern associated with energy deficit to one associated with satiety, even when no food is consumed yet. A real-time monitoring of neuronal activity ([Ca²⁺] fluctuations) in freely behaving mice, revealed that the extent of neuronal activity changed depending on the accessibility and palatability of the food¹³⁵.

Obesity has profound effects on the signaling capabilities of POMC neurons. For example, HFD feeding results in altered mitochondrial dynamics and mitochondria-endoplasmic reticulum (ER) interactions, leading to the inhibition of POMC neurons firing due to impaired Ca²⁺ handling^{137–}

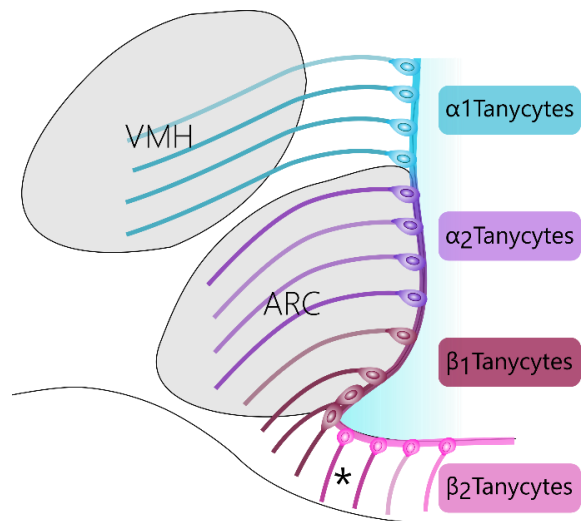
139.

3.3.1.3 Sensing properties of ARC neurons

NPY/AgRP and CART/POMC neurons in the ARC are in a perfect position for sensing circulating hormones and metabolites. Ghrelin, a hormone secreted by enteroendocrine cells of the gastrointestinal tract during hunger^{140–142}, once detected in the ARC can induce feeding by stimulating AgRP/NPY neuronal activity. AgRP/NPY knockout mice do not increase food intake in response to ghrelin, indicating that the detection of this hormone by AgRP/NPY neurons is required for the orexigenic effects of ghrelin^{143,144}. ARC AgRP neurons sense ghrelin via its receptor (GHSR) and stimulate food intake¹⁴⁵. Importantly, ghrelin inhibits the POMC neurons indirectly via inhibitory GABAergic inputs from the activated AgRP/NPY neurons¹⁴⁶, this providing evidence for the AgRP-POMC complementary network.

3.3.2 Tanycytes; the non-neuronal cells in the ARC bridging the circulation with the hypothalamus

The term tanycyte, from Greek meaning elongated cell, was introduced in 1954 by Horstmann¹⁴⁷ to describe ependymoglial cells whose processes extended over large distances. This term is now used for specialized elongated ependymoglial cells in the adult brain and spinal cord. In adult mammals, tanycytes line the third ventricle (3V), the dorsal and ventral walls of the mesencephalic aqueduct, and the floor of the fourth ventricle (4V).



The most common classification of tanycytes is based on their anatomic location. Tanycytes lying in the upper part of the 3V comprises the α_1 subtype, then descending towards the ventral ARC we find the α_2 , followed by the β_1 , and finally, the β_2 tanycytes whose somata line the floor of the 3V (Fig. I-9). However, since the different tanycytic subtypes likely continuously overlap heterogenic subpopulations, the tanycyte subtypes likely form more than the classical four subgroups; therefore, specific markers need to be

Fig. I-9 Anatomical organization of tanycytes across the 3V. Tanycytes identified¹⁴⁸. The diverse functions of these cells range from neural stem cells to neuronal *lying in the upper part of the 3V comprises the α_1 subtype, then descending towards the ventral ARC we find the α_2 , followed by the β_1 , and finally,* ¹⁴⁹

the β_2 tanycytes whose somata line the floor of the 3V. modulators, including the transduction of metabolism-related cues. In the following sections, we will discuss some of these roles emphasizing their transport capabilities.

3.3.2.1 Tanycytes control the access of molecules from the periphery to the hypothalamus.

Once circulating molecules have leaked from the fenestrated blood vessels of the Median Eminence (Fig. I. 9 (1)), these can access the ARC parenchyma by passing the following checkpoints: A) the ME-cerebrospinal fluid (CSF) (Fig. I. 9 (2)), and then the CSF-ARC interphases (Fig. I. 9 (3)), and/or B) the ME-ARC interphase (Fig. I. 9 (4)).

Lining the ME-CSF and the CSF-ARC interphases, tanycyte somata contact CSF in the 3V, while their cilium with varying number of microvilli and large protrusions from their apical surface extend into the brain parenchyma contacting neurons, glial cells and vessels. Tanycyte somata lying here, on the 3V wall and floor, express barrier proteins restricting the paracellular passage of molecules, potentially forcing a specific passage *through* the tanycytes and not in between them.

Both tanycyte somata and processes express a great variety of receptors for circulating molecules, as well as endo/exocytotic membrane vesicles. Altogether, these structural specializations mirror the tanycyte capacities to exchange different molecules between the nuclei parenchyma and the CSF. Cumulative evidence indicates that tanycytes potentially sense specific CSF and bloodborne molecules, that then are transmitted to the ARC neurons^{99,150–152}.

On the other hand, the β_1 tanycytes that make up the BHB extend their tight-junction coated processes in between the ME and the ARC. This subgroup of tanycytes specifically express *Spr1a*, a protein that participates in the impermeabilization of the skin¹²⁹. Correlations using permeability assays have led to the hypothesis that β_1 tanycytes might mechanically regulate the transit of molecules from the ME towards the ventral ARC¹⁵³.

Pioneer studies showed that the first hypothalamic nucleus to detect leptin, an adipokine released from the fat depots, is the ARC¹⁵⁴, particularly by the tanycytes located in between the ME and ARC (β_1 and β_2 tanycytes). These cells increase phosphorylated STAT3 (pSTAT3) in their processes and cell bodies within the first two minutes after the leptin administration⁹⁹. It is proposed that once leptin is extravasated from the fenestrated capillary plexus, it is internalized by tanycytic end-feet in clathrin-coated vesicles, a process mediated by LepR binding and activation. Next, this hormone is transported through the tanycytes process and released from their somata into the 3V CSF through an extracellular signal-regulated kinase (ERK)-dependent signaling pathway⁹⁹. Congruently, this transport mechanism is altered in high-fat diet (HFD)-fed mice⁹⁹.

Very likely, other hormones or metabolites rely on tanycytic transport to get into the CSF and/or ARC. This could be a specific transport pathway depending on different receptor subtypes expressed by the tanycytes. Malfunction of this transport system could be part of pathologies as diabetes and metabolic syndrome. Indeed, Balland *et al*⁹⁹ showed that the deficiency in ERKdependent leptin transport through tanycytes is involved in the pathophysiology of central

leptin resistance in high-fat fed obese mice. Under these conditions, leptin fails to activate STAT3 signaling in tanycytes and remains stuck in the median eminence (ME). The restoration of ERK signaling in obese mice restores leptin release in the mediobasal hypothalamus and promotes loss of body weight when switched to a standard chow diet.

Collectively, it is logic to suggest that tanycytic transport systems can affect the responses of ARC neurons in basal physiological conditions. Since physiology is regulated in circadian fashion, we propose that this transport system is also fine-tuned according to the time of the day by the SCN. We will discuss this further in chapter 3. Problem Statement and Hypothesis

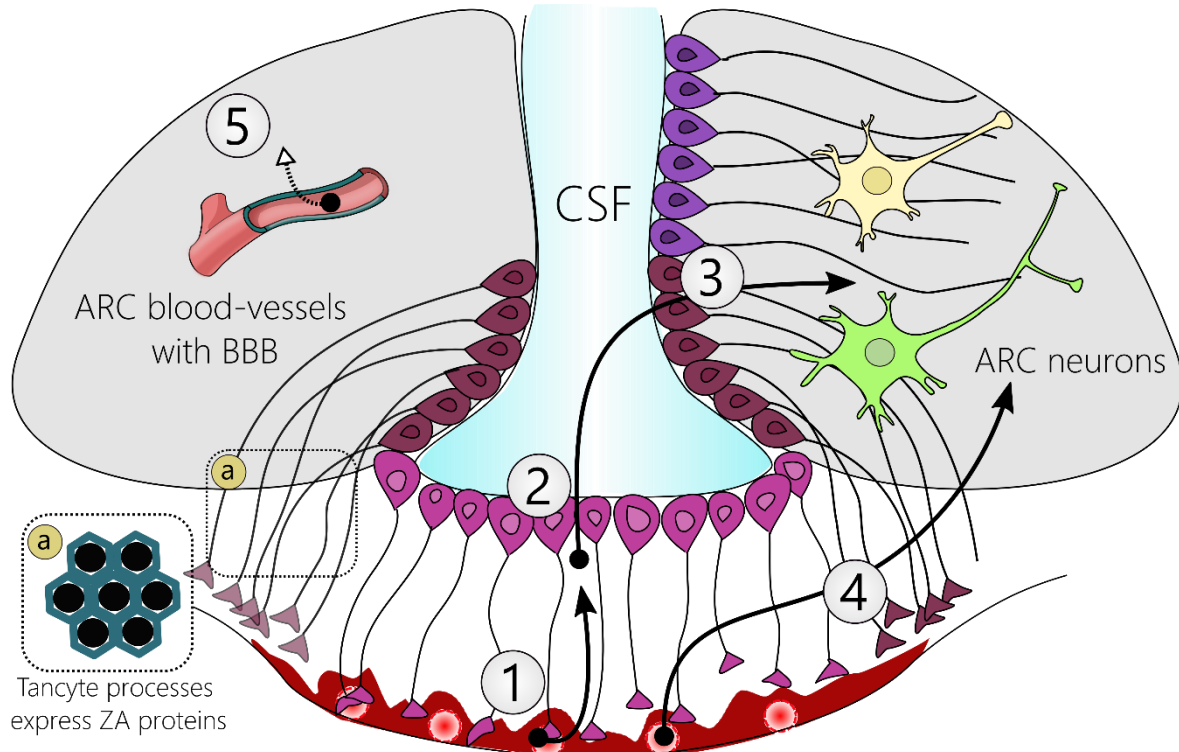


Fig. I-10 Tanycytes control the access of molecules from the periphery to the hypothalamus. Once circulating molecules have leaked from the fenestrated blood vessels of the Median Eminence (1), these can access the ARC parenchyma by passing the following checkpoints: A) the ME-cerebrospinal fluid (CSF) (2), and then the CSF-ARC interphases (3), and/or B) the ME-ARC interphase (4). Tanycytes at the ME-ARC interphase express key zonula adherens proteins that have promoted the hypothesis of these tanycytes forming a restrictive gate in between the ME and the ARC, putatively regulating the unspecific transit of molecules from the ME to the ARC and viceversa. The entrance of molecules through the vasculature of the ARC is tightly regulated by the functioning of the blood-brain barrier (BBB)

3.3.2.2 Other roles of tanycytes as metabolic regulators

The anatomical location of tanycytes, their variety of metabolic-related receptors, and the neurons structurally associated with them, promoted many hypotheses regarding their role in modulating peripheral metabolism. One of the first studies showing the relevance of tanycytes in metabolic regulation showed how ablation of the tanycyte layer following alloxan i.c.v. administration induced hyperphagia during refeeding after an overnight fasting¹⁵⁵. More recently, Yoo *et al* found that the conditional ablation of tanycytes through tamoxifen treatment induces hyperphagia in mice¹⁵⁶. Lacking tanycytes, visceral white fat accumulation occurs earlier than in

intact animals, before the appearance of hyperphagia, with no net change in energy expenditure¹⁵⁶.

Controversial results were obtained by research groups trying to elucidate the role of tanycytes in leptin signaling; for example, the ablation of tanycytes in the ARC and ME leads to increased susceptibility to obesity, yet does not alter the leptin sensitivity¹⁵⁶. Additionally, inactivation of leptin receptor expression in tanycytes did not result in an overt metabolic phenotype¹⁵⁷. Contrastingly, another research group reported that tanycytes are essential for the early internalization of leptin into the MBH being detected as soon as 2 minutes after i.p. labelled leptin injection⁹⁹. Next tanycyte-mediated leptin translocation to the MBH is essential for insulin-related pancreas functions and lipid metabolism¹⁵¹.

Tanycytes are also important transporters of lactate into the ARC parenchyma as the deletion of their monocarboxylate transporter 1 (MCT1), glucose transporter 2 (GLUT2), or glucokinase (GK) results in hyperphagia during refeeding^{158–160}. Although the mechanisms underlying these effects remain obscure, some evidence suggests these might be related with the modulation of NPY/AgRP and POMC/CART neurons by increasing or decreasing the neuropeptide gene expression^{152,155,158,159}, by regulating neuronal cell signaling^{99,161}, and/or by altering the neuronal membrane potential¹⁶².

Tanycytes secrete FGF21¹⁶³, and although the central effect of FGF21 is to increase energy expenditure¹⁶⁴, its specific deletion in tanycytes promotes lipid mobilization and browning of the white adipose tissue (WAT). Additionally, these mice exhibit increased energy expenditure during the active/dark phase via extensive fatty acid oxidation, as well as decreased fat accumulation; alongside with unchanged locomotor activity¹⁶³. The decrease in fat accumulation in this model did not depend on food intake, suggesting tanycytes can exert influence directly over the energy expenditure circuits.

Furthermore mice whose tanycytes miss the gene for fibroblast growth factor (FGF) 21, *Fgf21* displayed higher blood glucose levels after a glucose tolerance test (GTT)¹⁶³. β tanycytes express FGFR1 and FGFR2IIIc isoforms¹⁶⁷, allowing that plasma and cerebrospinal fluid-derived FGFs directly act on these cells¹⁶⁸. Interestingly, FGFs levels increase in the cerebrospinal fluid after a meal or after peripheral injection of glucose^{169,170} and central administration of FGF1 can lower circulating glucose and even induce diabetes remission in diabetic mice and rats independently of body weight loss¹⁷¹. Furthermore, central FGF1 administration induces robust c-Fos expression in tanycytes¹⁷², while antibody-mediated inhibition of FGFR1 also induces reversible weight loss due to a decrease in food intake and fat deposition and improved glucose control in mice, Siberian Hamsters, and monkeys^{173–175}.

More recently, Yoo and collaborators showed that, the ablation of ME and ARC tanycytes using tamoxifen injections in Rax-CreERT2 mice induces insulin insensitivity, suggesting that tanycytes may also modulate glucose by modifying insulin sensitivity¹⁶³. The underlying mechanisms remain largely unknown, but glucose could act via G protein-coupled receptors to directly trigger intracellular Ca²⁺ mobilization and transfer the signal to neighboring cells¹⁷⁶

Ground breaking studies showed that tanycytes are able to adapt the access of nutrients and hormones according to the organismal energetic conditions, with regulatory consequences^{99,177-179}. For example, during fasting, the tanycyte interface is reshaped resulting in the improvement of the access of peripheral molecules into the ARC¹⁸⁰. Importantly, these modifications were reversible upon the increase of peripheral glucose levels.

However, this study did not explain how the glucose into the ARC could be related with the glucose in periphery, but they showed that the changes in glycemia were somehow related to changes in the ARC glucose¹⁸¹.

3.4 Non-photic feedback to the SCN

Two kinds of inputs influence SCN neurons; photic input from the retina^{182,183}, and non-photic inputs from neurons from other parts of the brain¹⁸⁴. Commonly, these brain regions innervating the SCN sustain a bilateral communication with the clock neurons. One popular interpretation of the non-photic input to the SCN considers the logic that since the SCN does not express receptors for every peripheral molecule, this information should be provided by specialized structures. The whole concept resembles a “panopticum”, but in this case SCN is not sensing the periphery directly.

The current understanding is that the non-photic inputs to the SCN may serve to fine adapt the output of the SCN according to particular emergent conditions detected by these special brain regions, acutely. Popularly, the adaptation of the SCN output is termed as re-entrainment, however it is not completely known whether the oscillation of all the SCN neurons adapt in response to the acute situation, or just the neurons belonging to the circuit regulating that particular altered function.

Although the neuronal circuitry governing photoentrainment is well characterized^{183,184}, how non-photic information integrates with this system to create a comprehensive circadian response is poorly understood¹⁸⁵; nevertheless, there are some excellent examples we will discuss next.

3.4.1 Non-photic feedback from the ARC to the SCN

The arcuate nucleus (ARC), one of the main nuclei integrating metabolic information in realtime with other variables (reviewed in 2.3 Arcuate Nucleus of the hypothalamus, a hub for metabolic regulation.), is reciprocally interconnected with the SCN^{186,187}. Since the ARC can transmit metabolic information to the SCN^{96,97}, it was proposed as a critical provider of nonphotic entrainment to the master clock: the SCN¹⁸⁸. The ARC-SCN reciprocal communication has been reported by several research groups, including ours; however, the nature of the mutual projections is not entirely clear. Recently, there were reported kisspeptin expressing neurons in the ARC projecting to the SCN, with a determinant role synchronizing food intake, temperature and locomotor activity⁷⁶. Additionally, labelling studies have shown AgRP neurons from the

ARC sending projections to the SCN⁹⁷. In the opposite sense, the SCN projects back to the ARC via VIP⁹⁷, PK2⁹⁰.

Studies in rats showed that the neuronal communication between the SCN and the ARC is essential to express the circadian rhythm in corticosterone. This hormonal rhythm disappears when the SCN is mechanically disconnected from the ARC, even when the molecular clock in the SCN, assessed by *Per1* transcription gene remains rhythmical⁹⁷. We have hypothesized that this interdependency might be due to the need of the SCN to receive information about corticosterone concentration in the periphery to adjust the daily levels. Indeed, the ARC is the first place in the brain to detect this hormone, which is crucial for the negative feedback regulation of glucocorticoids¹⁰².

Besides corticosterone being a feedback signal to the SCN, this hormonal cue helps to robust rhythms in peripheral organs linked to the time of the day. Corticosterone in circulation (cortisol, in humans) peaks right before the activity period¹⁸⁹. The influence of this hormone extends over numerous peripheral tissues as glucocorticoids can modify the expression of 20% of the genome¹⁹⁰ thanks to the glucocorticoid responsive element (GRE) in their promoter sequence¹⁹¹. A transcriptome study found that 100 out of 169 cycling genes in the liver lost rhythmicity upon adrenalectomy¹⁹², while experiments *in vitro* showed how the administration of corticosterone or dexamethasone at key time points synchronize clock gene cycling in cultured rat fibroblasts¹⁹³; additionally, *in vivo* tests showed that corticosterone can entrain liver, kidney, and heart¹⁹⁴. Finally, in mice exposed to changing light schedules, glucocorticoid disruption accelerated the behavioral entrainment and realignment of peripheral clock gene cycling¹⁹⁵. However, in spite of the profound influence of glucocorticoids over several tissues, these are not required for the global clock gene cycling¹⁹².

Additional to the effect on corticosterone secretion, the mechanical disconnection of the ARC-SCN circuit also ablates the locomotor rhythm in constant darkness⁹⁷, implying that the feedback from the ARC is necessary for the SCN to implement the daily locomotor activity, too.

Lesion studies, first suggested that ARC could be involved in the rhythm of feeding^{196–199}. Later, it was shown in mice that ablating leptin-responsive neurons in the ARC using an injection of saporin toxin bound to leptin, flattened the food intake rhythm in L/D conditions, while animals kept in constant darkness completely lost this rhythm²⁰⁰. Importantly, the same injection of saporin toxin but in the ventromedial hypothalamus (VMH), which also has leptin-responsive neurons, showed no effects on food intake, revealing the specificity of this regulatory mechanism²⁰⁰.

In rats, their core body temperature is low during the day and high during the night and these changes are dependent on the SCN²⁰¹. Interrupting the SCN-ARC communication eliminates this rhythm in animals under constant darkness⁹⁷, again suggesting that SCN-ARC direct communication is essential for maintaining this rhythm.

3.5 Other sources of non-photoc feedback to the SCN

3.5.1 Circumventricular organs

For open thermodynamic systems like living beings, real time monitoring of the inner conditions is essential to keep the organism alive. The central nervous system receives diverse inputs from afferent neurons, circulating hormones, and absorbed nutrients, to then integrate this information resulting in key outputs that maintain systemic metabolic homeostasis⁹⁸. The brain being a massive integrator must have access to the periphery it controls, as direct as possible but without sacrificing other aspects of this delicate tissue. Since the functioning of the brain is based on a very exquisite balance of ions and other signaling molecules, the brain milieu must be as stable as possible, avoiding dramatic perturbations when eating, exercising or fasting, for example. Coincidentally, the brain vasculature is characterized by the presence of the blood-brain barrier (BBB), a very selective physical-chemical entity separating the circulating blood from the brain parenchyma.

As a massive controller, how does the SCN get to know the values of the variables it controls in real time? Besides the sensory branches of the Autonomic Nervous System (ANS) that can provide feedback signals to regulatory areas, there are some special brain regions lacking BBB. These BBB-less regions have privileged access to nutrients in circulation, metabolites, and hormones, released by peripheral organs such as the liver, adipose tissue, pancreas and the gastrointestinal tract, for instance. These nuclei are called Circumventricular Organs (CVOs).

The neurons and other cell types in the CVOs have access to the composition of the circulating blood and the cerebrospinal fluid (CSF), congruently, these regions express receptors and ion channels for specific circulatory molecules/minerals. Importantly, the SCN receives direct input from the CVOs, consequently these nuclei are hypothesized as real-time feedback providers of the SCN.

A couple of great examples of CVOs interacting with the SCN are the Organum Vasculosum of the Laminae Terminalis (OVLT), and the anatomic complex of the Arcuate Nucleus-Median eminence (ARC-ME). The OVLT controls water intake and mineral balance in mammals, both being circadian variables. Recently, it was shown that the SCN^{AVP} neurons receive a direct activator input from sodium-sensing OVLT neurons expressing glutamic acid decarboxylase (OVLT^{GAD})⁷⁸.

3.5.1.1 Hormonal feedback: melatonin

The SCN controls the synthesis of melatonin through a tonic inhibition of noradrenergic stimulation of the pineal gland during the light period. This hormone, sustains an evident link between external light and internal physiological cycles, and interestingly, since 1980's it has already been known that melatonin can influence circadian rhythms¹⁹⁶. The melatonin feedback signal is received through melatonin receptors M1 and M2 highly expressed in the SCN²⁰⁴. For example, MT2 receptor was shown to mediate the phase-shifting of the SCN neuronal firing²⁰⁵,

while *in vitro* experiments showed that melatonin can regulate the phase and amplitude of the electric circadian activity of SCN explants^{206,207}. Additionally, in rats kept in constant dark and in blind humans, melatonin entrained free-running rhythms^{208–211}.

Importantly, melatonin as an SCN feedback signal has certain limitations. For instance, *in vivo* experiments showed that mice physiology kept rhythmic under stable light-dark conditions even when melatonin signaling was disrupted. However, as expected, the entrainment of these mice to new light schedules showed impaired²¹². Also, human studies showed how in shift workers and blind people, excess or absent light, respectively, disturbs melatonin rhythms, with variable desynchronization of the sleep/wake pattern, core body temperature and cortisol^{213,214}. Patients with disordered sleep, for example, are prescribed with 0.5-10mg of melatonin in the late afternoon to induce sleep and phase advance the clock²¹⁵; the same clinical application benefits subjects experiencing acute phase-shifts due to jet-lag. Thus, although melatonin might not be essential for the generation of circadian rhythms, it helps to entrain the whole-body physiological rhythms.

3.6 Disruption of circadian physiology as a risk factor for metabolic diseases

The SCN works inside a larger neuronal network of tightly linked oscillatory feedback circuits whose integrity is crucial to keep physiology and behavior synchronized. The uncoupling of these oscillators by modified photoperiods (constant light, L/L) or disrupted sleep/wake cycles, such as in shift work, social jetlag, late-night food intake, or chronic jetlag; have disruptive effects on metabolic/mental balance, impacting the quality of life directly. The installation of these modern society-derived behavioral modifications contributes to metabolic disturbances, including type 2 diabetes (T2D)^{216–218}.

For instance, rats kept under constant light L/L display profound disruption in the pancreatic islet clock function characterized by the impairment in the amplitude and the phase islet clock oscillations, while rats forced to be active during their rest period develop metabolic syndrome symptoms such as the impairment of the glucose homeostasis, a central feature in T2D²¹⁹.

The incidence of T2D has tripled during the last two decades, reaching pandemic proportions²²⁰. In order to improve our preventive recommendations to avoid T2D, and to enhance the treatment of existing patients it is crucial to understand all the mechanisms regulating glycemia homeostasis, including the understanding of the cyclicity in glycemia through the circadian cycle.

4 Problem Statement and Hypothesis

The circadian system headed by the SCN establishes different set-points for hormones and circulating metabolites, according to 1) the time of the day, and 2) to emergent conditions such as the season, reproductive state, fasting, sickness, or stress⁶⁶. We, as others, hypothesize that

this subtle variation of set-points might result from a daily modulation of the sensitivity of key sensory structures⁶⁷.

As reviewed before, the SCN largely depends on diverse non-photic feedback signals to express certain rhythms. In the particular case of glucose homeostasis, the relevance of the interaction with the ARC is special. The ARC houses first-order neurons, whose depolarization/hyperpolarization depends on glucose concentration in the ARC milieu; also, the neurons in this nucleus possess anatomical pathways to influence key peripheral organs such as the liver and pancreas. However, ARC tanycytes, but not neurons, are in direct contact with the content of the cerebrospinal fluid, and are ideally positioned to transport the glucose into the ARC.

Taken together, we hypothesized that these non-neuronal cells might be under SCN circadian control, and by gating the transport capabilities of tanycytes, the SCN might modulate glucose entry into the ARC parenchyma. Furthermore, by controlling the glucose access into the ARC, the SCN could fine-tune glucose-responsive neurons output according to the time of the day.

5 General Objective

Determine whether the SCN sets the circadian values of glycemia via the modification of glucose penetration into the ARC, and if so elucidate the mechanism.

5.1 Particular objectives

1. Evaluate if the penetration of circulating molecules into the ARC parenchyma changes across the L/D cycle, via the use of Evans Blue
 - a. If so, determine the time points of higher and lower penetration into the ARC
2. Evaluate if the ME-ARC, the CSF-ARC barriers are submissive to circadian regulation
 - a. If so, determine which barrier molecules change during these different states
3. Determine whether the SCN influences the penetration of peripheral molecules to the ARC parenchyma
 - a. If so, determine if the SCN facilitates or restricts the access of circulatory molecules to the ARC
 - b. Identify the neurotransmitter(s) mediating this influence
4. Determine whether the penetrability of glucose to the ARC parenchyma differs at the acrophase and bathiphase of the glycemia rhythm
 - a. If so, modify amount of glucose that penetrates into the ARC, and measure the consequences in the circulating glycemia

6 Methodology

6.1 Experimental model and subject details

Young adult male Wistar rats weighing 250–350 g (P50-P65) were used in this study. The animals were obtained from the Animal facility of the Faculty of Medicine, UNAM, and from the Animal Facility of the

Instituto de Investigaciones Biomédicas, UNAM. Once the rats arrived, they were allocated in our local bioterium and were allowed to adapt to the new conditions before any surgical procedure were done. During the adaptation period, the rats were kept in groups of 4–6 under a 12-h light/dark cycle (lights on at 7 A.M. or Zeitgeber time (ZT) 0), at room temperature of 22–25°C. Commercial rodent chow (Tekland Global Diets 18% protein 2018C) and tap water were available to all animals. Rats were randomly assigned to different time points for the experiments. Care was taken to reduce the stress and discomfort of the animals as well as to optimize and minimize the number of animals used. Experiments were performed following the regulations of the Universidad Nacional Autónoma de México and Instituto de Investigaciones Biomédicas (project 245), according to Mexican norms for animal handling (Norma Oficial Mexicana, NOM-062-ZOO-1999) and the law for animal protection published by the University Animal Care Committee in Mexico City, Mex. (February 2002).

6.2 Experimental protocols

6.2.1 Intrajugular cannulation

Were performed under anesthesia via i.p. injection of Ketamine (Anesket, PiSA, Mexico, 50 mg/kg) and Xylazine (Procin, PiSA, Mexico, 8mg/kg). A silicon cannula (0.025in internal diameter, 0.047in external diameter, 11 cm long, Intech, USA) was implanted in the right branch of the internal jugular vein, introduced 3cm towards the heart; the rest of the cannula was exteriorized subcutaneously through the shoulder girdle and filled with a mix of Glycerol (60%J. T. Baker, USA), Heparin (PiSA, USA, 20%), sterile saline solution 0.9% (10%), and antibiotic (Amphotericin B, Penicillin, Streptomycin; GIBCO, USA, 10%), to maintain the cannula accessible.

The rats were allowed to recover for 10-12 days in individual cages while monitored and handled daily. After the recovery period, the animals wore a hand-made vest for 2 days before the experiment in order to help joining the cannula to a long tube 12h prior to the experiment. The long tube was interiorized in a spring connected to a swivel, ensuring free movement of the animals. Animals that did not recovered well or that lost more than 20% of their weight during the recovery period were discarded.

6.2.2 SCN lesioning

Bilateral or unilateral electrolytic SCN lesions were performed stereotaxically under i.p. anesthesia (as above), using a standard Kopf stereotaxic apparatus. Coordinates were adapted from the atlas of Paxinos and Watson (0.2 mm posterior and 8.4 mm ventral from the surface of the brain; for the lateral coordinate sinus was used as reference, putting the electrode 0.2 mm away from the border of the vein). After the surgery, all animals had free access to water, food and were monitored and handled daily. Experiments were done after a recovery period of 12-15 days. The entirety of the SCN-lesion was verified by a postmortem analysis of vasoactive intestinal peptide VIP immunostaining. Only animals lacking VIP immunoreactivity in the SCN were used for further analysis.

6.2.3 ICV cannula

Wistar male rats weighting 250g were anesthetized using i.p. injections of ketamine 100 mg/mL (0.18 mL/kg im; Anesket, PiSA Agropecuaria, S.A. de C.V.) and xylazine 20 mg/mL (0.1 mL/kg i.p.; Procin, PiSA Agropecuaria, S.A. de C.V.). A stainless-steel guide cannula was stereotaxically implanted into the third ventricle (coordinates: -0.7mm anterior from bregma, -0.18mmlateral from midline, and -2.8 mm below brain surface; tooth bar set at -3.5 mm).

6.2.4 Fasting

Wistar male rats (300–350 g) were subjected to 72 hours fasting with ad libitum-fed access to tap water (ZT11 n=3, ZT22 n=3). The fasting period started at the same ZT time the animals were sacrificed later. The animals of each group were housed in the same cage.

6.2.5 Permeability assays

For EB permeability assay, rats were sacrificed at ZT2 (n=5), ZT6 (n=5), ZT11 (n=5), ZT14 (n=3), and ZT22 (n=6). Vital dye Evans blue (Cat. Number E2129, Sigma-Aldrich, USA) was diluted 5% in saline solution. Evans blue was administered in a dose of 50mg/kg i.v. through the cannula and circulated for 5 min before administration of a lethal dose of pentobarbital i.v. (100 mg/kg; Pisabental, Pisa Agropecuaria). Animals were immediately perfused intracardially with 200mL of 0.1M pH 7.2 phosphate buffered paraformaldehyde (PFA) 4% (rate 20mL/min). Then the brains were extracted and post-fixed in PFA for 24 h and subsequently changed to 30% sucrose with 0.02% sodium azide in 0.1 M PBS for cryoprotection until cut. Brains from different time points were processed in a similar time post-sucrose to avoid differences in EB wash. Coronal sections were cut at 30mm, at -28°C using a cryostat (Lupetec, Brazil) and collected on gelatinized slides for analysis with confocal microscopy (Nikon A1R+ laser scanning confocal, scanning head coupled to an Eclipse Ti-E inverted microscope, Nikon Corporation; Tokyo, Japan). Samples were imaged using a CFI Plan Fluor 10X N.A. 0.3 objective and the signal was amplified and digitized through both standard and gallium arsenide phosphide (GaAsP) detectors. All images were acquired with the same resolution and pinhole size.

Analysis of EB penetration was limited to medial area of the ARC using morphological criteria.

Microphotographs from different time points (8-10 micrographs) were analyzed using ImageJ v 2.0.0, 2018.66 To determine EB entrance into the ARC, a section of 100mm x 550mm, 45° inclination was taken from the acquired image per each side of the ARC, and a histogram of the grey value per mm was generated; the 0 mm was always positioned at the ventricular wall. Values of 8-10 pictures per animal were averaged (See Figure 1B).

The quantification in SCN_x animals followed the same procedure. To evaluate the impact of the unilateral SCN lesion, we calculated the ratio between the intensity of EB signal in the ARC at the lesioned (Ls) and non-lesioned side (NonLs) in the same animals (Ls vs NonLs).

The signal in the SCN_{xx} images was measured in both sides of the ARC and compared with animals with misplaced lesions near to the SCN. To evaluate the impact of the bilateral SCN lesion, we calculated the ratio of the EB intensity in the ARC in an SCN_{xx} animals and animals receiving lesions outside the SCN. To quantify EB penetration in other CVOs, a region of interest (ROI) of fixed size was positioned right in the middle of the structure (SFO 300x300mm, OVLT 100x300mm, AP 450x450mm, ME 100x50mm) and the Integrated Density of Fluorescence was averaged (3-5 pictures per structure, per rat).

Blood and liver samples were obtained before the PFA started to perfuse the animal and used for EB measurement to determine circadian changes in circulating EB or tissue uptake.

6.2.6 2-NBDGlucose penetration assays

For the 2-NBDGlucose (2-deoxy-2-[(7-nitro-2,1,3-benzoxadiazol-4-yl) amino]-D-glucose) penetration assays (2 assays), rats bearing a jugular cannula (described above) were sacrificed at ZT11 (n=4) and ZT22 (n=3). 2NBDG (Cat. Number 14325, Cayman, USA) was diluted in 0.9% saline solution. A dose of

0.83mg/kg was administered i.v. through the cannula and circulated 5 minutes before administration of a lethal dose of pentobarbital i.v. (100 mg/kg; Pisabental, Pisa Agropecuaria). Animals were decapitated, brains were extracted and immediately frozen on dry ice. Coronal sections were cut at 30mm, at -20_C using a cryostat (Lupetec, Brazil) and collected on gelatinized slides. Confocal microphotographs were acquired using Nikon A1R+ laser scanning confocal (same as above). Images from all groups were obtained using the same pinhole size, brightness, and contrast setting. Microphotographs from different time points (5-10 micrographs) were analyzed using ImageJ v 2.0.0, 2018. To determine the penetration into the ARC we used the same ROI and protocol as with the EB.

The measurement of the 2-NBDGlucose penetration in the control areas (hippocampus and SFO) was done by placing a region of interest (ROI) of fixed size right in the middle of the structure.

6.2.7 Intracerebroventricular injections

Resveratrol was injected i.c.v. via a cannula placed 10-15 days before the injection. At the day of the experiment; a dose of 0.5mg/kg (0.15mg/ 2uL) (n=4 and n=3 for ZT22 and ZT11 respectively) was injected using a needle adapted to a Hamilton syringe. Glucose levels were measured immediately before and 5, 10, 30 and 40 minutes after the i.c.v. injection using a hand-held glucometer (Accu- Check Active). Rats were decapitated; brains dissected and cut to determine the placement of the cannula. The vasopressin antagonist was administered at a dose of 200ng/per animal in a final volume of 2uL, n=8 and n=3 for ZT22 and ZT11 respectively. Vehicles ZT22 n=6 and ZT11 n=3.

6.2.8 Immunohistochemistry and data analysis

Unless differently specified, all the brains for the immunostainings were extracted from perfused rats with 4% PFA, then post-fixed in PFA for 24 h and subsequently immersed in 30% sucrose with 0.02% sodium azide in 0.1 M PBS for cryoprotection until cut. The brains were differently marked using a needle to incubate the tissue from both time points in the same well in order to avoid the differences associated with the immunostaining procedure.

To analyze the ME-ARC barrier, 30mm coronal sections from the same brains used for permeability assays were incubated free-floating with anti-vimentin antibody overnight at 4°C (ZT11 n=10; ZT22 n=9). After 3 washes of 5min each with PBS, sections were incubated 2h at RT with the secondary antibody. Sections were collected on gelatinized slides, dried and incubated with DAPI for 10min. Then the sections were immersed in Vectashield mounting medium. Images were acquired using confocal microscope equipped with a CFI Plan Fluor 20X N.A. 0.3 objective. For the analysis of tanycytes length, Z-projections of 20 mm were obtained (n=3 per animal) (40X). For the analysis of ME-ARC barrier intensity, and ME intensity of the signal 5-10 micrographs were taken per animal. For the staining of ZO1, rats were deeply anesthetized with pentobarbital (100 mg/kg; Pisabental, Pisa Agropecuaria) and subsequently decapitated. The brains were then quickly extracted, placed on a dry ice bed, and cut immediately (n=3 per group). Coronal sections of 20um were collected on gelatinized slides. Immediately after cutting the fresh tissue, the sections were fixed for 1 min in cold methanol (-20_C) and dried at RT.

Sections were incubated for 2 hours with anti-ZO-1 in a humid chamber, washed and incubated with secondary antibodies one hour at RT. Finally, sections were incubated in DAPI solution and mounted.

Confocal microscopy was used to acquire pictures as a z-stack performed at 40x to quantify ZO-1 immunofluorescence. To analyze beta-catenin in the ME thirty mm coronal sections were placed in antigen retrieval solution (EDTA 0.1M, pH 8) at 80°C for 20 minutes, then washed. Since the antibodies against

Vimentin and beta-catenin were produced into different animal species (antivimentin produced in mice, anti-beta catenin in rabbit), and no overlapping staining could be detected, we then incubated the brain sections in a cocktail of anti-beta catenin and vimentin antibodies overnight (ZT11 n=6; ZT22 n=6). After washes, sections were incubated in secondary antibody for 2h at RT. Sections were collected on gelatinized slides, incubated with DAPI during 10 min, and then covered. Microphotographs were obtaining at 20x magnification (n=5-10 micrographs per animal). All the analyses were performed used the software ImageJ v 2.0.0, 2018.

6.2.9 Immunofluorescence protocol and image analysis for GLUT1/Vimentin/CD31

The combination of GLUT1/Vimentin/ CD31 allowed us to evaluate the distribution and immunoreactivity GLUT1 glucose in tanycytes and microvessels. ZT11 or ZT22 brain slices from intact (n=6 per group) animals or SCN lesioned (n=3) followed the same procedure described for vimentin staining. Sections were incubated overnight at 4°C with a cocktail containing anti-GLUT1; anti Vimentin and anti-CD31/PECAM in a blocking solution under slight shaking. Microphotographs were obtained at 20x magnification (n=5-10 micrographs per animal). We used morphological criteria to quantify the fluorescence of the staining in the tanycyte somas or in the projections to the ARC, as well as to identify the localization of a and b beta tanycytes. The immunoreactivity of GLUT1 was measured in the CD31+ areas (microvessels length lesser than 10mm), or in tanycytes determined by Vimentin (tanycyte soma or projections).

6.2.10 Aurothioglucose staining

Wistar male rats weighting 350-300 received 0.37 mg/uL aurothioglucose ($C_6H_{11}AuO_5S$) dissolved in sterile PBS through an intrajugular cannula (same process as described above). The aurothioglucose circulated 20 min and the animal was sacrificed and perfused with saline (0.9%) / paraformaldehyde (4%). The brains were removed and placed in 4% paraformaldehyde overnight and then transferred to sucrose (30%). The brain was sectioned using a cryostat at 30um, -25°C; the sections were collected in PBS and mounted on gelatinized slides, exposed to UV light for 2h, and then rinsed 5 times with deionized water. Aurothioglucose particles were visualized using a protocol adapted from Hacker's et al., technique (ref 67). To reveal the particles, we prepared three different solutions. 1) Solution A: we dissolved 100 mg silver acetate ($AgC_2H_3O_2$) in 50 mL of deionized water 2) Citrate buffer solution (pH 3.8): 25.5g citric acid ($C_6H_8O_7.H_2O$) and 23.5 g trisodium citrate ($C_6H_5Na_3O_7.2H_2O$) were dissolved in distilled water to make 100 ml. The pH was adjusted to 3.8 using citric acid ($C_6H_8O_7$). 3) Solution B: 125 mg of Hydroquinone ($C_6H_6O_2$) were dissolved in 25 ml of Citrate Buffer.

In order to amplify the signal of the aurothioglucose we mixed 25 ml of solution A with 25 ml of solution B. The tissue was incubated in this solution at 26°C for 70 min, then the slides were transferred to a 5% sodium thiosulfate ($Na_2S_2O_3$) solution and incubated them for 10 min. Finally, we removed the thiosulfate, washed the slides with deionized water for 20 min and cover the slides. Slices processed from rats without aurothioglucose administration did not display the signal observed in the Figure S3F.

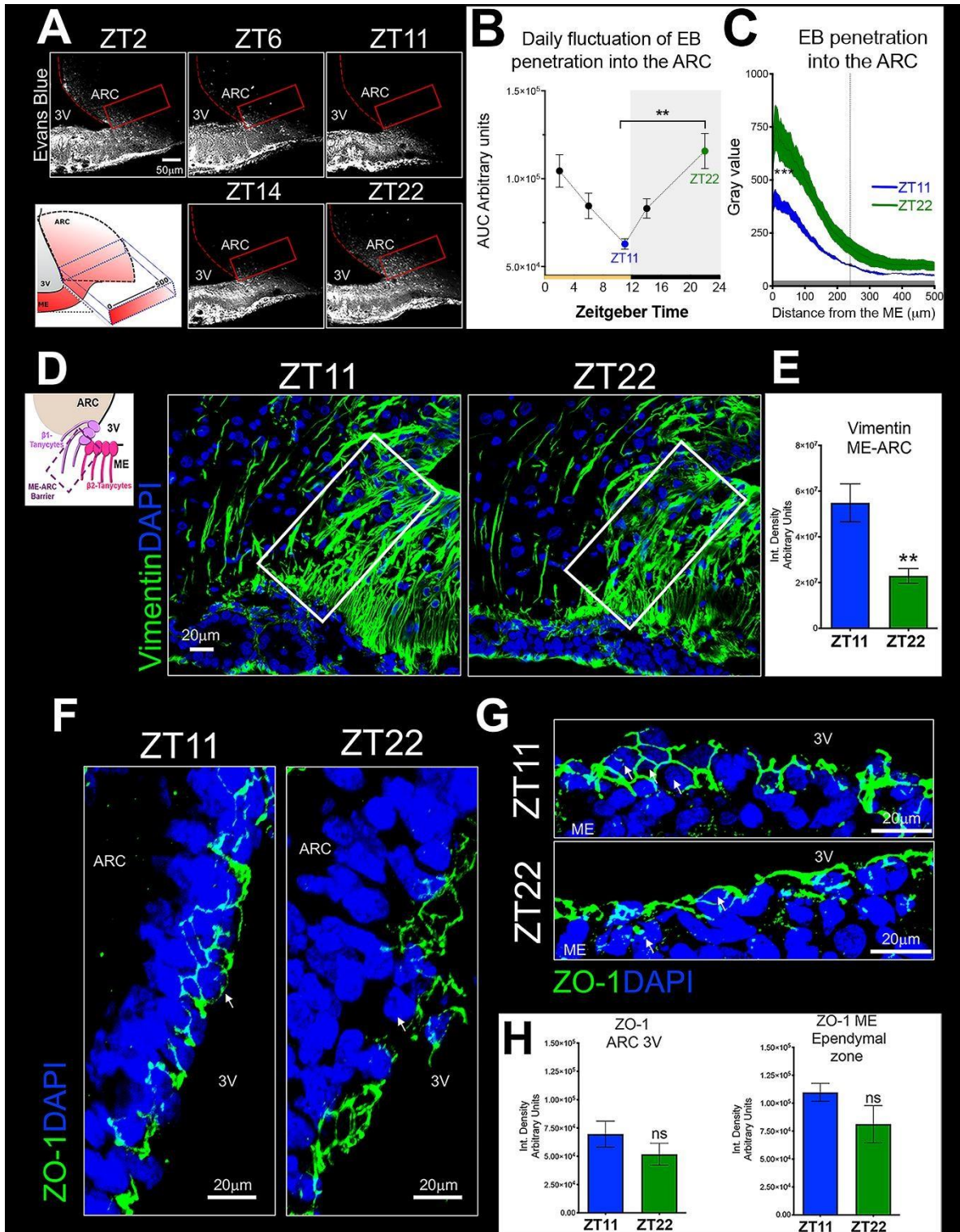
6.3 Quantification and statistical analysis

Animals were randomly assigned to experimental protocols as well as time points. The analysis of the collected data was a blind process. Data from no animals were excluded from the present study. The statistical analysis was performed using GraphPad Prism Software v9. All data were normally distributed and reported as the mean +/- standard error of the mean (SEM). The statistical details of each experiment can be found embedded in the results section and in the figure legends, including the type of statistical test used and the exact value of n, where n represents the number of individual animals employed in each experiment. Differences between groups were considered significant at a p-value <0.05.

7 Results

7.1.1 The entry of circulating molecules into the ARC fluctuates daily

We first investigated whether the access of blood-borne molecules into the ARC fluctuated through the LD cycle. We administered the vital dye Evans Blue (EB, MW=960.81Da or ~70kDa when bound to albumin) at ZT2_(n=5), ZT6_(n=5), ZT11_(n=5), ZT14_(n=3) and ZT22_(n=5) to adult Wistar rats under stress-free conditions through a remote jugular vein cannula. Throughout the LD cycle, EB penetration into the ARC parenchyma was the highest at ZT22, while ZT11 exhibited the lowest levels compared to other time points (One-way ANOVA $F_{(4, 19)}=6.811$, post hoc Tukey's test ZT22 vs. ZT11 $p=0.0012$) (**Figure 1A, 1B**). Multiple comparison analyses also revealed differences between ZT11 and ZT2 (Tukey's test $p=0.0078$) but not between other time points (Figure 1B). Linear regression showed higher intensity of EB in the first microns into the ARC at ZT22 compared to ZT11 (Y-intercept gray value ZT11_(n=5)=324.1 vs ZT22_(n=5)=601.7). It remained significantly higher until 220 microns indicating that EB penetrated the ARC parenchyma deeper at ZT22 than at ZT11 (Figure 1C) (Slopes analysis: Mann Whitney test, $p=0.0079$).



▲ Figure 1 Entrance of Evans Blue into the arcuate nucleus varies with the day/night cycle.

(A) Representative microphotographs (10 \times) showing entrance of Evans blue (EB, white) into the ARC throughout the day-night cycle. Cartoon depicting quantification method, red rectangle indicates the area where EB penetration was measured. Note the EB signal in the rectangle is higher at ZT22 than observed at ZT11. (B) Histogram illustrates EB penetration at ZT11 and ZT22 into the ARC (500 microns). Significant differences between ZT11 (n=5) and ZT22 (n=5) are observed from the starting point of measurement (0) until 220 microns. Two-way ANOVA, post-hoc Unpaired Student's t test. * $p < 0.05$, ** $p < 0.01$. Data are shown as the mean \pm SEM. (C) Graph shows the area under the curve for the histograms quantifying penetration of EB into the ARC at ZT2 (n=5), ZT6 (n=5), ZT11 (n=5), ZT14 (n=3) and ZT22 (n=5). Note the peak of EB penetration is at ZT22 while ZT11 shows the lowest levels. One-way ANOVA, $F(4, 19) = 6.811$. One-way ANOVA, post-hoc Tukey's test. ** $p < 0.01$. Data are shown as the mean \pm SEM. (D) Z-projections of confocal imaging reconstructions of ZT11 and ZT22 (40 \times), showing immunoreactivity of Vimentin (green) in tanyctytic processes located in the median eminence (ME)-ARC barrier. The cartoon illustrates the quantified region of vimentin immunoreactivity in the ME-ARC barrier at ZT11 (n=10) and ZT22 (n=9). Note that vimentin immunoreactivity is lower at ZT22 than at ZT11 in ME-ARC zone. (E) Integrated density measurements of Vimentin immunoreactivity in the quantified region. Mann Whitney U=9, ** $p = 0.0021$, two-tailed. Graph shows individual data and the mean \pm SEM. (F) Z-projections microphotographs of ZO-1 protein immunostaining (green) in the somas of $\alpha 2$ and $\beta 1$ tanyctes lining the 3V in the ARC-CSF interface, and (G) on the floor of the 3V (ME), at the level of $\beta 2$ tanyctes. Microphotographs reveal changes in ZO-1 distribution in ZT22. (H) Integrated density of ZO-1 in the 3V-ARC and (I) in the Ependymal zone of the ME ZT11 (n=3) and ZT22 (n=3). Unpaired Student's t test. Graph shows the individual data and the mean \pm SEM. See also Figure S1.

We evaluated EB extravasation into other circumventricular organs (CVOs); permeability in the *organum vasculosum of the laminae terminalis* (OVLT) was also lower at ZT11_(n=4) than at ZT22_(n=5) (Unpaired t-test $t = 2.813$, $df = 7$, $p = 0.0261$). EB penetration into the subformal organ (SFO) and Area Postrema (AP) did not show time-related differences (Figure S1A).

For the scope of this work, we focused on ARC's variations with the lowest levels at ZT11 and peaking at ZT22. To investigate whether the permeability differences were circadian driven or due to light input, we assessed permeability to EB in constant darkness at CT 2 and CT11. Also, under these circadian conditions, similar EB permeability differences were observed CT11_(n=6) and CT2_(n=10) (Unpaired Student's t-test, $t = 2.385$, $df = 14$, $p = 0.0317$).

7.1.2 Structural changes in ME-ARC and CSF-ARC barriers correlate with permeability states.

Time-dependent differences in EB penetration into ARC parenchyma can be due to a) variations in its extravasation into the ME, b) differences in EB uptake by peripheral organs leading to differences in circulating EB, c) changes in the blood-brain barrier (BBB) of the ARC blood vessels, d) changes in permeability of the ME-ARC barrier, or due to e) changes in ME-CSF and CSF-ARC interphases.

We did not find differences in EB penetration into the ME (One-way ANOVA, $F_{(4, 13)} = 0.9045$, $p = 0.8503$) (Figure S1B), nor in the number of fenestrated vessels as demonstrated by panendothelial Cell Antigen (MECA-32) at ZT2_(n=5), ZT11_(n=4), ZT19_(n=5) (Kruskal-Wallis test $p = 0.3022$, post-hoc Dunn's multiple comparisons test $p = 0.3917$). Collectively, the absence of differences in these parameters discards changes in ME extravasation.

Neither EB uptake by the liver nor dye content in the blood were different at ZT11_(n=3) and ZT22_(n=3) (Unpaired Student's t-test. For blood $t = 0.6631$, $df = 4$, $p = 0.5435$. For liver $t = 0.5293$,

df=4 $p=0.6246$) (Figure S1C), indicating that a local mechanism promotes these daily changes in the ARC rather than a difference in circulating EB.

Next, we evaluated the robustness of the ARC BBB at ZT11 and ZT22 through the distribution of Zonula Occludens protein 1 (ZO-1), one of the most explicit markers of barrier integrity^{221,222}. We did not observe changes in the length of ZO-1 immunoreactivity along the microvessels of the ARC's BBB capillaries, nor in the total intensity of ZO-1 in the ARC between ZT11_(n=3) and ZT22_(n=3) (Unpaired Student's t-test, length $p=0.9952$, integrative intensity $p=0.9319$) (Figure S1D-E), making the BBB an unlikely contributor to the variations in EB penetration into the ARC.

The access of blood-borne molecules into the ARC can be influenced at two additional levels. First, β_1 tanycytes extending their tight-junction coated processes between the ME and the ARC can limit the transport into the ARC^{129,223}. Second, the tanycytes lining the ventricular wall, expressing barrier proteins, may restrict paracellular passage of molecules from the CSF into the ARC^{99,178}.

Tanycytes forming ME-ARC and CSF-ARC barriers are subdivided into α_1 , α_2 , β_1 or β_2 depending on their location²²³ and undergo structural plasticity via cytoskeleton modulation²²⁴⁻²²⁶. Vimentin, an intermediary-filament protein, the major structural cytoskeleton element in tanycytes, has been implicated in permeability functions in other tissues^{227,228}. To study this significant component of the ME-ARC barrier, we assessed the organization of tanycytes at time points corresponding to maximal (ZT22) and minimal (ZT11) EB penetration. Examination of vimentin immunoreactivity revealed a higher density of β_1 -tanycyte processes in the ME-ARC transition area at ZT11_(n=10) than at ZT22_(n=9) (Mann Whitney U=9, $p=0.0021$, two-tailed) (Figure 1D-1E). Similarly, Z-projection reconstructions showed that, while the processes of β_1 -tanycytes extend into the ventral part of the ARC at ZT11_(n=4), they appear to be shorter at ZT22_(n=4) (Unpaired Student's t-test $t=3.005$ df=6, $p=0.0032$) (Figure S1G).

No differences in the pattern or intensity of Vimentin in the ependymal layer nor the internal zone of the ME were observed. However, the end-feet of β_2 tanycytes surrounding the blood vessels in the external zone of the ME were more abundant at ZT11_(n=6) than at ZT22_(n=5) (Unpaired Student's t-test $t=2.386$ df=9, $p=0.0408$) (Figure S1H-L).

Next, we examined the organization of the CSF-ARC barrier. We observed a continuous honeycomb pattern of ZO-1 highlighting somata of α_2 and β_1 tanycytes lining the third ventricle (3V) at ZT11 while exhibiting a diffuse pattern at ZT22 (Figure 1F, white arrows). Moreover, while ZO-1 staining delineated the somas of the ME β_2 tanycytes at ZT11, it appeared interrupted at ZT22 (Figure 1F-G, white arrows), with no significant difference in total ZO-1 intensity (Figure 1H-I). This organizational pattern of ZO-1 protein suggests that tanycytes lining the ventricular walls create a tighter barrier at ZT11, preventing paracellular diffusion from the ME to the CSF and preventing it into the ARC parenchyma. In contrast, the discontinuous arrangement of the ventricular ZO-1 at ZT22 suggests more penetrable ventricular walls.

In addition to ZO-1, we evaluated β -catenin, a key structural component of adherent junctions crucial for forming and maintaining tight-junctions^{153,229}. We found higher immunoreactivity of this protein at ZT11_(n=6) compared to ZT22_(n=6) in the transition zone between the ME and ARC (Mann Whitney test, Mann Whitney U=9, $p=0.0043$, two-tailed), as well as in the projections into the ARC (Unpaired t-test $t=3.824$ $df=10$, $p=0.0033$) (Figure S1M-Q).

The tighter organization of the ME-ARC barrier and the CSF-ARC interphase at ZT11 correlates with lower EB penetration into the ARC. In contrast, the loose organization of the ME-ARC barrier at ZT22 is associated with more penetrability. Therefore, we hypothesized that the differences in EB penetration into the ARC are mediated by changes in the ME-ARC and CSF-ARC barriers, suggesting these two barriers undergo a daily regulation.

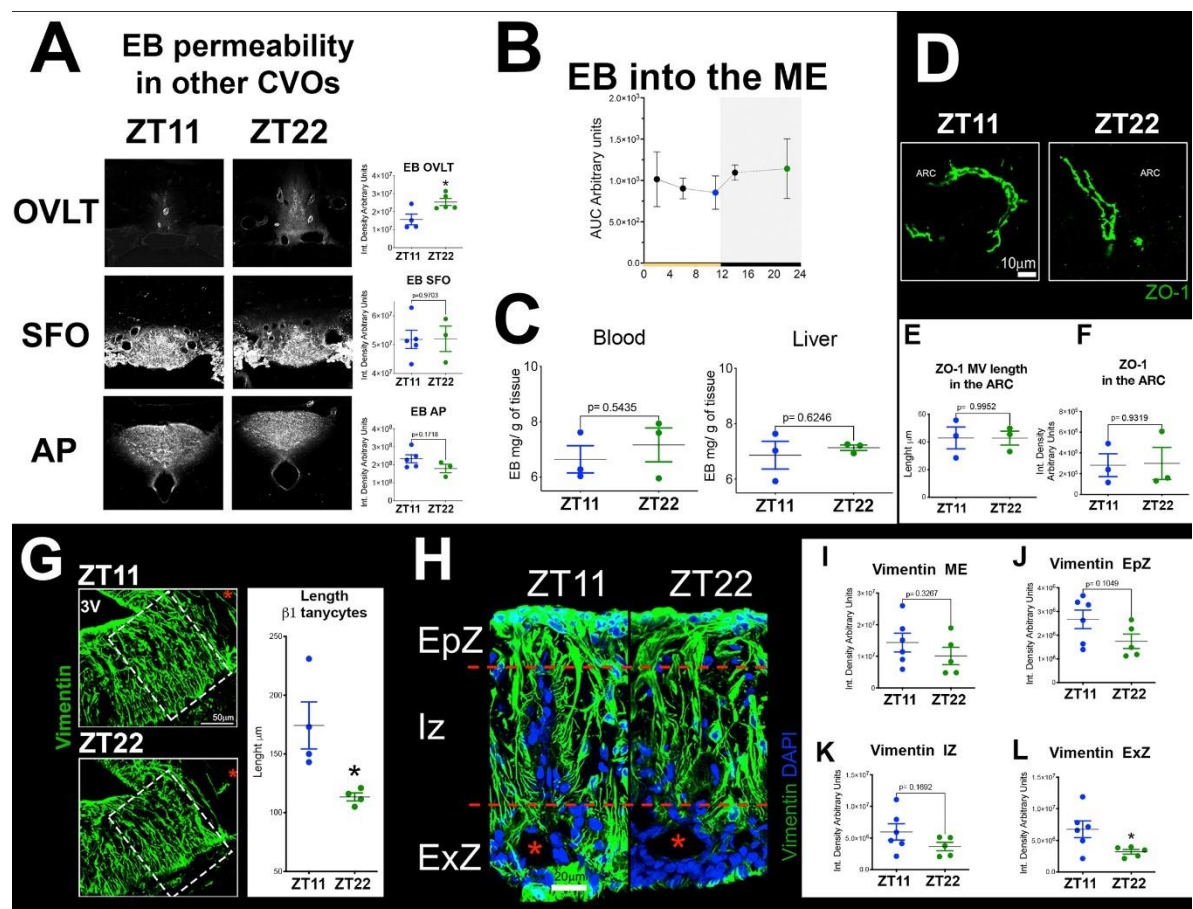


Fig Figure S 1 continues in the next page together with its legend ▼

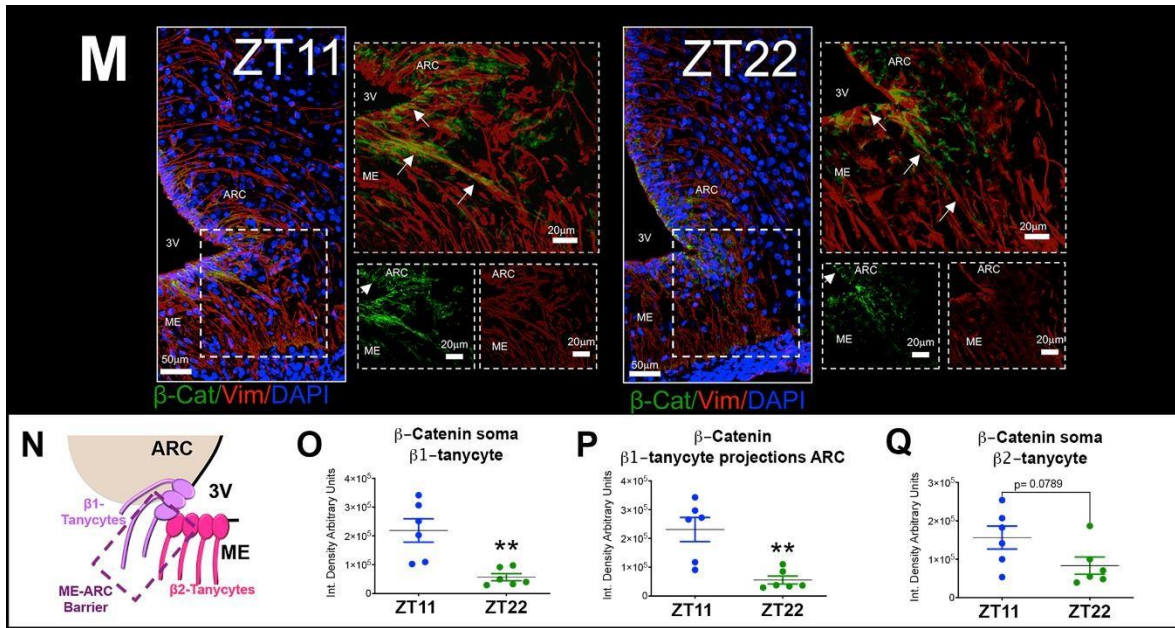


Figure S 1 Permeability of Evans blue in other CVOs at ZT11 and ZT22 (A) Representative images of Evans blue (EB) penetration in the Organum Vasculosum of the Lamina Terminalis (OVLT, up), Subfornical organ (SFO, middle) and Area Postrema (AP, bottom). OVLT but no other circumventricular organs display differences in EB penetration, showing more EB at ZT11 ($n=4$) than at ZT22 ($n=5$) (Unpaired t -test $t=2.813$, $df=7$, $p=0.0261$). $*p<0.05$. Data are presented as the mean \pm SEM. (B) Graph showing the integrated density of fluorescence of the median eminence (ME). The EB penetration in the ME is not statistically different throughout the light/dark cycle. at ZT2 ($n=5$), ZT6 ($n=5$), ZT11 ($n=5$), ZT14 ($n=3$) and ZT22 ($n=5$). (One-way ANOVA, $F(4, 13) = 0.9045$, $p=0.8503$). Data are shown as the mean \pm SEM. (C) EB content in the blood and liver in animals is not different between ZT11 ($n=3$) and ZT22 ($n=3$). Unpaired Student's t test. Data are presented as the mean \pm SEM. (D) Representative confocal images of ZO-1 (green) in the ARC microvessels (MV) showing tight junctions' continuity of the BBB. (E) (F) Quantification of the length and the intensity of ZO-1 signal in the MV within the ARC at ZT11 ($n=3$) and ZT22 ($n=3$). Unpaired Student's t test. Data are presented as the mean \pm SEM. (G) Vimentin staining (green) and quantification of in the ME-ARC interface shows more continuous trajectories of the tanyctic processes at ZT11 ($n=4$) to the ventral aspect of the ME compared to ZT22 ($n=4$). Unpaired Student's t test. $*p<0.05$. Data are shown as the mean \pm SEM. (H) Vimentin staining (green) in the Ependymal Zone (EpZ), Internal zone (Iz) and External Zone (ExZ) of the ME. (I-L) Quantification of vimentin fluorescence in ME zones at ZT11 ($n=6$) and ZT22 ($n=5$). Unpaired Student's t test. $*p<0.05$. Data are presented as the mean \pm SEM. (M) Representative confocal images of β Catenin immunostaining (green) in tanyocytes (vimentin positive, red), show a higher immunoreactivity for β -Catenin at ZT11 ($n=6$) compared to ZT22 ($n=6$). 40 \times . (N-Q) Quantification of the β -Catenin integrated density of fluorescence in the somata and projections of β 1-tanycytes, and in somata of β 2-tanycytes. Cartoon at the left illustrates the region that was quantified. Mann Whitney test. $**p<0.01$. Data are presented as the mean \pm SEM. $**p<0.01$.

7.1.3 The Suprachiasmatic nucleus mediates the opening of the ME-ARC barrier at ZT22

The variations in the structure of the ME-ARC barrier indicate that the SCN is involved in its regulation. Such regulation can be mediated via direct neuronal pathways from the SCN or indirectly via hormonal secretion. Initially, we lesioned the SCN bilaterally (SCNx) and compared EB penetration in these animals at ZT22 vs animals receiving misplaced lesions (Misp Les) (Figure 2A). The ratio of EB penetration between these two conditions (SCNx vs Misp Les) showed a sharp decrease in EB penetration into the ARC in the SCNx condition (Figure

2B). The area under the curve is significantly smaller in SCN_{xx}(_{n=4}) animals than in intact animals at ZT22(_{n=3}) (Unpaired Student's t-test, $t=7$, $df=5$, $p=0.0005$), indicating that the SCN regulates the extravasation of peripherally-circulating molecules into the ARC, either directly or indirectly.

Unlike bilaterally lesioned animals, unilaterally lesioned animals preserve their circadian rhythms⁹⁷, allowing to evaluate the effect of removing the SCN innervation on barrier permeability and morphology. Animals bearing a unilateral lesion of the SCN (SCNx) showed an ipsilateral decrease in EB penetration into the ARC at ZT22, not at ZT11 (ratio of penetration no lesion side vs. lesion side in ZT11 and ZT22 (Unpaired Student's t-test, $t=3.845$ $df=5$) (Figure 2C, 2D). In parallel to the changes in permeability, the ME-ARC area exhibited unilateral changes in the tanycytes organization. Specifically, the density of tanycytes processes extending into the ventral ARC increased ipsilaterally to the SCN lesion at ZT22(_{n=3}) (Paired Student's t-test $t=17.5$, $df=2$, $p=0.0034$), acquiring a similar pattern as observed in intact animals at ZT11 (Unpaired t-test $t=10.51$, $df=4$, $p=0.0005$) (Figure 2E-G).

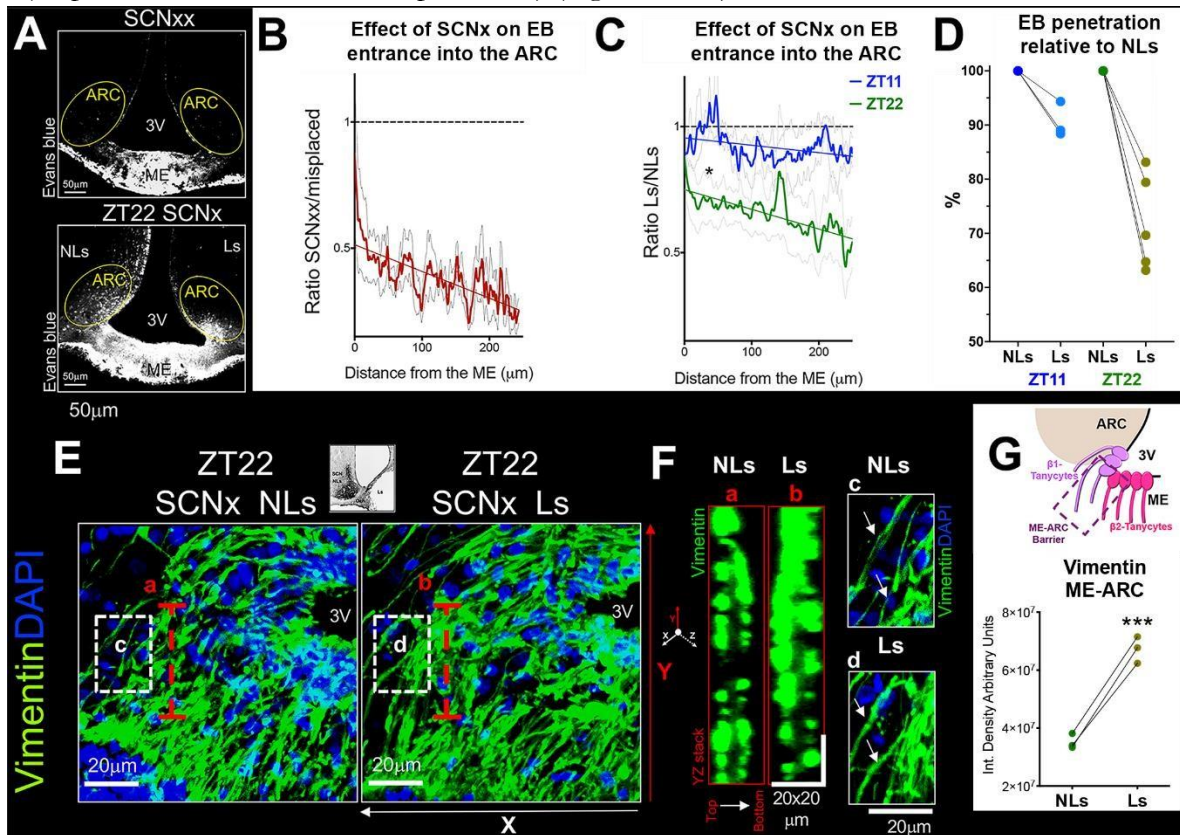


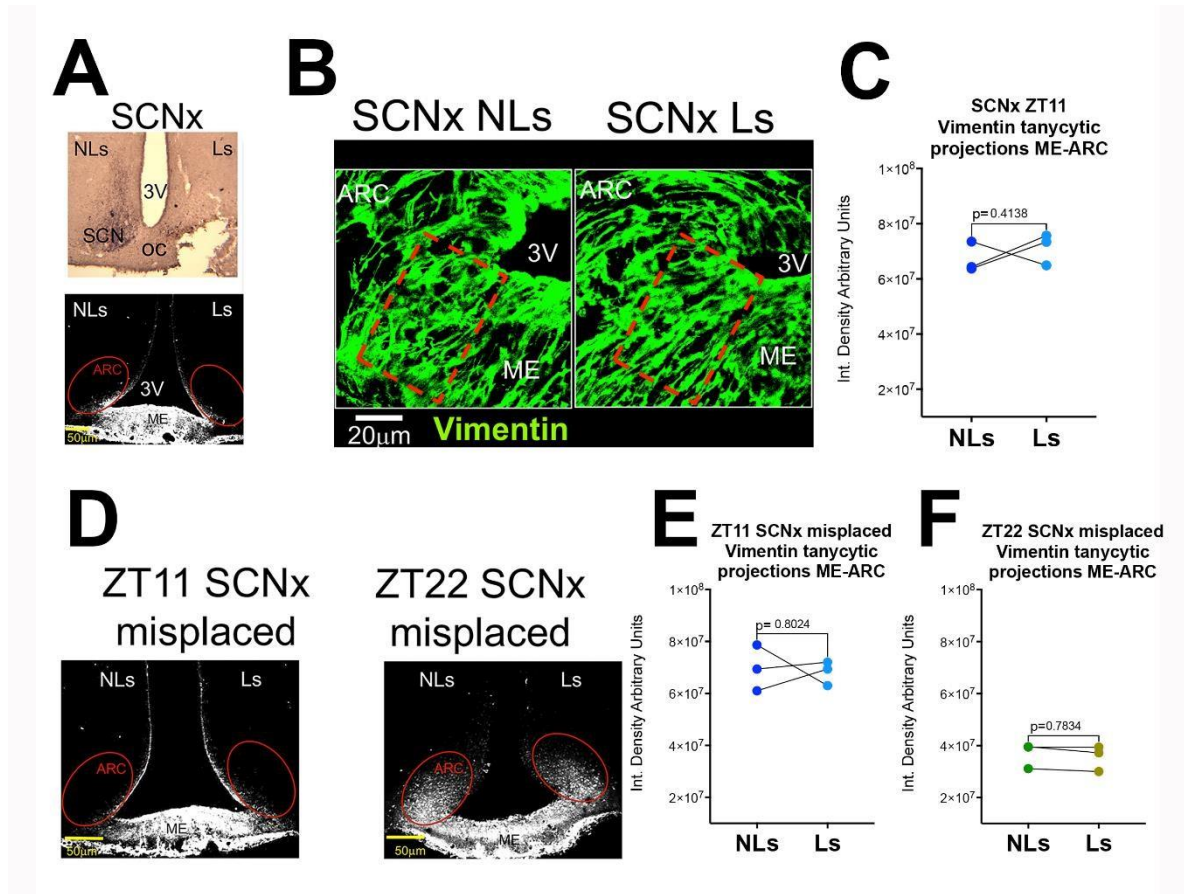
Figure 2 The Suprachiasmatic nucleus opens ME-ARC barrier at ZT22.

(A) Representative images of Evans blue (EB) penetration in a bilaterally lesioned (SCN_{xx}, up) and a unilaterally lesioned animal (SCNx, bottom) at ZT22. (B) Ratio of EB penetration between SCN_{xx} and misplaced lesioned animals shows a consistent diminishment in the ARC of SCN_{xx} animals at ZT22. (C) Ratio of EB penetration in the ARC between lesioned side (Ls) and not lesioned side (NLs) in SCN_x animals exhibits a significant decrease across 250 microns at ZT22(_{n=4}) but not at ZT11(_{n=3}) where EB penetration in the shows similar values making the ratio close to 1. (D) Percentage of EB penetration into the ARC in SCN_x animals. The graph shows the percentage of the EB fluorescence in the Lesioned side (Ls) relative to the non-Lesioned side (NLs), both at ZT11 and ZT22. (E) Z-projections of ME-ARC barrier from SCN_x animals at ZT22 showing Vimentin (green) increases at

the lesioned side. The upper inset shows a representative picture of vasoactive intestinal peptide (VIP) immunostaining used to verify the unilateral SCN lesion. (F) Accumulated fluorescence of Vimentin in an optical slide of 20 microns in the NLs (a) and in the Ls (b), taken from (E) (red dotted line) illustrating increased Vimentin immunoreactivity in the Ls. The (c) and (d) panels are magnified insets from the images in E (white dotted rectangle). (G) Quantification of vimentin immunoreactivity in the NLs and Ls at ZT22 (n=3). Unpaired t-test. ***p<0.001. Data are shown as the mean ± SEM. See also Figure S2. ▲

These results suggest that SCN-input opens the ME-ARC barrier at ZT22; raising the possibility that also SCN-input decreases the permeability at ZT11. However, SCNx animals sacrificed at ZT11 (n=3), similarly to animals bearing a misplaced lesion, showed no changes in EB extravasation into the ARC (Unpaired t-test p=0.012 t=3.845 df=5) (Figure S2A) nor in the organization of tancytic processes (Figure S2B-C), indicating that the SCN does not contribute actively to the barriers closure at ZT11, and that the closed state is the outcome of absence of SCN input. The results of the complete SCN lesion support this conclusion. Collectively, the lesion experiments suggest that the closed state is the basal condition of the barriers unless the SCN provides an opening signal.

Figure S 2 SCNx at ZT11 or SCNx misplaced lesions do not induce bilateral changes in Evans blue penetration into the ARC or



vimentin immunoreactivity. (A) Representative image of immunostaining of vasointestinal peptide (VIP) after a unilateral misplaced or

partial SCN lesion (up), show that Evans blue (EB) penetration into the ARC at ZT11 in an SCNx misplaced animal did not

exhibit unilateral changes. (B) representative confocal images of vimentin (green) in SCN \times misplaced at ZT11 show no differences in

ME-ARC barrier. (C) Quantification of vimentin in the ME-ARC zone in SCN \times misplaced at ZT11 (n=3). Paired Student's t

test. Data are presented as the mean \pm SEM. (D) Representative images of EB penetration in animals with lesions outside the SCN

at ZT11 misplaced and ZT22 misplaced. Note the difference the higher penetration of EB into the ARC at ZT22. (E-F) Integrated

density of fluorescence of tanyctye processes in animals with lesions outside the SCN at ZT11 (n=3) and ZT22 (n=3) do not display

differences between the lesioned side (Ls) and the non-Lesioned side (NLs). Paired Student's t test. Data are presented as the mean \pm

SEM. ▲

7.1.4 High tanyctytic GLUT1 at ZT22 promotes glucose entrance into the ARC

ZT11 and ZT22 are crucial time windows for animal physiology. At ZT11, a rodent begins preparations for the activity period, while following ZT22, the animal gets ready to rest. ZT11 is characterized by high levels of glycemia, while at ZT22, the levels are low^{230,231}. Since the ARC plays a central role in glucose homeostasis^{232,233}, we studied glucose penetration by examining the extravasation of a fluorescent derivative of Glucose, the 2-NBDGlucose (2-deoxy-2-[(7-nitro-2,1,3-benzoxadiazol-4-yl)amino]-D-glucose).

Analysis of 2-NBDGlucose penetration into the ARC shows a higher penetration into the ARC parenchyma at ZT22_(n=3) (when glycemia is low) than at ZT11_(n=4) (glycemia acrophase) (Unpaired Student's t-test $t=3.874$, $df=5$, $p=0.0117$) (Figure 3A-C), indicating that similar to EB penetration, glucose entrance into the ARC is time-dependent. Notably, other brain regions, such as the SFO and hippocampus (used as control regions), did not show differences (Figure S3A) at these time points.

Transport of Glucose from the CSF into the brain parenchyma is a GLUT1 dependent and gradient-independent process^{234,235}. We evaluated whether changes in tanyctytic GLUT1 at the

CSF-ARC interphase contributed to the differences in glucose penetration. GLUT1 levels are significantly higher at ZT22_(n=6-11) than at ZT11_(n=6-11), both in somas of α_2 tanycytes (Unpaired Student's t-test $t=2.878$, $df=20$, $p=0.0164$) and β_1 tanycytes (Unpaired Student's t-test $t=3.239$, $df=20$, $p=0.0089$), as well as in their processes into the ARC (Unpaired Student's t-test $t=2.255$, $df=20$, $p=0.0355$) (Figure 3D-I).

Levels of GLUT1 immunoreactivity were not time-dependent in α_1 tanycytes (Figure 3F), ARC capillaries (CD31+ cells), and ependymal cells at the level of the ventromedial hypothalamus (VMH) (Unpaired Student's t-test. For ARC microvessels $t=1.62$, $df=10$, $p=0.2723$; for ependymal cells $t=1.608$, $df=4$, $p=0.2723$) (Figure S3B-D); indicating that the increased glucose entrance into the ARC at ZT22 might be related to increased expression of GLUT1 in the α_2 and β_1 tanycytes in the 3V.

The evident changes in GLUT1 expression in the 3V wall, and the presence of aurothioglucose, a non-metabolizable analogous of Glucose, in the ARC near the 3V wall after an i.v. injection, suggests that Glucose penetrates from the CSF into the ARC (Figure S3F).

Increased tanycytic GLUT1 occurred at ZT22 when glycemia is typically low; while diminished GLUT1 was observed at the glycemia acrophase (ZT11), suggesting an opposed relationship between these two variables.

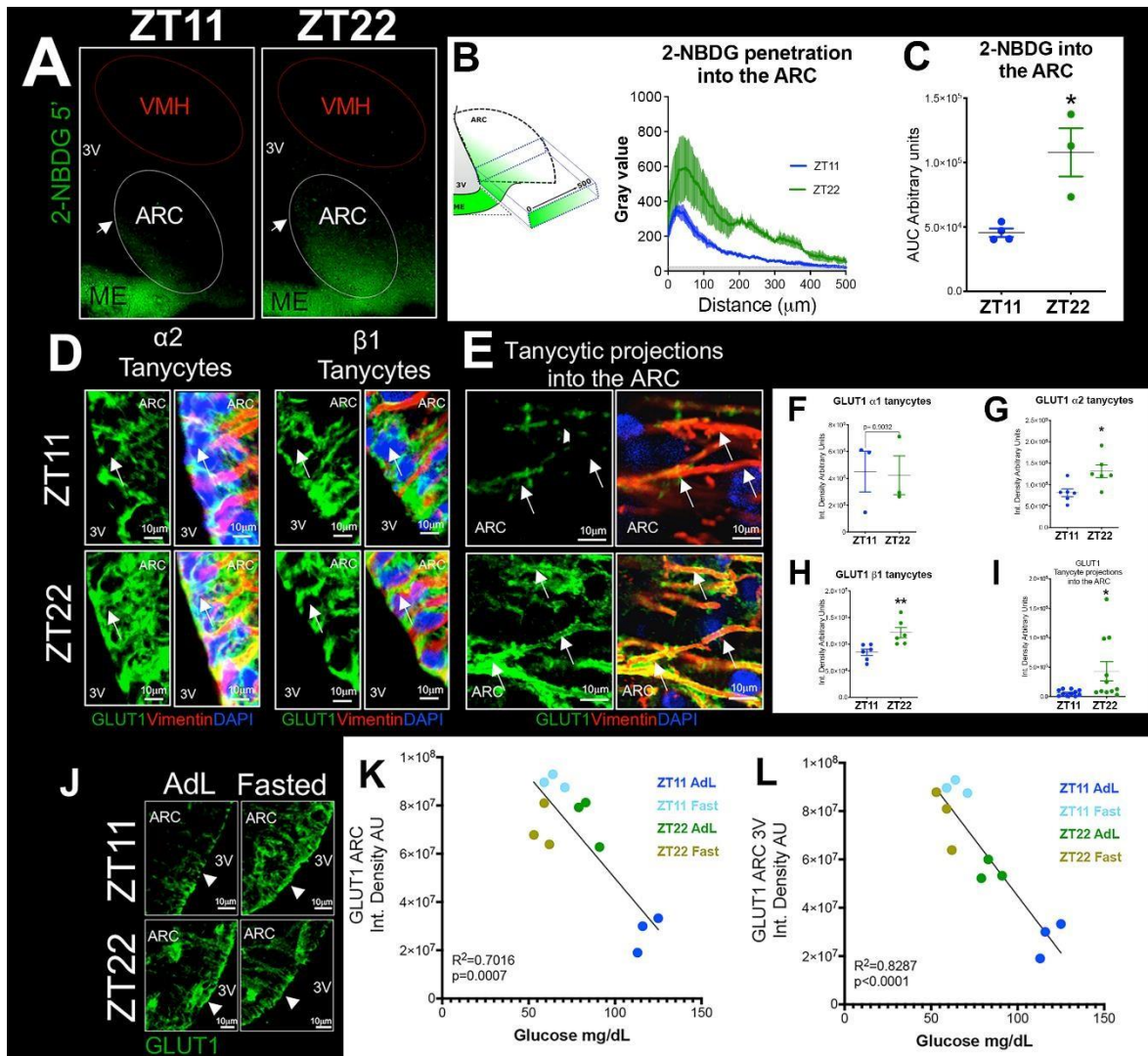


Figure 3 Glucose access into the ARC is time-dependent and mediated by tanyctic GLUT1

(A) Representative images of 2-NBDG glucose (green) penetration into the ARC. Note the higher 2-NBDG glucose intensity in the ARC at ZT22 compared to ZT11. VMH, ventromedial hypothalamus; ME, Median Eminence. (B) Histogram of 2-NBDG glucose penetration (500 microns) into the ARC at ZT11 (n=4) and ZT22 (n=4). (C) Quantification Area under the curve of 2-NBDG glucose penetration at ZT11 (n=4) and ZT22 (n=4). Unpaired Student's t-test. * $p < 0.05$. Data are shown as the mean \pm s.e.m. (D) Immunofluorescence of GLUT1 (40X) in $\alpha 2$ and $\beta 1$ tanyctes shows higher intensity at ZT22 compared to ZT11. (E) Micrographs show that GLUT1 immunoreactivity (40X) in tanyctic projections into the ARC is higher at ZT22 than ZT11. (F-I) Quantification of GLUT1 immunoreactivity in $\alpha 1$ (F), $\alpha 2$ (G), $\beta 1$ tanyctes (H), and in tanyctic projections in the ARC (I) in ZT22 (n=6-11) and ZT11 (n=6-11). Unpaired Student's t-test. * $p < 0.05$, ** $p < 0.01$. Data shown as the mean SEM. (J) Representative images of GLUT1 immunoreactivity in *ad libitum*-fed (AdL) and fasted animals at ZT11 and ZT22 show an increase in GLUT1 at ZT11 in fasting conditions. (K-L) Correlation of glycemia with GLUT1 intensity in the whole ARC (K); or just in $\alpha 2$ and $\beta 1$ tanyctes somata (L), in AdL and fasted animals. Note that high GLUT1 immunoreactivity in tanyctes correlates with low glycemia levels and viceversa. See also Figure S3 and S4

GLUT1 expression in ARC tanyctes showed an inverse correlation with peripheral Glucose in *ad libitum*-fed animals; this correlation became even more robust when GLUT1 in ARC tanyctes was considered solely, instead of GLUT1 in the whole ventricle wall. This correlation was maintained even after 72h-fasting, a condition whereby glycemia is substantially low (linear

correlation GLUT1 in the ARC with systemic glucose $R^2=0.7016$ $p=0.0007$; linear correlation GLUT1 in the 3V tanycytes with systemic glucose $R^2=0.8287$ $p<0.0001$) (Figure 3J-L, Figure S4). For example, 72-h fasting decreased peripheral Glucose at ZT11 and increased GLUT1 intensity in α_2 (One-way ANOVA $F_{(3,8)}=8.607$, post-hoc Tukey's test, $p=0.0069$) and β_1 tanycytes (One-way ANOVA $F_{(3,8)}=13.33$, post-hoc Tukey's test, $p=0.0018$), as well as in tanycytic projections into the ARC (One-way ANOVA $F_{(3,8)}=6.665$, post hoc Tukey's test, $p=0.0144$) (Figure S4).

To examine how the SCN could influence ventricular glucose uptake, we analyzed GLUT1 immunoreactivity in SCNx animals at ZT22_(n=4). We observed a unilateral decrease in GLUT1 levels in somata (Paired Student's t-test $t=4.236$, $df=3$, $p=0.0241$) and in the processes of β_1 tanycyte extending into the ARC's side ipsilateral to the SCN lesion (Paired Student's t-test $t=4.333$, $df=3$, $p=0.0227$) (Figure 4), no significant changes were observed in α_2 tanycytes (Figure 4).

In SCNx animals at ZT22, no differences were found in GLUT1 immunoreactivity of ARC microvessels between lesioned and intact sides (Figure S3G), indicating that the SCN enhances glucose penetration at ZT22 by increasing the expression of tanycytic GLUT1. In contrast, SCNx animals sacrificed at ZT11_(n=3) did not display unilateral changes in GLUT1 expression nor in the 3V zone (Figure S3I-K). This result suggests that low expression of GLUT1 constitutes the basal state in the absence of SCN input.

In addition to ME-ARC barrier opening for large molecules, as illustrated by the penetration of EB (bound to circulating albumin with high affinity in a ~ 70 kDa complex), the results indicate that the SCN also enhances penetrability of Glucose by increasing GLUT1 expression in β_1 tanycytes.

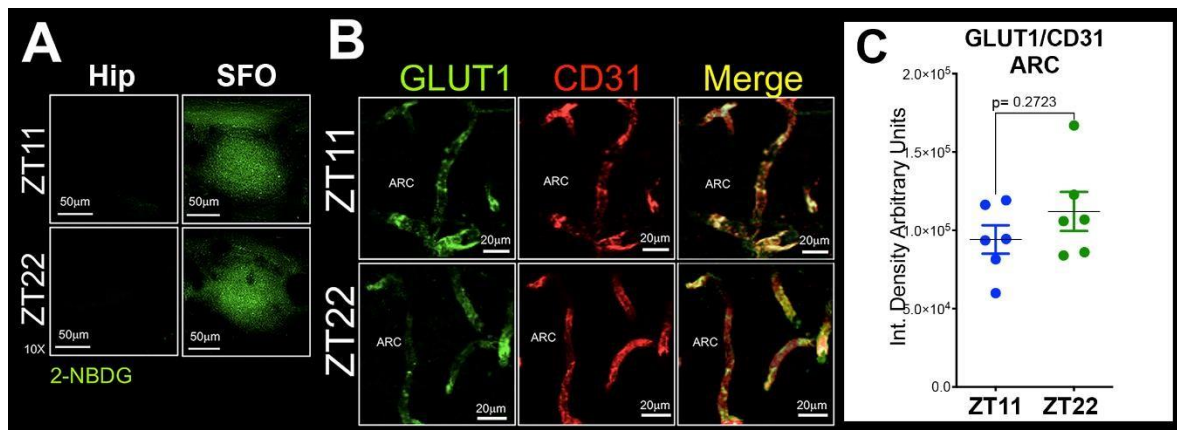


Fig. S3 continues in the next page with its legend.

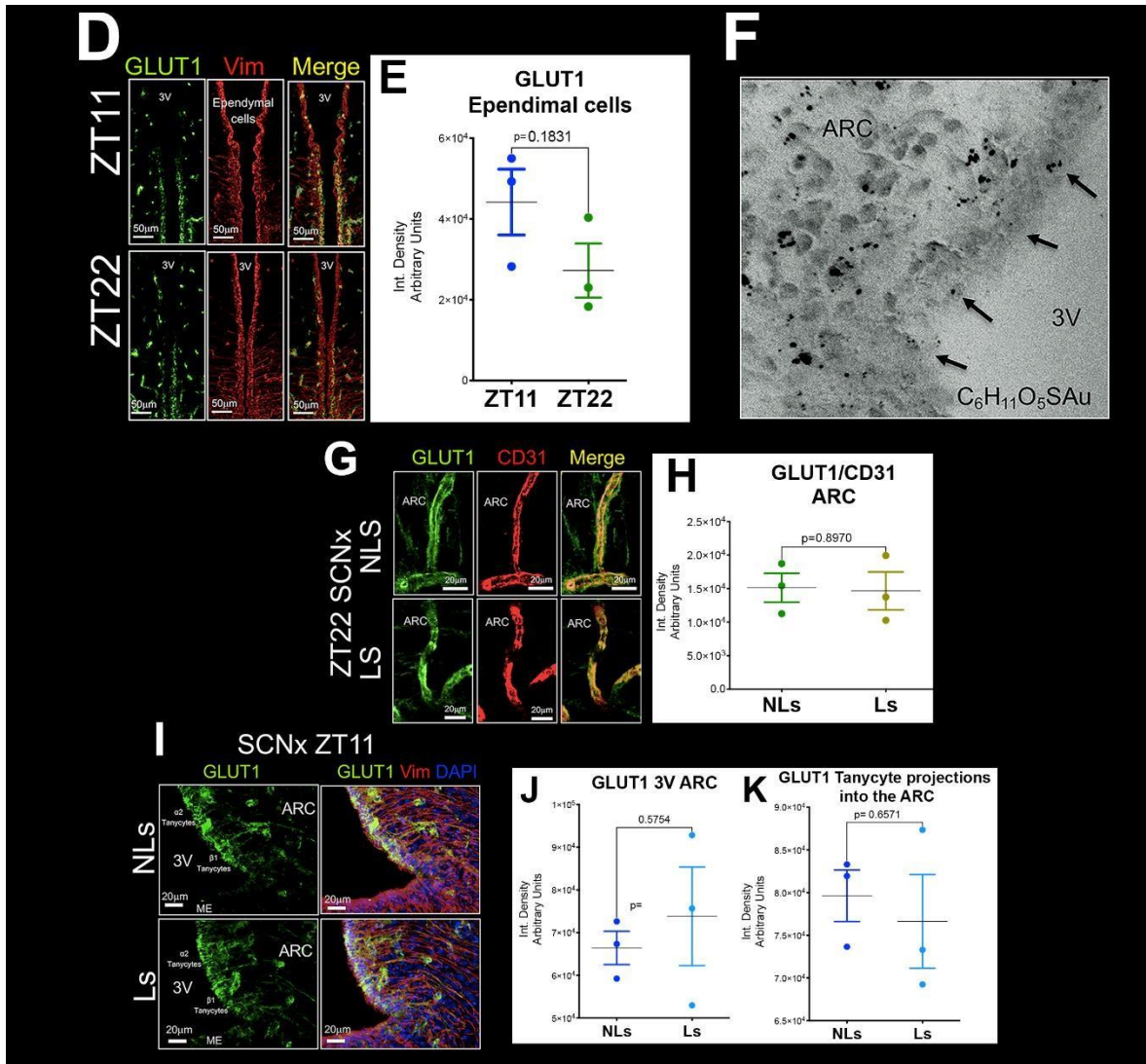


Figure S 3 Permeability of Evans blue in other CVOs at ZT11 and ZT22 (A) Representative images of Evans blue (EB) penetration in the Organum Vasculosum of the Lamina Terminalis (OVLT, top), Subfornical organ (SFO, middle) and Area Postrema (AP, bottom). OVLT but no other circumventricular organs display differences in EB penetration, showing more EB at ZT11 (n=4) than at ZT22 (n=5) (Unpaired t-test $t=2.813$, $df=7$, $p=0.0261$). $*p<0.05$. Data are presented as the mean \pm SEM. (B) Graph showing the integrated density of fluorescence of the median eminence (ME). The EB penetration in the ME is not statistically different throughout the light/dark cycle, at ZT2 (n=5), ZT6 (n=5), ZT11 (n=5), ZT14 (n=3) and ZT22 (n=5). (One-way ANOVA, $F(4, 13) = 0.9045$, $p=0.8503$). Data are shown as the mean \pm SEM. (C) EB content in the blood and liver in animals is not different between ZT11 (n=3) and ZT22 (n=3). Unpaired Student's t test. Data are presented as the mean \pm SEM. (D) Representative confocal images of ZO-1 (green) in the ARC microvessels (MV) showing tight junctions' continuity of the BBB. (E) (F) Quantification of the length and the intensity of ZO-1 signal in the MV within the ARC at ZT11 (n=3) and ZT22 (n=3). Unpaired Student's t test. Data are presented as the mean \pm SEM. (G) Vimentin staining (green) and quantification of in the ME-ARC interface shows more continuous trajectories of the tanyctic processes at ZT11 (n=4) to the ventral aspect of the ME compared to ZT22 (n=4). Unpaired Student's t test. $*p<0.05$. Data are shown as the mean \pm SEM. (H) Vimentin staining (green) in the Ependymal Zone (EpZ), Internal zone (Iz) and External Zone (ExZ) of the ME. (I-L) Quantification of vimentin fluorescence in ME zones at ZT11 (n=6) and ZT22 (n=5). Unpaired Student's t test. $*p<0.05$. Data are presented as the mean \pm SEM. (M) Representative confocal images of β Catenin immunostaining (green) in tanyocytes (vimentin positive, red), show a higher immunoreactivity for β -Catenin at ZT11 (n=6) compared to ZT22 (n=6). 40x. (N-Q) Quantification of the β -Catenin integrated density of fluorescence in the somata and projections of β 1-tanyocytes, and in somata of β 2-tanyocytes. Cartoon at the left illustrates the region that was quantified. Mann Whitney test. $**p<0.01$. Data are presented as the mean \pm SEM. $**p<0.01$. \blacktriangle

7.1.5 Glucose entrance into the ARC is essential for low glycemia

To examine the functional significance of the increase in ARC GLUT1 expression, we applied a GLUT1 competitive blocker, 3,5,4-trihydroxystilbene (Resveratrol)²³⁶, at ZT11_(n=3) and ZT22_(n=4). Intracerebroventricular (i.c.v.) administration of resveratrol, but not vehicle_(n=4), inhibited glucose entrance into the ARC and induced a rapid increase in glycemia at ZT22 (Two-way ANOVA, time x condition, $F_{15,45}=3.507$, post-hoc Tukey's test, $p=0.0006$) (Figure S5A), peaking 20 min after the resveratrol administration and returning to baseline levels 40 min postinjection. The same injection at ZT11 did not affect the glucose levels in the periphery (Figure 5A), indicating the time dependency of this regulation.

Next, we examined how the SCN could mediate its effects on the barriers. We observed Vasopressin (VP) containing fibers along the 3V walls, in the vicinity of β_1 tanycytes somata belonging to the ARC-ME barrier, appearing more abundantly at ZT22 than at ZT11 (qualitative findings, Figure 4A). Furthermore, we observed that VP fibers in the tanycytes area, but not in the internal or external zone of the ME, nearly disappeared ipsilaterally after a unilateral SCN lesion, indicating that this innervation originates from the SCN in agreement with previous tracing studies from the SCN⁹⁶ (Figure 5B, See also Figure S5B).

Since circadian-driven release of VP from the SCN starts around ZT18^{32,33}, and the 3V walls show robust expression of the V1aR^{237,238}, we hypothesized that VP from the SCN could act on tanycytes to increase glucose transport into the ARC. To test whether VP at ZT22 contributes to changes in systemic glycemia, we inhibited the VP receptor using V1aR antagonist (DeaminoPen¹, O-Mer-Tyr², Arg⁸). I.c.v administration of V1aR antagonist but not vehicle significantly decreased penetration of 2-NBDGlucose into the ARC (Unpaired Student's t-test $t=4.615$, $df=5$, $p=0.0058$), similar as resveratrol (Figure 5C). In addition to the changes in 2-NBDGlucose penetration into the ARC, administration of V1aR antagonist significantly increased systemic glucose levels at ZT22_(n=4) (Two-way ANOVA, time x condition, $F_{15,45}=3.507$, $p=0.0006$). Furthermore, a sharp increase in glycemia was observed within 10 minutes after drug application, reaching levels normally seen at the circadian acrophase (~ 125 mg/dL) (post-hoc Tukey's test $p<0.05$) (Figure 5D), persisting for 20 minutes post-administration (post-hoc Tukey's test $p<0.0001$). Collectively, it indicates that increased glucose penetration into the ARC at ZT22 is essential to lower glycemia at this time point.

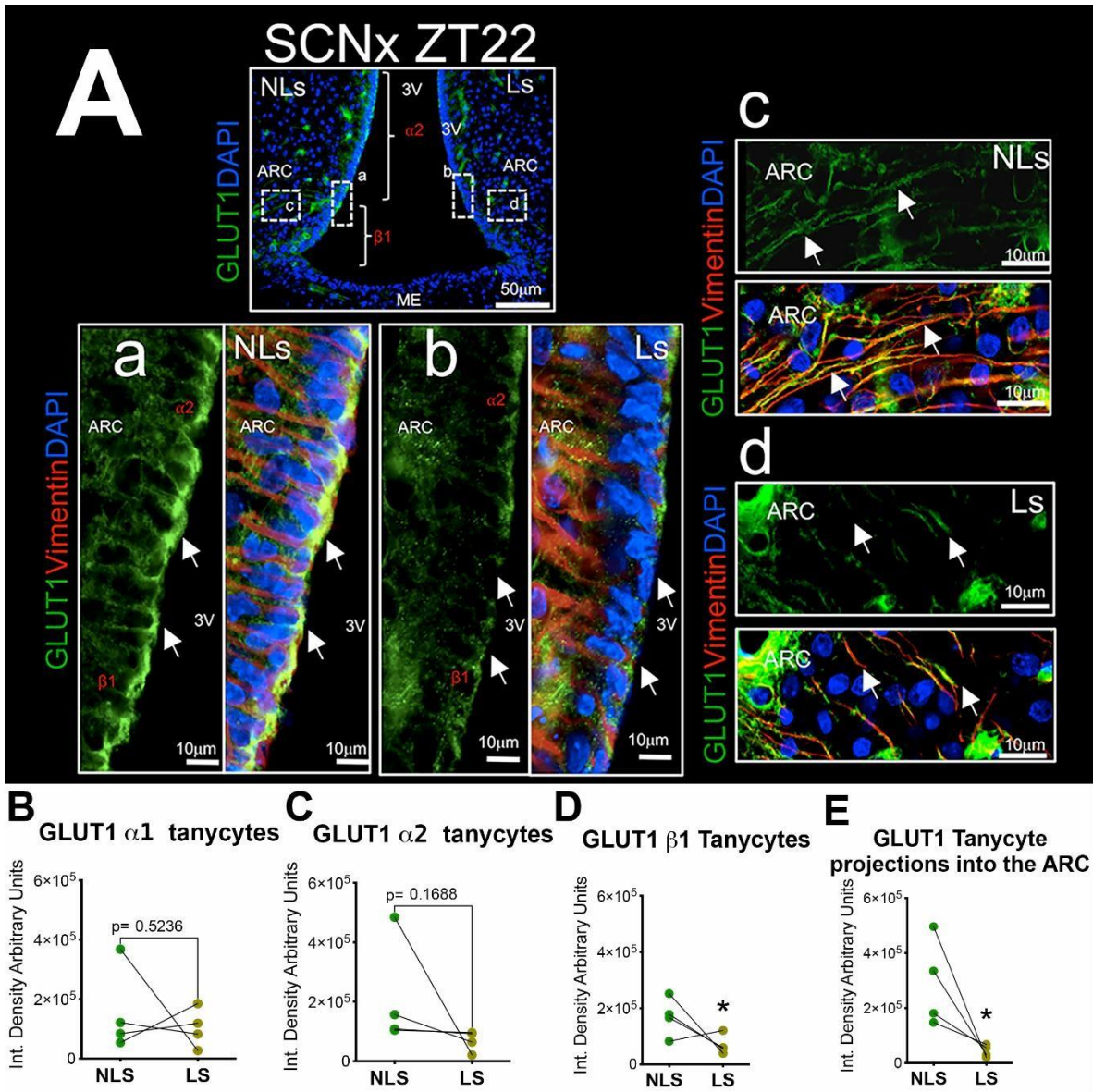


Figure 4. Suprachiasmatic nucleus mediates increase of GLUT1 in $\beta 1$ tanycytes.

(A) Representative image of GLUT1 immunoreactivity in SCN \times condition at ZT22 shows an ipsilateral decrease of GLUT1 in the ARC. Insets show GLUT1 in 3V tanycytes in the intact side (NLS) (a), in the lesioned side (LS) (b); in tanycyte processes in the NLS (c), and in the LS (d). (B-E) Quantification of GLUT1 immunoreactivity in SCN \times animals comparing lesioned and Intact sides of the ARC in $\alpha 1$, $\alpha 2$, $\beta 1$ tanycytes and tanycytic projections at ZT22 (n=4). *p<0.05. Paired Student's t-test. Data shown as mean \pm SEM. See also Figure S4

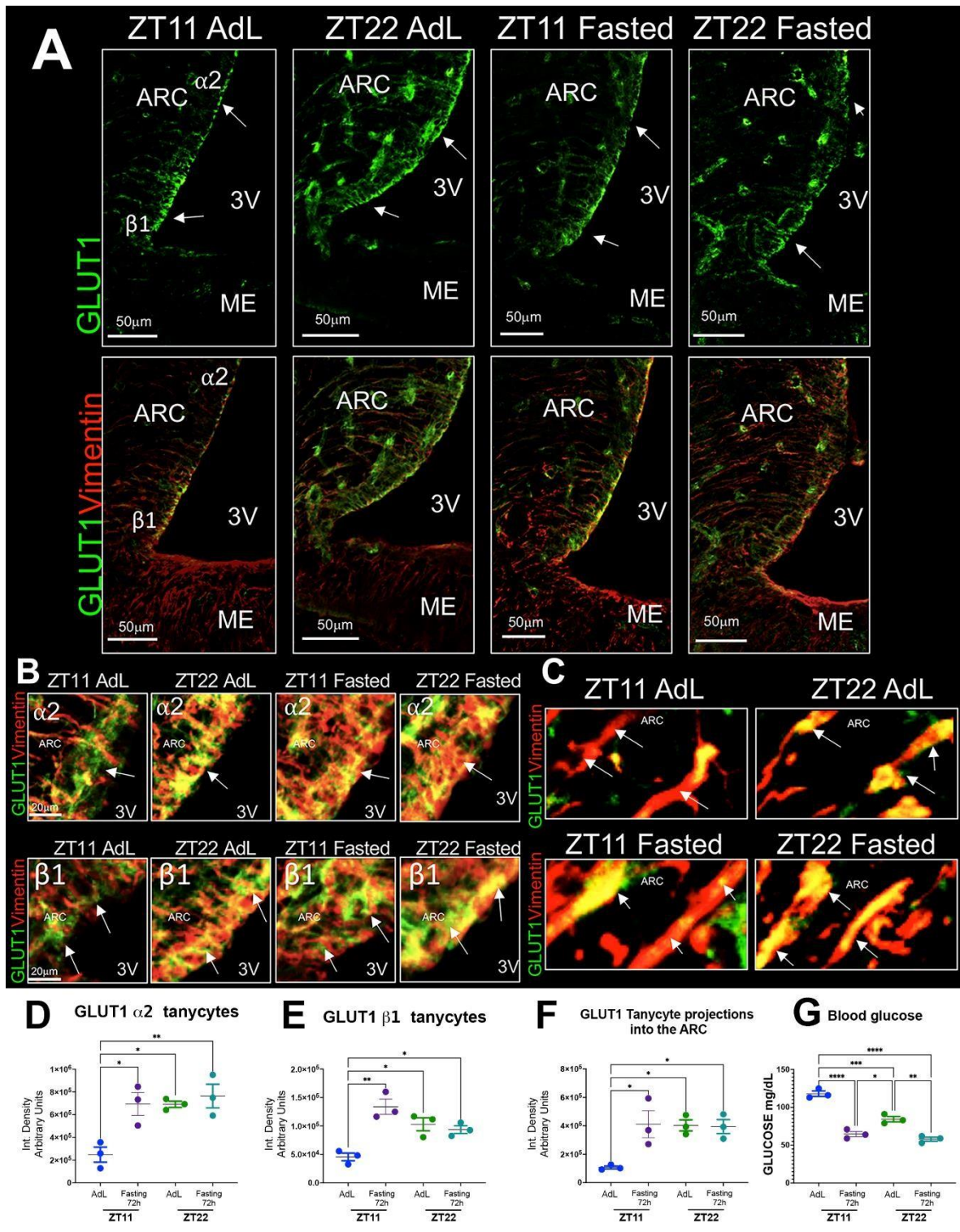
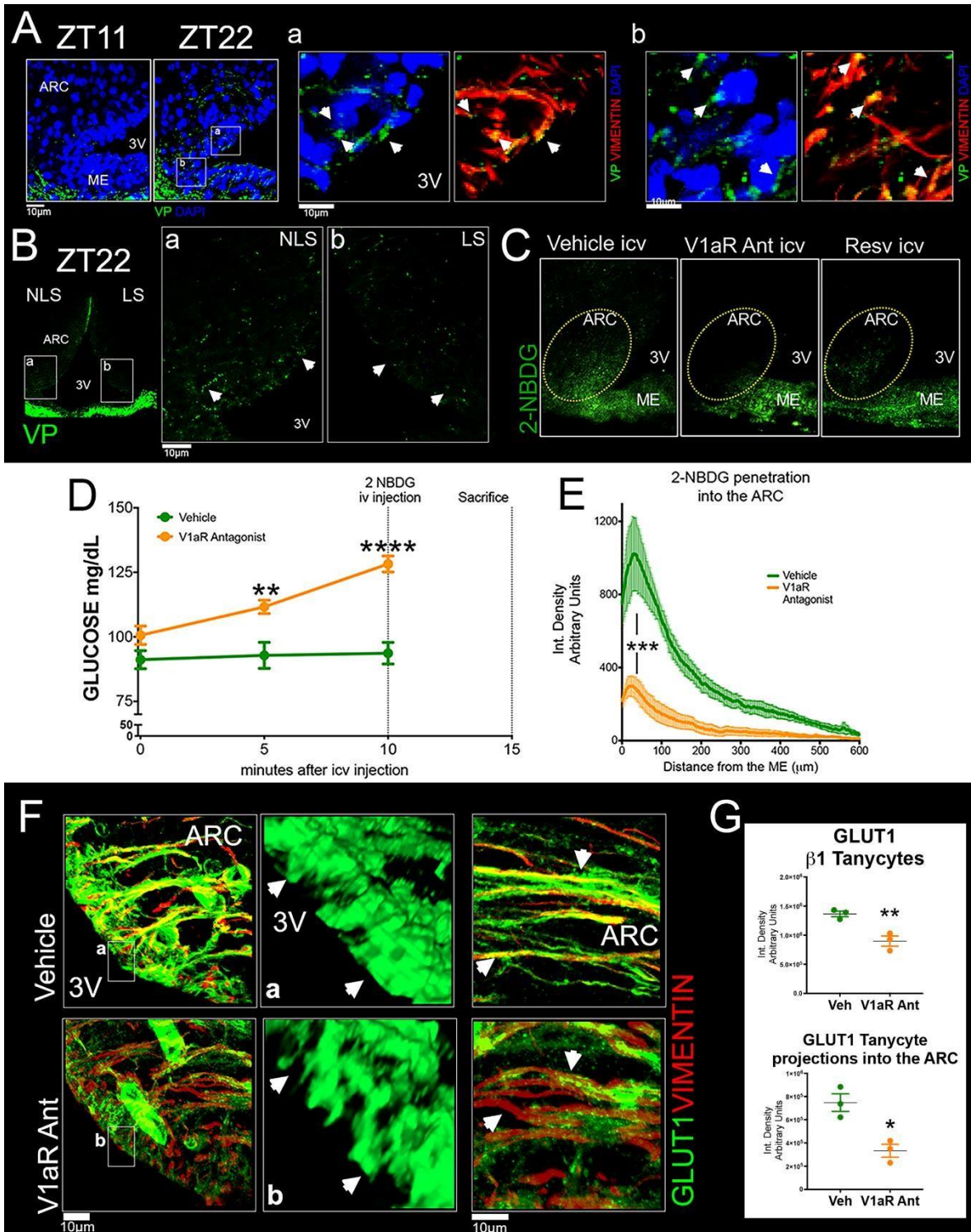


Figure S 4 Fasting increases GLUT1 in the ARC only at ZT11 when peripheral glucose levels decrease significantly (A) Confocal images showing the immunoreactivity of GLUT1 (green) in tanyocytes (vimentin, red) in the ARC of ad libitum (AdL) and 72-h fasted animals (20 \times). Note the increase of GLUT1 only in ZT11 fasted animals. (B-C) Immunoreactivity of GLUT 1 in the $\alpha 2$ and $\beta 1$ tanyocyte somas (vimentin, red), as well as in their processes in the ARC, in both AdL and fasted animals. (D-F) Quantification shows that fasting at ZT11 increased the GLUT1 immunoreactivity in the $\alpha 2$ and $\beta 1$ tanyocyte somas, and in their projections into the ARC similarly to the levels observed in ad libitum at ZT22. ZT11 AdL(n=3), ZT11 Fasted(n=3), ZT22 AdL(n=3), ZT22 Fasted(n=3)

Fasted($n=3$). One-way ANOVA, post hoc Tukeys test. $*p<0.05$, $**p<0.01$, $***p<0.001$. Data are presented as the mean \pm SEM. (G) Glucose levels in ad libitum and fasting conditions, at ZT22 and ZT11. ZT11 AdL($n=3$), ZT11, fasted ($n=3$), ZT22 AdL($n=3$), ZT22 Fasted($n=3$). Note that higher GLUT1 in tanycytes coincide with lower glucose levels. One-way ANOVA, post hoc Tukeys test. $*p<0.05$, $**p<0.01$, $***p<0.001$. Data are presented as the mean \pm SEM. \blacktriangle



\blacktriangle Figure 5 Vasopressin modulates the glucose entrance into the ARC and induces low glycemia (A) Representative microphotographs of vasopressin (VP) fibers in the ARC at ZT11 and ZT22. (a) Magnification from (A) (white

squares, right) shows abundant VP fibers in the 3V zone in the ARC, and (b) in tanyctic processes at ZT22. (B) Representative image of the VP immunoreactivity (green) in the ARC in an SCN \times animal at ZT22; inset (a) shows the non-lesioned side (NLS) and (b) and lesioned side (LS) (40 \times). Note the decrease in VP fibers in the 3V at the level of the ARC (white arrows). (C) Representative microphotographs show the decrease in 2NBDGlucose penetration into the ARC at ZT22, 10 minutes following i.c.v. administration of V1aR antagonist, or resveratrol compared to vehicle. (D) Glycemia increased significantly after the i.c.v. administration of V1aR(n=4) antagonist, compared to the vehicle(n=4) at ZT22. Two-way ANOVA, post-hoc Tukey's test. ** $p < 0.01$, *** $p < 0.001$. Data are shown as the mean \pm SEM. (E) Histogram shows decrease in 2NBDGlucose penetration into the ARC, 15 minutes after the i.c.v. administration of V1aR antagonist compared to vehicle. (F) Representative microphotographs show decrease of GLUT1 immunofluorescence in β 1 tanyctes (left) after i.c.v. administration of V1aR antagonist compared to vehicle. Insets (a) and (b) show a 3D reconstruction of the 3V zone (white rectangle) of GLUT1 immunoreactivity after i.c.v. administration of vehicle (a) or V1aR antagonist (b). Right panels show a lower intensity of GLUT1 immunofluorescence in tanyctic projections into the ARC after administration of V1aR antagonist compared to vehicle. (G) Graphs show the intensity of GLUT1 in β 1 tanyctes and tanyctic projections into the ARC after vehicle(n=3) or V1aR(n=3) antagonist at ZT22. Unpaired Student's t-test. * $p < 0.01$, ** $p < 0.001$. Data are shown as the \pm SEM. See also Figure S5.

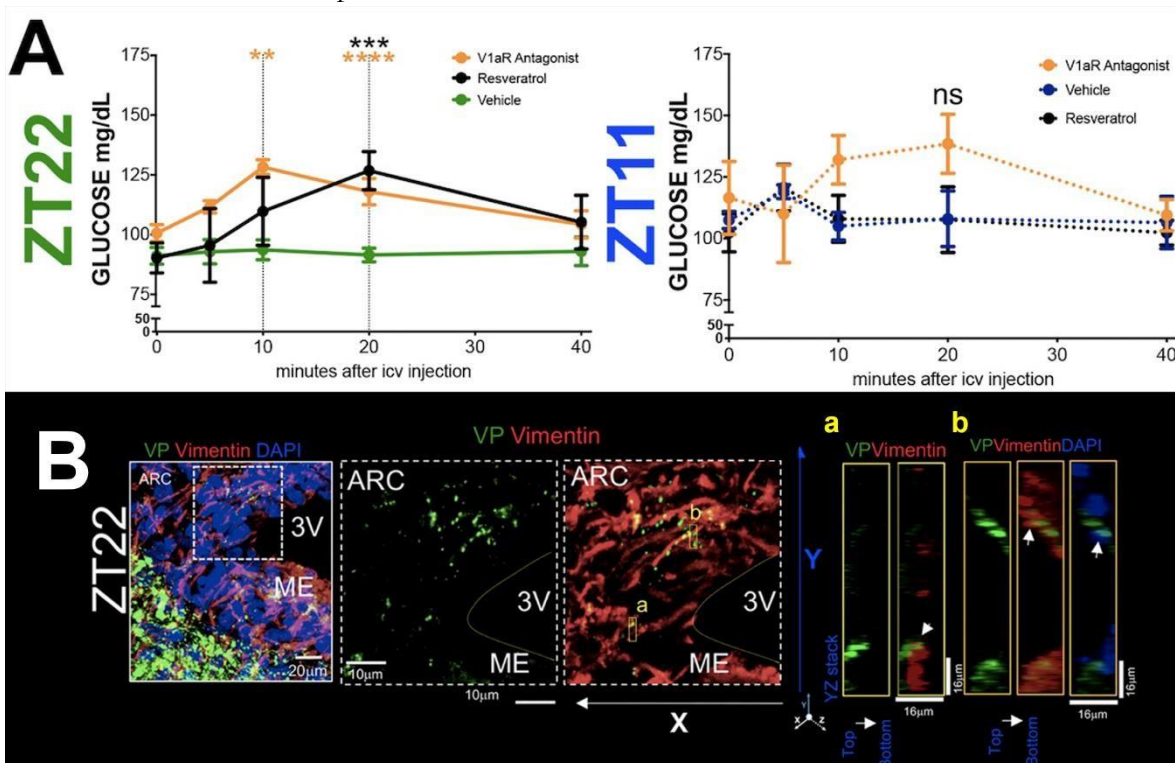
When the cannula did not reach the ventricle, VP antagonist administration did not alter

glycemia (Figure S5C) nor glucose entrance into the ARC (Data not shown). Further, other brain areas such as SFO, ME or hippocampus at ZT22 did not exhibit 2NBDGlucose changes after i.c.v administration of V1aR (Figure S5D-E).

Confirming the action of VP on the tanyctic GLUT1 in the ARC; the i.c.v. V1aR antagonist injection at ZT22(n=3) induced a significant decrease in GLUT1 immunoreactivity in the somata of β 1 tanyctes (Unpaired Student's t-test $t=5.511$, $df=4$, $p=0.0053$), and in their projections into the ARC (Unpaired Student's t-test $t=4.426$, $df=4$, $p=0.0115$) (Figure 5F-G).

The intensity of Vimentin in the ME-ARC zone did not show statistically significant changes (Unpaired Student's t-test, $t=0.8694$,

$df=4$, $p=0.4337$) (Figure S5F-G), suggesting that changes in the tanyctic GLUT1 in the 3VARC zone mediate most of the penetration of 2-NBDGlucose.



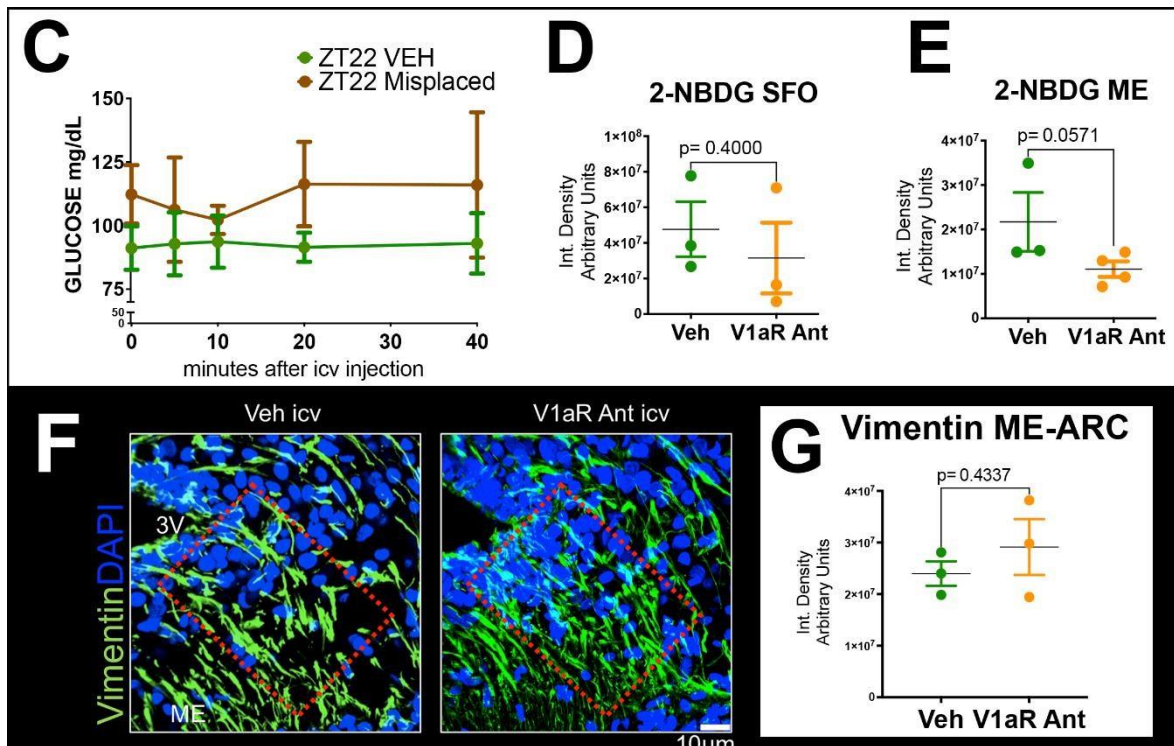


Figure S 1 (A) Glycemia levels increase after *i.c.v.* infusion of resveratrol (ZT22($n=3$); ZT11($n=3$)) and vasopressin (VP) antagonist V1aR (ZT22($n=4$); ZT11($n=3$)), compared to vehicle (ZT22($n=4$); ZT11($n=3$)). Two-way ANOVA, post-hoc Tukey's test. $**p<0.01$, $***p<0.001$, $****p<0.0001$. Data are presented as the mean \pm SEM. (B) Representative image of VP (green) and vimentin (red) in the ME-ARC interface at ZT22 (40X) and magnification of the area within the dotted square showing the immunoreactivity of VP alone (left) or together with vimentin (right). Insets (a) and (b) from areas enclosed in yellow rectangles show VP fibers in contact with tanyctic processes (white arrows). (C) Glycemia levels after *i.c.v.* infusion of vehicle or V1aR antagonist in rats with a misplaced cannula at ZT22($n=4$) compared to vehicle at ZT22($n=4$). Two-way ANOVA, post-hoc Tukey's test. Data are presented as the mean \pm SEM. (D) Graphs show the integrated density of fluorescence of the 2-NBDG glucose in the subfornical organ (SFO) (left) and in the median eminence (ME) (right) following the *i.c.v.* administration of vehicle or V1aR antagonist at ZT22. Unpaired Student's *t* test. Data are presented as the mean \pm SEM. (E) Representative confocal images of vimentin (green) following the *i.c.v.* administration of vehicle or V1aR antagonist at ZT22 and the quantification of vimentin intensity in ME-ARC zone. Unpaired Student's *t* test. Data are presented as the mean \pm SEM. ▲

8 General Discussion

The first evidence suggesting that the brain influences glucose metabolism was provided by Claude Bernard in 1849, when he was still a student. He observed that stimulating the base of the fourth ventricle in rabbits caused a pronounced rise in glycemia. As he wrote in the *Memoires and Communications of Compte Rendu des Seances de L'Academie des Sciences*: "It modifies the constitution of the urine, and the sugar is made to appear there. Injuring a certain part of the floor of the fourth ventricle, (...) urine which before this operation was turbid, alkaline and devoid of sweet matter, is now abundant, clear, acid and containing a large amount of sugar in solution, (...) it becomes analogous to what we have known in diabetes".

Nowadays, the current understanding of glycemia regulation contemplates an extra layer of complexity, the circadian periodicity displayed in glycemia fluctuations given by the SCN²³⁹. The SCN promotes glycemia concentration to rise before the start of the activity period and decrease prior the resting phase²³⁹. Although the differences in glucose concentration between the acrophase and bathiphase are not dramatic, having the acrophase values at bathiphase time would be a prediabetic symptom, while having the reverse would be a sign of acute hypoglycemia. However how these variations are controlled so accurately in time was not fully understood.

Our data give a mechanistic explanation of basal glycemia whereby the SCN drives tanycytemediated entry of glucose from the CSF and ME into the ARC, a brain area involved in adjusting glycemia. A high influx of glucose promotes a decrease in circulating levels just before the onset of sleep; while anticipating the activity period, a reduction in SCN-AVP input leads to a decrease in glucose entrance into the ARC, resulting in a gradual increase in glycemia (Fig. D1). Glucose influx into the ventral ARC and the VP dependent expression of GLUT1 in the β_1 tanycytes at the 3V border indicate that ventricular tanycytes mediate the primary regulation of glucose access to the ARC and, marginally, the ARC/ME barrier.

What we propose is in contrast with what was assumed for a long time: glucose concentration in the whole brain always follows the peripheral glucose concentration. Under basal conditions at different time points, we observed that glucose entry into the ARC milieu is inversely proportional to the values in the periphery. Similarly, we also found that in a fasting state at different times of the day, the GLUT1 immunoreactivity is inversely proportional to glycemia. Similar findings considering fasting, were found by another group that showed glucose entrance into the ARC during fasting, to be inverse to peripheral glycemia¹⁷⁹. This led us to propose that glucose flux into the ARC sets, at least in part, the concentration of peripheral glycemia.

Likely, the general assumption about the peripheral glycemia being mirrored into the whole brain still applies for regions using glucose exclusively as a fueling molecule such as the hippocampus, cortex motor etc., but not for nuclei using this same molecule for regulatory functions such as the ARC.

Our contribution considering the circuit for glycemia regulation, would lie in having described the role of the ARC via tanycyte-neuron interactions and its participation detecting glucose in real time. Given the reciprocal connection with the SCN, the ARC then can integrate the time signal (conveyed by the SCN) with the rest of the glucose regulatory circuitry.

The SCN neurons coordinating the changes in glucose entrance into the ARC are, at least, the AVP⁺. These neurons also consist of several diverse populations targeting different areas; hereby, the SCN, via the activity rhythm of the SCN^{AVP} neurons, might regulate different synchronous processes, all associated with the resting phase: (1) SCN^{AVP} projections to the PVN inhibit corticosterone secretion during the light period primarily via PVN autonomic projections influencing the adrenal. (2) SCN^{AVP} projections to the medial preoptic area (MnPO) mediate the

decrease in body temperature at the beginning of the resting phase. (3) SCN^{AVP} projections to the OVLT elicit drinking behavior just before the resting phase. And (4) SCN^{AVP} neurons are also essential to lower glycemia before and at the beginning of the rest period.

The interconnection of the SCN-ARC, first evidenced by early tracing studies^{96,240,241}, has been recognized as an essential interaction for expressing certain rhythms, such as locomotor and corticosterone rhythms⁹⁷. Another direct consequence of this SCN-ARC interaction is the SCN-dependent activity acrophase of a small population of POMC neurons, essential for the correct timing of the daily decrease in temperature whereby the interplay of SCN^{VP} neurons and ARC^{POMC} neurons plays an essential role⁷³.

The methods and techniques used in the present study allow us to suggest that the vasopressin regulating tanycyte GLUT1 mainly comes from neuronal terminals on the tanycytes, and not from the 3V, since unilateral ablation of the SCN induces unilateral diminishment in Evans Blue penetration, and GLUT1 immunoreactivity. However, the high density of V1aR in the tanycytes lining the 3V at the level of the ARC and VMH may indicate these cells could also play a role in transmitting the rhythmic vasopressin from the 3V into these hypothalamic nuclei. One of the

◀ Fig. D1 Graphical summary.

Suprachiasmatic nucleus

regulates access of circulating glucose into the arcuate. Via vasopressin the SCN drives tanyocyte-mediated entry of glucose

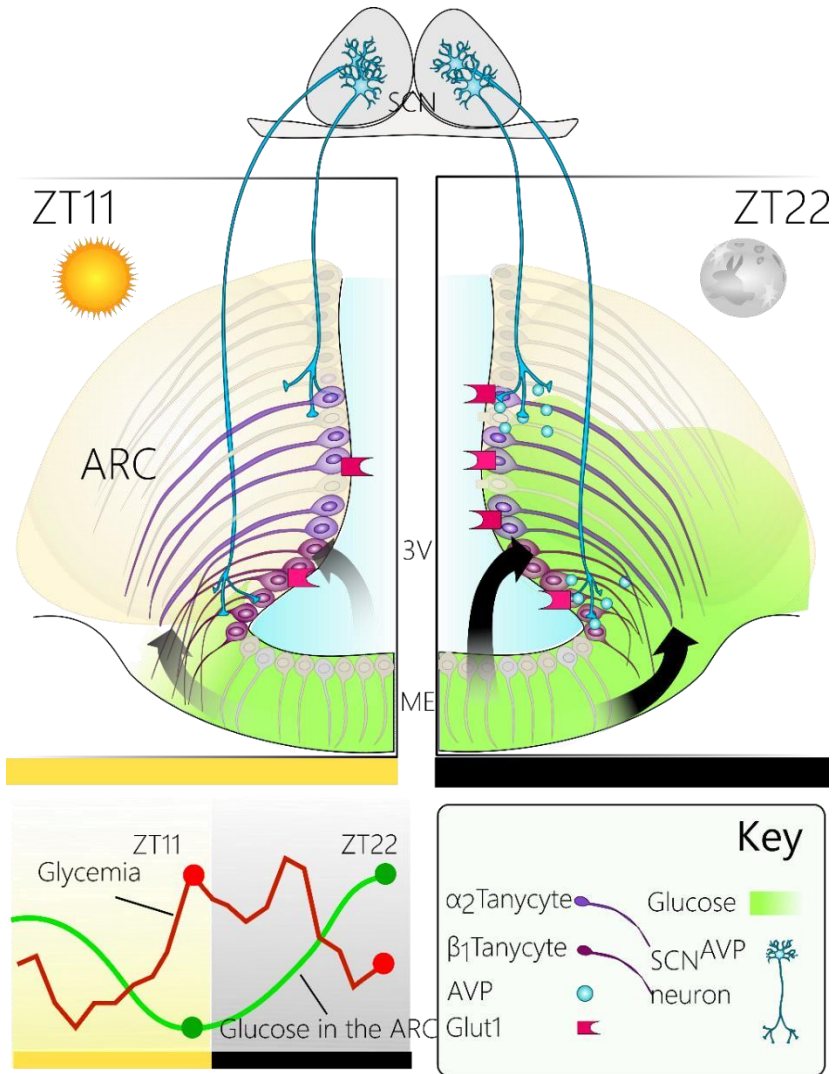
into the ARC and this SCN-vasopressin-driven glucose entrance into the ARC lowers blood glucose levels prior the resting phase. This tanyocyte-mediated entry of glucose into the arcuate nucleus explains not only circadian variations in peripheral blood glucose but we think it is a general mechanism adjusting glycemia in fasting states.

implications of what we described here might imply that tanyocytes play an extra role internalizing the SCN^{AVP} from the ventricle and taking it to the neurons in the VMH or ARC.

Noticeably, tanyocytes and astrocytes, but not neurons, are in direct contact with the cerebrospinal fluid and blood vessels, and thus ideally positioned to quickly detect glucose

fluctuations through both routes. Besides their location, the notion that tanyocytes could participate in glucose regulation is also based on the glucose-sensing properties these cells show. For example, they express GLUT2, GK, and KATP channels¹⁷⁶, crucial elements in glucose detection. The first association between diabetes and tanyocytes dates back to the 1980s when Bestetti and Rossi²⁴⁵ showed that peripheral injections of streptozotocin, a toxic agent for glucose sensing β cell leading to diabetes, induced profound alteration in tanyocyte morphology. Later, it was found that tanyocytes can initiate a calcium wave through taste receptors in response to glucose analogs^{246,247}.

Comparable results were observed upon alloxan injection (another killer of insulin-producing β cells) in the third ventricle. A central injection of alloxan, a pharmacological inhibitor of the glucokinase (GK) activity leads to the destruction of the α and β 1 tanyocytes, and a concomitant impairment in glucose counterregulation, as well as higher fasting glycemia¹⁵⁵. Noticeably, the failure in glucose counterregulation was reversed with restoring the tanyocyte layer.



The need for a dedicated glucose sensor cell populations that are not ARC neurons is further supported by evidence showing that POMC neurons cannot detect glucose fluctuations by themselves²⁴⁸. Further experiments in awake, freely-moving, and healthy animals subject to peripheral changes in glycemia could demonstrate this. Our observation that increasing glucose in the ARC has an opposite effect on peripheral glucose levels merits further analysis to understand which ARC neurons are involved in this circadian regulation.

Finally, in 1964 Anand²⁴² and Oomura²⁴³, almost at the same time discovered the so-called “glucose-sensitive” neurons in the hypothalamus, one using cats and the other dogs²⁴⁴. Later, further work from Oomura’s laboratory demonstrated that activity of hypothalamic neurons was directly influenced by glucose *in vitro*²⁴⁵, they named *glucose responsive*, the neurons increasing their activity upon glucose injections, and *glucose sensitive*, those that decreased their activity as glucose increased²⁴³. Today we classify these types of neurons as glucose-excited (GE) if they increase their electrical activity when glucose level rises, and glucose-inhibited (GI) those neurons getting hyperpolarized upon glucose increase in the bath.

Despite the well-defined concepts explaining the GI and GE functioning, the evidence backing the theory of neuronal glucose sensing, initially harvested either *in vitro* or using nonphysiological glucose concentrations, have not been confirmed in awake animals under basal conditions. The main issue with these studies is that the techniques used to characterize GI and GE skip the existence of the blood-brain barrier.

For neurons to be considered glucose sensors, they should meet minimal criteria as the following, but not limited to:

- 1) Graded and proportional responses according to the glucose concentration in the circulation
- 2) Functional glucose detection operating in parallel with intact BBB
- 3) Connected to integrative nuclei or to the autonomic nervous system (ANS), the effector branch

Point 1 and 2. Until now there is no direct evidence showing the functioning, let alone defining GE or GI neurons in non-anesthetized free-moving animals, using graded changing glucose concentrations within physiological ranges.

A fruitful comparison of the glucose detection theory needs to compare this system with osmosensitive neuronal mechanisms. Here, researchers have measured action potentials elicited upon intraperitoneal injection (i.p.) or oral salt solutions with different concentration of sodium chloride, in awake, free moving mice, in real time²⁴⁶. A similar approach could clarify the real potential of the supposedly glucose sensitive neurons. Assuming that such injections do not disturb sensory systems in the stomach or intestine....

Point 3. Tanycytes might transmit glycemia information to ARC neurons (α_2 and β_1 tanycyte processes contact ARC neurons²⁴⁷), either in form of lactate, or other intermediary molecules, as suggested in a recent study¹⁵⁰. From that, the ARC, a hub for metabolic integration, would

transduce the computed output to downstream nuclei, finally modulating peripheral organs via the autonomous nervous system (ANS). These downstream nuclei connected with the ARC include at least the PVN, BNST, PBN and NTS^{113,232,248–250}. ARC^{AgRP}, via dedicated networks, can modify the insulin release from the pancreas, as the chemogenetic activation of AgRP neurons induces acute peripheral insulin resistance, increasing plasma insulin within one hour without changes in glucagon or corticosterone levels¹¹³.

The basal physiology of living organisms is cyclical and fluctuates through the 24 h; therefore, the comprehension of critical physiological variables, as glycemia, could benefit if we treat them as circadian variables. Further understanding of the mechanisms by which the SCN establishes different circadian setpoints in physiology is relevant, especially for type 2 diabetes, where the daily increase in glycemia before activity onset is still present, despite the already high circulating glucose⁶⁴, or as in diabetes type 1 where nocturnal hypoglycemia is recurrent^{65,66}. Consequently, the dynamic way the SCN influences these setpoints is another variable that needs to be considered when studying these diseases.

9 Perspectives

While the neuron-neuron communication between the SCN and its targets is the most studied, the communication of SCN neurons with non-neuronal populations remains poorly explored. Here, we suggest an anatomical association between SCN^{AVP} neurons and tanycytes. The soma of the tanycytes contacts the ventricular fluid in the 3V, while their single process penetrates into the brain parenchyma.

Given that 1). SCN^{AVP} fibers traverse the walls of the 3V, surrounding the somata and processes of tanycytes; and 2) removing just one side of the SCN, induces an ipsilateral change in tanycyte morphology and modifies the expression of a glucose receptor (GLUT1); in future studies we will try to demonstrate that SCN^{AVP} neurons communicate functionally with tanycytes (a neuron-tanycyte interaction). Since one of the main strategies used by the SCN is to fine-tune regulatory processes according to the circadian cycle, which is achieved by changing the sensitivity of sensory structures according to the time of the day; and that given the tanycyte properties as massive chemosensors; we will also test whether the SCN can to modulate tanycytic sensitivity according to the time of the day.

10 Tanycytes targets for treatment in type 2 diabetes?

Copious documentation evidenced that desynchronizing our daily life from the environmental cycles, such as in nocturnal workers, leads to severe metabolic disturbances^{251–253}. Indeed, circadian desynchronization has been recognized as a major risk factor for developing metabolic syndrome; reducing life quality and lifespan of people from all socioeconomic backgrounds (reviewed in^{254–256}). The most straightforward solution to this problem would be to avoid latenight activities; however, this is not possible for essential night workers such as nurses, and emergency room physicians. Despite the clear correlations between circadian desynchrony and

the surge of metabolic disorders, we have not developed measurements to ameliorate the health costs for medical personnel, for example.

As the scientific focus of circadian neurobiology moves increasingly to cellular and molecular studies, how will these elegant molecular explanations enhance the life quality of people from all economic contexts around the world? The need to translate these elegant molecular findings from basic research, into tools to improve the metabolic/mental health of the world population is still unsatisfactory.

In the model we propose, the circadian dysregulation due to night work could impair circadian ARC glucose entrance, resulting in increased glycemia at night, increasing the risks of developing metabolic syndrome and Type 2 diabetes. Tanycytes are putative players in the pathophysiology of these diseases, consequently becoming potential targets for new treatments thanks to their accessible anatomical position²⁵⁷.

11 Acknowledgements

Agradezco al Programa de Doctorado en Ciencias Biomédicas, UNAM por la formación recibida, el apoyo económico proveído por el Consejo Nacional de Ciencia y Tecnología (CONACyT) (CVU/número de beca: 646866/626173). También agradezco el financiamiento PAPIIT DGAPA IG-201321, al Instituto de Investigaciones Biomédicas, UNAM, y a la biblioteca “Dionisio Nieto Gómez” y a su personal (Lic Lucía Brito Ocampo y a María Petra Muñoz García) por sus excelente servicios bibliotecarios.

12 Bibliography

1. Prasai, M. J., Pernicova, I., Grant, P. J. & Scott, E. M. An Endocrinologist's Guide to the Clock. *J. Clin. Endocrinol. Metab.* **96**, 913–922 (2011).
2. Weaver, D. R. The Suprachiasmatic Nucleus: A 25-Year Retrospective. *J. Biol. Rhythms* **13**, 100–112 (1998).
3. Hastings, M. H., Maywood, E. S. & Brancaccio, M. Generation of circadian rhythms in the suprachiasmatic nucleus. *Nat. Rev. Neurosci.* **2018 198** **19**, 453–469 (2018).
4. Konopka, R. J. & Benzer, S. Clock mutants of *Drosophila melanogaster*. *Proc. Natl. Acad. Sci. U. S. A.* **68**, 2112–2116 (1971).
5. Vitaterna, M. H. *et al.* Mutagenesis and mapping of a mouse gene, clock, essential for circadian behavior. *Science (80-.)*. **264**, 719–725 (1994).
6. Colwell, C. S. Linking neural activity and molecular oscillations in the SCN. *Nat. Rev. Neurosci.* **12**, 553–69 (2011).
7. Patton, A. P. & Hastings, M. H. The suprachiasmatic nucleus. *Curr. Biol.* **28**, R816–R822 (2018).
8. Deery, M. J. *et al.* Proteomic Analysis Reveals the Role of Synaptic Vesicle Cycling in Sustaining the Suprachiasmatic Circadian Clock. *Curr. Biol.* **19**, 2031–2036 (2009).
9. Chiang, C. K. *et al.* The Proteomic Landscape of the Suprachiasmatic Nucleus Clock Reveals Large-Scale Coordination of Key Biological Processes. *PLoS Genet.* **10**, e1004695 (2014).
10. Akhtar, R. A. *et al.* Circadian cycling of the mouse liver transcriptome, as revealed by cDNA microarray, is driven by the suprachiasmatic nucleus. *Curr. Biol.* **12**, 540–550 (2002).
11. Bozek, K. *et al.* Regulation of Clock-Controlled Genes in Mammals. *PLoS One* **4**, e4882 (2009).
12. Zhang, S. L., Yue, Z., Arnold, D. M., Artushin, G. & Sehgal, A. A Circadian Clock in the Blood-Brain Barrier Regulates Xenobiotic Efflux. *Cell* **173**, 130–139.e10 (2018).
13. Lavery, D. J. & Schibler, U. *Circadian transcription of the cholesterol 7 α hydroxylase gene may involve the liver-enriched bZIP protein DBP.* <http://genesdev.cshlp.org/content/7/10/1871.full.pdf>.
14. Mitropoulos, K. A., Balasubramaniam, S., Gibbons, G. F. & Reeves, B. E. A. *Diurnal variation in the activity of cholesterol 7- α -hydroxylase in the livers of fed and fasted rats.* vol. 27 <https://febs.onlinelibrary.wiley.com/doi/pdf/10.1016/0014-5793%2872%292980620-3> (1972).
15. Damiola, F. *et al.* Restricted feeding uncouples circadian oscillators in peripheral tissues from the central pacemaker in the suprachiasmatic nucleus. *Rabinowitz* (1996) doi:10.1101/gad.183500.
16. Lavery, D. J. *et al.* *Circadian Expression of the Steroid 15-Hydroxylase (Cyp2a4) and Coumarin 7-Hydroxylase (Cyp2a5) Genes in Mouse Liver Is Regulated by the PAR Leucine Zipper Transcription Factor DBP.* *MOLECULAR AND CELLULAR BIOLOGY* vol. 19 <http://mcb.asm.org/> (1999).
17. Ishikawa, K. & Shimazu, T. *Daily rhythms of glycogen synthetase and phosphorilase activities in rat liver: influences of food and light.* *Life Sciences* vol. 19 https://ac.els-cdn.com/0024320576901193/1-s2.0-0024320576901193-main.pdf?_tid=7fdec500-c3db-4484-ad82-770e54325c39&acdnat=1540255794_c697312c096773900f560a6916237e93 (1976).

18. Guo, H., Brewer, J. M., Champhekar, A., Harris, R. B. S. & Bittman, E. L. *Differential control of peripheral circadian rhythms by suprachiasmatic-dependent neural signals.* www.pnas.org/cgi/doi/10.1073/pnas.0409734102 (2005).
19. Reddy, A. B. *et al.* Glucocorticoid signaling synchronizes the liver circadian transcriptome. *Hepatology* **45**, 1478–1488 (2007).
20. Terazono, H. *et al.* Adrenergic regulation of clock gene expression in mouse liver. *Proc. Natl. Acad. Sci.* **100**, 6795–6800 (2003).
21. Kalsbeek, A., Fleur, S. La, Heijningen, C. Van & Buijs, R. M. Suprachiasmatic GABAergic Inputs to the Paraventricular Nucleus Control Plasma Glucose Concentrations in the Rat via Sympathetic Innervation of the Liver. *J. Neurosci.* **24**, 7604–7613 (2004).
22. Lang, C. H. Inhibition of Central GABAA Receptors Enhances Hepatic Glucose Production and Peripheral Glucose Uptake. *Brain Res. Bull.* **37**, 611–616 (1995).
23. Cailotto, C. *et al.* The suprachiasmatic nucleus controls the daily variation of plasma glucose via the autonomic output to the liver: are the clock genes involved? *Eur. J. Neurosci.* **22**, 2531–2540 (2005).
24. Lamont, E. W., Robinson, B., Stewart, J. & Amir, S. The central and basolateral nuclei of the amygdala exhibit opposite diurnal rhythms of expression of the clock protein Period2. *Proc. Natl. Acad. Sci. U. S. A.* **102**, 4180–4184 (2005).
25. Feillet, C. A., Mendoza, J., Albrecht, U., Pévet, P. & Challet, E. Forebrain oscillators ticking with different clock hands. *Mol. Cell. Neurosci.* **37**, 209–221 (2008).
26. Amir, S., Lamont, E. W., Robinson, B. & Stewart, J. A Circadian Rhythm in the Expression of PERIOD2 Protein Reveals a Novel SCN-Controlled Oscillator in the Oval Nucleus of the Bed Nucleus of the Stria Terminalis. *J. Neurosci.* **24**, 781–790 (2004).
27. Cermakian, N., Waddington Lamont, E., Boudreau, P. & Boivin, D. B. Circadian clock gene expression in brain regions of Alzheimer's disease patients and control subjects. *J. Biol. Rhythms* **26**, 160–170 (2011).
28. Colwell, C. S. Linking neural activity and molecular oscillations in the SCN. *Nat. Rev. Neurosci.* *2011 1210* **12**, 553–569 (2011).
29. Legates, T. A., Fernandez, D. C. & Hattar, S. Light as a central modulator of circadian rhythms, sleep and affect. *Nat. Rev. Neurosci.* *2014 157* **15**, 443–454 (2014).
30. Fernandez, D. C., Chang, Y. T., Hattar, S. & Chen, S. K. Architecture of retinal projections to the central circadian pacemaker. *Proc. Natl. Acad. Sci. U. S. A.* **113**, 6047–6052 (2016).
31. Evans, J. A., Leise, T. L., Castanon-Cervantes, O. & Davidson, A. J. Dynamic interactions mediated by nonredundant signaling mechanisms couple circadian clock neurons. *Neuron* **80**, 973–983 (2013).
32. Honma, S., Shirakawa, T., Nakamura, W. & Honma, K. I. Synaptic communication of cellular oscillations in the rat suprachiasmatic neurons. *Neurosci. Lett.* **294**, 113–116 (2000).
33. CASTEL, M. & MORRIS, J. F. Morphological heterogeneity of the GABAergic network in the suprachiasmatic nucleus, the brain's circadian pacemaker. *J. Anat.* **196 (Pt 1)**, 1–13 (2000).

34. Albus, H., Vansteensel, M. J., Michel, S., Block, G. D. & Meijer, J. H. A GABAergic mechanism is necessary for coupling dissociable ventral and dorsal regional oscillators within the circadian clock. *Curr. Biol.* **15**, 886–893 (2005).
35. Pauls, S. D., Honma, K. I., Honma, S. & Silver, R. Deconstructing Circadian Rhythmicity with Models and Manipulations. *Trends Neurosci.* **39**, 405–419 (2016).
36. Taub, A. *et al.* Arginine Vasopressin-Containing Neurons of the Suprachiasmatic Nucleus Project to CSF. *eNeuro* **8**, (2021).
37. Colwell, C. S. *et al.* Disrupted circadian rhythms in VIP- and PHI-deficient mice. *Am. J. Physiol. - Regul. Integr. Comp. Physiol.* **285**, 939–949 (2003).
38. Harmar, A. J. *et al.* The VPAC2 Receptor Is Essential for Circadian Function in the Mouse Suprachiasmatic Nuclei. *Cell* **109**, 497–508 (2002).
39. Hastings, M. H., Brancaccio, M. & Maywood, E. S. Circadian Pacemaking in Cells and Circuits of the Suprachiasmatic Nucleus. *J. Neuroendocrinol.* **26**, 2–10 (2014).
40. Maywood, E. S., Chesham, J. E., O'Brien, J. A. & Hastings, M. H. A diversity of paracrine signals sustains molecular circadian cycling in suprachiasmatic nucleus circuits. *Proc. Natl. Acad. Sci. U. S. A.* **108**, 14306–14311 (2011).
41. Welsh, D. K., Takahashi, J. S. & Kay, S. A. Suprachiasmatic nucleus: Cell autonomy and network properties. *Annu. Rev. Physiol.* **72**, 551–577 (2009).
42. Wen, S. *et al.* Spatiotemporal single-cell analysis of gene expression in the mouse suprachiasmatic nucleus. *Nat. Neurosci.* **2020 233 23**, 456–467 (2020).
43. Prosser, H. M. *et al.* Prokineticin receptor 2 (Prokr2) is essential for the regulation of circadian behavior by the suprachiasmatic nuclei. *Proc. Natl. Acad. Sci. U. S. A.* **104**, 648–653 (2007).
44. Zhou, Q. Y. & Cheng, M. Y. Prokineticin 2 and circadian clock output. *FEBS J.* **272**, 5703–5709 (2005).
45. Lu, Q. & Kim, J. Y. Mammalian circadian networks mediated by the suprachiasmatic nucleus. *FEBS J.* (2021) doi:10.1111/FEBS.16233.
46. Silver, R. *et al.* Multiple regulatory elements result in regional specificity in circadian rhythms of neuropeptide expression in mouse SCN. *Neuroreport* **10**, 3165–3174 (1999).
47. Jin, X. *et al.* A Molecular Mechanism Regulating Rhythmic Output from the Suprachiasmatic Circadian Clock. *Cell* **96**, 57–68 (1999).
48. Jones, J. R., Tackenberg, M. C. & McMahon, D. G. Manipulating circadian clock neuron firing rate resets molecular circadian rhythms and behavior. *Nat. Neurosci.* **2015 183 18**, 373–375 (2015).
49. Meng, Q. J. *et al.* Setting Clock Speed in Mammals: The CK1 ϵ tau Mutation in Mice Accelerates Circadian Pacemakers by Selectively Destabilizing PERIOD Proteins. *Neuron* **58**, 78–88 (2008).
50. Brancaccio, M., Patton, A. P., Chesham, J. E., Maywood, E. S. & Hastings, M. H. Astrocytes Control Circadian Timekeeping in the Suprachiasmatic Nucleus via Glutamatergic Signaling. *Neuron* **93**, 1420–1435.e5 (2017).
51. Santos, J. W. Q. *et al.* Circadian variation in GFAP immunoreactivity in the mouse suprachiasmatic nucleus. <https://doi.org/10.1080/09291010400028906> **36**, 141–150 (2007).

52. Lavialle, M. & Servière, J. Developmental study in the circadian clock of the golden hamster: a putative role of astrocytes. *Dev. Brain Res.* **86**, 275–282 (1995).
53. Prosser, R. A., Edgar, D. M., Craig Heller, H. & Miller, J. D. A possible glial role in the mammalian circadian clock. *Brain Res.* **643**, 296–301 (1994).
54. Prolo, L. M., Takahashi, J. S. & Herzog, E. D. Circadian Rhythm Generation and Entrainment in Astrocytes. *J. Neurosci.* **25**, 404–408 (2005).
55. Barca-Mayo, O. *et al.* Astrocyte deletion of Bmal1 alters daily locomotor activity and cognitive functions via GABA signalling. *Nat. Commun.* **2017 81 8**, 1–14 (2017).
56. Brancaccio, M., Patton, A. P., Chesham, J. E., Maywood, E. S. & Hastings, M. H. Astrocytes Control Circadian Timekeeping in the Suprachiasmatic Nucleus via Glutamatergic Signaling. *Neuron* **93**, 1420-1435.e5 (2017).
57. Tso, C. F. *et al.* Astrocytes Regulate Daily Rhythms in the Suprachiasmatic Nucleus and Behavior. *Curr. Biol.* **27**, 1055–1061 (2017).
58. Gachon, F., Nagoshi, E., Brown, S. A., Ripperger, J. & Schibler, U. The mammalian circadian timing system: from gene expression to physiology. *Chromosoma* **113**, 103–112 (2004).
59. Buijs, R. M. & Kalsbeek, A. Hypothalamic integration of central and peripheral clocks. *Nat. Rev. Neurosci.* **2**, 521–526 (2001).
60. Decker, M. J., Rye, D. B., Lee, S. Y. & Strohl, K. P. Paradoxical Sleep Suppresses Immediate Early Gene Expression in the Rodent Suprachiasmatic Nuclei. *Front. Neurol.* **1**, (2010).
61. PJ, L., LW, E. & JP, C. Characterization of the multisynaptic neuronal control of the rat pineal gland using viral transneuronal tracing. *Eur. J. Neurosci.* **10**, 128–145 (1998).
62. Moore, R. Y. Neural control of the pineal gland. *Behav. Brain Res.* **73**, 125–130 (1996).
63. Moore, R. Y. Entrainment pathways and the functional organization of the circadian system. *Prog. Brain Res.* **111**, 103–119 (1996).
64. Roseboom, P. H. *et al.* Melatonin synthesis: analysis of the more than 150-fold nocturnal increase in serotonin N-acetyltransferase messenger ribonucleic acid in the rat pineal gland. *Endocrinology* **137**, 3033–3045 (1996).
65. Pevet, P. & Challet, E. Melatonin: Both master clock output and internal time-giver in the circadian clocks network. *J. Physiol.* **105**, 170–182 (2011).
66. Mrosovsky, N. *Rheostasis: The physiology of change.* (Oxford University Press, 1990).
67. Buijs, R. M., Guzmán Ruiz, M. A., Méndez Hernández, R. & Rodríguez Cortés, B. The suprachiasmatic nucleus; a responsive clock regulating homeostasis by daily changing the setpoints of physiological parameters. *Auton. Neurosci.* **218**, 43–50 (2019).
68. Schwartz, W. J. & Reppert, S. M. Neural regulation of the circadian vasopressin rhythm in cerebrospinal fluid: A pre-eminent role for the suprachiasmatic nuclei. *J. Neurosci.* **5**, 2771–2778 (1985).
69. Jolkkonen, J., Tuomisto, L., van Wimersma Greidanus, T. B. & Riekkinen, P. J. Vasopressin levels in the cerebrospinal fluid of rats with lesions of the paraventricular and suprachiasmatic nuclei. *Neurosci. Lett.* **86**, 184–188 (1988).

70. Södersten, P., De Vries, G. J., Buijs, R. M. & Melin, P. A daily rhythm in behavioral vasopressin sensitivity and brain vasopressin concentrations. *Neurosci. Lett.* **58**, 37–41 (1985).
71. Kalsbeek, A., Heerikhuizen, J. J. van, Wortel, J. & Buijs, R. M. A Diurnal Rhythm of Stimulatory Input to the Hypothalamo–Pituitary–Adrenal System as Revealed by Timed Intrahypothalamic Administration of the Vasopressin V1 Antagonist. *J. Neurosci.* **16**, 5555–5565 (1996).
72. Kalsbeek, A., Van Der Vliet, J. & Buijs, R. M. Decrease of endogenous vasopressin release necessary for expression of the circadian rise in plasma corticosterone: A reverse microdialysis study. *J. Neuroendocrinol.* **8**, 299–307 (1996).
73. Guzmán-Ruiz, M. *et al.* The suprachiasmatic nucleus changes the daily activity of the arcuate nucleus α -MSH neurons in male rats. *Endocrinology* **155**, 525–535 (2014).
74. Gizowski, C., Zaelzer, C. & Bourque, C. W. Clock-driven vasopressin neurotransmission mediates anticipatory thirst prior to sleep. *Nature* **537**, 685–688 (2016).
75. Leak, R. K. & Moore, R. Y. Innervation of Ventricular and Periventricular Brain Compartments. *Brain Res.* **1463**, 51 (2012).
76. Padilla, S. L. *et al.* Kisspeptin Neurons in the Arcuate Nucleus of the Hypothalamus Orchestrate Circadian Rhythms and Metabolism. *Curr. Biol.* **29**, 592–604.e4 (2019).
77. Guzmán-Ruiz, M. A. *et al.* Role of the suprachiasmatic and arcuate nuclei in diurnal temperature regulation in the rat. *J. Neurosci.* **35**, 15419–15429 (2015).
78. Gizowski, C. & Bourque, C. W. Sodium regulates clock time and output via an excitatory GABAergic pathway. *Nature* **583**, 421–424 (2020).
79. Gizowski, C., Zaelzer, C. & Bourque, C. W. Activation of organum vasculosum neurons and water intake in mice by vasopressin neurons in the suprachiasmatic nucleus. *J. Neuroendocrinol.* **30**, (2018).
80. Buijs, R. M. Anatomical and functional demonstration of a multisynaptic suprachiasmatic nucleus adrenal (cortex) pathway. *Eur. J. Neurosci.* **11**, 1535–1544 (1999).
81. Ulrich-Lai, Y. M., Arnhold, M. M. & Engeland, W. C. Adrenal splanchnic innervation contributes to the diurnal rhythm of plasma corticosterone in rats by modulating adrenal sensitivity to ACTH. *Am. J. Physiol. Regul. Integr. Comp. Physiol.* **290**, (2006).
82. Ishida, A. *et al.* Light activates the adrenal gland: Timing of gene expression and glucocorticoid release. *Cell Metab.* **2**, 297–307 (2005).
83. Lehman, M. N. *et al.* Circadian rhythmicity restored by neural transplant. Immunocytochemical characterization of the graft and its integration with the host brain. *J. Neurosci.* **7**, 1626–1638 (1987).
84. Ralph, M. R., Foster, R. G., Davis, F. C. & Menaker, M. Transplanted suprachiasmatic nucleus determines circadian period. *Science* **247**, 975–978 (1990).
85. Lesauter, J., Romero, P., Cascio, M. & Silver, R. Attachment site of grafted SCN influences precision of restored circadian rhythm. *J. Biol. Rhythms* **12**, 327–338 (1997).
86. Ahissar, E. *et al.* A diffusible coupling signal from the transplanted suprachiasmatic nucleus controlling circadian locomotor rhythms. *Nat.* **382**, 810–813 (1996).

87. Silver, R., LeSauter, J., Tresco, P. A. & Lehman, M. N. A diffusible coupling signal from the transplanted suprachiasmatic nucleus controlling circadian locomotor rhythms. *Nature* vol. 382 810–813 (1996).
88. Kramer, A. *et al.* Regulation of Daily Locomotor Activity and Sleep by Hypothalamic EGF Receptor Signaling. *Science (80-.)*. **294**, 2511–2515 (2001).
89. Prosser, H. M. *et al.* Prokineticin receptor 2 (Prokr2) is essential for the regulation of circadian behavior by the suprachiasmatic nuclei. *Proc. Natl. Acad. Sci. U. S. A.* **104**, 648–653 (2007).
90. Cheng, M. Y. *et al.* Prokineticin 2 transmits the behavioural circadian rhythm of the suprachiasmatic nucleus. *Nature* **417**, 405–410 (2002).
91. Kraves, S. & Weitz, C. J. A role for cardiotrophin-like cytokine in the circadian control of mammalian locomotor activity. *Nat. Neurosci.* 2006 92 **9**, 212–219 (2006).
92. Ono, D., Honma, S. & Honma, K. ichi. Differential roles of AVP and VIP signaling in the postnatal changes of neural networks for coherent circadian rhythms in the SCN. *Sci. Adv.* **2**, (2016).
93. Buijs, R. M., Hurtado-Alvarado, G. & Soto-Tinoco, E. Vasopressin: An output signal from the suprachiasmatic nucleus to prepare physiology and behaviour for the resting phase. *J. Neuroendocrinol.* **33**, e12998 (2021).
94. Yao, Y., Taub, A. B., LeSauter, J. & Silver, R. Identification of the suprachiasmatic nucleus venous portal system in the mammalian brain. *Nat. Commun.* 2021 121 **12**, 1–9 (2021).
95. Prager-Khoutorsky, M. & Bourque, C. W. Anatomical organization of the rat organum vasculosum laminae terminalis. *Am. J. Physiol. - Regul. Integr. Comp. Physiol.* **309**, R324–R337 (2015).
96. Yi, C. X. *et al.* Ventromedial arcuate nucleus communicates peripheral metabolic information to the suprachiasmatic nucleus. *Endocrinology* **147**, 283–294 (2006).
97. Buijs, F. N. *et al.* Suprachiasmatic nucleus interaction with the arcuate nucleus; Essential for organizing physiological rhythms. *eNeuro* **4**, (2017).
98. Jais, A. & Brüning, J. C. Arcuate Nucleus-Dependent Regulation of Metabolism—Pathways to Obesity and Diabetes Mellitus. *Endocr. Rev.* **43**, 314–328 (2022).
99. Balland, E. *et al.* Hypothalamic Tanycytes Are an ERK-Gated Conduit for Leptin into the Brain. *Cell Metab.* **19**, 293–301 (2014).
100. Uyama, N., Geerts, A. & Reynaert, H. Neural connections between the hypothalamus and the liver. *Anat. Rec. - Part A Discov. Mol. Cell. Evol. Biol.* **280**, 808–820 (2004).
101. Elias, C. F. *et al.* Leptin Activates Hypothalamic CART Neurons Projecting to the Spinal Cord. *Neuron* **21**, 1375–1385 (1998).
102. Leon-Mercado, L. *et al.* The Arcuate Nucleus: A Site of Fast Negative Feedback for Corticosterone Secretion in Male Rats. *eNeuro* **4**, ENEURO.0350-16.2017 (2017).
103. Chami, N., Preuss, M., Walker, R. W., Moscati, A. & Loos, R. J. F. The role of polygenic susceptibility to obesity among carriers of pathogenic mutations in MC4R in the UK Biobank population. *PLoS Med.* **17**, (2020).
104. Yeo, G. S. H. *et al.* A frameshift mutation in MC4R associated with dominantly inherited human obesity. *Nat. Genet.* **20**, 111–112 (1998).

105. Ollmann, M. M. *et al.* Antagonism of central melanocortin receptors in vitro and in vivo by agouti-related protein. *Science* **278**, 135–138 (1997).
106. Aponte, Y., Atasoy, D. & Sternson, S. M. AGRP neurons are sufficient to orchestrate feeding behavior rapidly and without training. *Nat. Neurosci.* *2011 143* **14**, 351–355 (2011).
107. Beutler, L. R. *et al.* Dynamics of Gut-Brain Communication Underlying Hunger. *Neuron* **96**, 461475.e5 (2017).
108. Tong, Q., Ye, C. P., Jones, J. E., Elmquist, J. K. & Lowell, B. B. Synaptic release of GABA by AgRP neurons is required for normal regulation of energy balance. *Nat. Neurosci.* *2008 119* **11**, 998–1000 (2008).
109. Krashes, M. J., Shah, B. P., Koda, S. & Lowell, B. B. Rapid versus delayed stimulation of feeding by the endogenously released AgRP neuron mediators GABA, NPY, and AgRP. *Cell Metab.* **18**, 588–595 (2013).
110. Dicken, M. S., Hughes, A. R. & Hentges, S. T. Gad1 mRNA as a reliable indicator of altered GABA release from orexigenic neurons in the hypothalamus. *Eur. J. Neurosci.* **42**, 2644–2653 (2015).
111. Engström Ruud, L., Pereira, M. M. A., de Solis, A. J., Fenselau, H. & Brüning, J. C. NPY mediates the rapid feeding and glucose metabolism regulatory functions of AgRP neurons. *Nat. Commun.* *2020 111* **11**, 1–12 (2020).
112. Betley, J. N., Cao, Z. F. H., Ritola, K. D. & Sternson, S. M. Parallel, redundant circuit organization for homeostatic control of feeding behavior. *Cell* **155**, (2013).
113. Steculorum, S. M. *et al.* AgRP Neurons Control Systemic Insulin Sensitivity via Myostatin Expression in Brown Adipose Tissue. *Cell* **165**, 125–138 (2016).
114. Atasoy, D., Nicholas Betley, J., Su, H. H. & Sternson, S. M. Deconstruction of a neural circuit for hunger. *Nat.* *2012 4887410* **488**, 172–177 (2012).
115. Luquet, S., Perez, F. A., Hnasko, T. S. & Palmiter, R. D. NPY/AgRP neurons are essential for feeding in adult mice but can be ablated in neonates. *Science* **310**, 683–685 (2005).
116. Gropp, E. *et al.* Agouti-related peptide-expressing neurons are mandatory for feeding. *Nat. Neurosci.* **8**, 1289–1291 (2005).
117. Cavalcanti-de-Albuquerque, J. P., Bober, J., Zimmer, M. R. & Dietrich, M. O. Regulation of substrate utilization and adiposity by Agrp neurons. *Nat. Commun.* *2019 101* **10**, 1–13 (2019).
118. Alhadeff, A. L. *et al.* A Neural Circuit for the Suppression of Pain by a Competing Need State. *Cell* **173**, 140-152.e15 (2018).
119. Betley, J. N. *et al.* Neurons for hunger and thirst transmit a negative-valence teaching signal. *Nat.* *2015 5217551* **521**, 180–185 (2015).
120. Bai, L. *et al.* Genetic Identification of Vagal Sensory Neurons That Control Feeding. *Cell* **179**, 1129-1143.e23 (2019).
121. Harno, E., Ramamoorthy, T. G., Coll, A. P. & White, A. POMC: The physiological power of hormone processing. *Physiol. Rev.* **98**, 2381–2430 (2018).
122. Andermann, M. L. & Lowell, B. B. Toward a Wiring Diagram Understanding of Appetite Control. *Neuron* **95**, 757–778 (2017).

123. Quarta, C., Fioramonti, X. & Cota, D. POMC Neurons Dysfunction in Diet-induced Metabolic Disease: Hallmark or Mechanism of Disease? *Neuroscience* **447**, 3–14 (2020).
124. Krashes, M. J., Lowell, B. B. & Garfield, A. S. Melanocortin-4 receptor-regulated energy homeostasis. *Nat. Neurosci.* **19**, 206–219 (2016).
125. Cone, R. D. Studies on the physiological functions of the melanocortin system. *Endocr. Rev.* **27**, 736–749 (2006).
126. Zhan, C. *et al.* Acute and long-term suppression of feeding behavior by POMC neurons in the brainstem and hypothalamus, respectively. *J. Neurosci.* **33**, 3624–3632 (2013).
127. Quarta, C. *et al.* POMC neuronal heterogeneity in energy balance and beyond: an integrated view. *Nat. Metab.* **3**, 299–308 (2021).
128. Lam, B. Y. H. *et al.* Heterogeneity of hypothalamic pro-opiomelanocortin-expressing neurons revealed by single-cell RNA sequencing. *Mol. Metab.* **6**, 383–392 (2017).
129. Campbell, J. N. *et al.* A molecular census of arcuate hypothalamus and median eminence cell types. *Nat. Neurosci.* **20**, 484–496 (2017).
130. Hentges, S. T., Otero-Corchon, V., Pennock, R. L., King, C. M. & Low, M. J. Proopiomelanocortin expression in both GABA and glutamate neurons. *J. Neurosci.* **29**, 13684–13690 (2009).
131. Jarvie, B. C. & Hentges, S. T. Expression of GABAergic and glutamatergic phenotypic markers in hypothalamic proopiomelanocortin neurons. *J. Comp. Neurol.* **520**, 3863–3876 (2012).
132. Sohn, J. W. *et al.* Serotonin 2C receptor activates a distinct population of arcuate proopiomelanocortin neurons via TRPC channels. *Neuron* **71**, 488–497 (2011).
133. Biglari, N. *et al.* Functionally distinct POMC-expressing neuron subpopulations in hypothalamus revealed by intersectional targeting. *Nat. Neurosci.* **24**, 913–929 (2021).
134. Koch, M. *et al.* Hypothalamic POMC neurons promote cannabinoid-induced feeding. *Nat.* **519**, 45–50 (2015).
135. Chen, Y., Lin, Y. C., Kuo, T. W. & Knight, Z. A. Sensory detection of food rapidly modulates arcuate feeding circuits. *Cell* **160**, 829–841 (2015).
136. Borgmann, D. *et al.* Gut-brain communication by distinct sensory neurons differently controls feeding and glucose metabolism. *Cell Metab.* **33**, 1466-1482.e7 (2021).
137. Paeger, L. *et al.* Energy imbalance alters Ca²⁺ handling and excitability of POMC neurons. *Elife* **6**, (2017).
138. Schneeberger, M. *et al.* Mitofusin 2 in POMC neurons connects ER stress with leptin resistance and energy imbalance. *Cell* **155**, (2013).
139. Diano, S. *et al.* Peroxisome proliferation-associated control of reactive oxygen species sets melanocortin tone and feeding in diet-induced obesity. *Nat. Med.* **17**, 1121–1128 (2011).
140. Tschöp, M. *et al.* Circulating ghrelin levels are decreased in human obesity. *Diabetes* **50**, 707–709 (2001).
141. Cummings, D. E. *et al.* A preprandial rise in plasma ghrelin levels suggests a role in meal initiation in humans. *Diabetes* **50**, 1714–1719 (2001).

142. Shiiya, T. *et al.* Plasma Ghrelin Levels in Lean and Obese Humans and the Effect of Glucose on Ghrelin Secretion. *J. Clin. Endocrinol. Metab.* **87**, 240–244 (2002).
143. Chen, H. Y. *et al.* Orexigenic action of peripheral ghrelin is mediated by neuropeptide Y and agouti-related protein. *Endocrinology* **145**, 2607–2612 (2004).
144. Luquet, S., Phillips, C. T. & Palmiter, R. D. NPY/AgRP neurons are not essential for feeding responses to glucoprivation. *Peptides* **28**, 214–225 (2007).
145. Wang, Q. *et al.* Arcuate AgRP neurons mediate orexigenic and glucoregulatory actions of ghrelin. *Mol. Metab.* **3**, 64–72 (2013).
146. Cowley, M. A. *et al.* The distribution and mechanism of action of ghrelin in the CNS demonstrates a novel hypothalamic circuit regulating energy homeostasis. *Neuron* **37**, 649–661 (2003).
147. Ernst Horstmann, V. DIE FASERGLIA DES SELACHIERGEGHIRNS*. *Bd. 39, S* 588–617 (1954).
148. Langlet, F. Tanycyte gene expression dynamics in the regulation of energy homeostasis. *Front. Endocrinol. (Lausanne)*. **10**, 286 (2019).
149. Prevot, V. *et al.* The versatile tanycyte: A hypothalamic integrator of reproduction and energy metabolism. *Endocr. Rev.* **39**, 333–368 (2018).
150. Lhomme, T. *et al.* Tanycytic networks mediate energy balance by feeding lactate to glucoseinsensitive POMC neurons. *J. Clin. Invest.* **131**, (2021).
151. Duquenne, M. *et al.* Leptin brain entry via a tanycytic LepR–EGFR shuttle controls lipid metabolism and pancreas function. *Nat. Metab.* 2021 **38** **3**, 1071–1090 (2021).
152. Bolborea, M., Pollatzek, E., Benford, H., Sotelo-Hitschfeld, T. & Dale, N. Hypothalamic tanycytes generate acute hyperphagia through activation of the arcuate neuronal network. *Proc. Natl. Acad. Sci. U. S. A.* **117**, 14473–14481 (2020).
153. Mullier, A., Bouret, S. G., Prevot, V. & Dehouck, B. Differential distribution of tight junction proteins suggests a role for tanycytes in blood-hypothalamus barrier regulation in the adult mouse brain. *J. Comp. Neurol.* **518**, 943–962 (2010).
154. Faouzi, M. *et al.* Differential accessibility of circulating leptin to individual hypothalamic sites. *Endocrinology* **148**, 5414–5423 (2007).
155. Sanders, N. M., Dunn-Meynell, A. A. & Levin, B. E. *Third Ventricular Alloxan Reversibly Impairs Glucose Counterregulatory Responses.* (2004).
156. Yoo, S. *et al.* Tanycyte ablation in the arcuate nucleus and median eminence increases obesity susceptibility by increasing body fat content in male mice. *Glia* [glia.23817](https://doi.org/10.1002/glia.23817) (2020) doi:10.1002/glia.23817.
157. Yoo, S., Cha, D., Kim, D. W., Hoang, T. V. & Blackshaw, S. Tanycyte-Independent Control of Hypothalamic Leptin Signaling. *Front. Neurosci.* **13**, 240 (2019).
158. Barahona, M. J. *et al.* Glial hypothalamic inhibition of GLUT2 expression alters satiety, impacting eating behavior. *Glia* **66**, 592–605 (2018).
159. Elizondo-Vega, R. *et al.* Inhibition of hypothalamic MCT1 expression increases food intake and alters orexigenic and anorexigenic neuropeptide expression. *Sci. Reports 2016 61* **6**, 1–13 (2016).

160. Uranga, R. M. *et al.* Adenovirus-mediated suppression of hypothalamic glucokinase affects feeding behavior. *Sci. Rep.* **7**, 1–13 (2017).
161. Bolborea, M., Helfer, G., Ebling, F. J. P. & Barrett, P. Dual signal transduction pathways activated by TSH receptors in rat primary tanycyte cultures. *J. Mol. Endocrinol.* **54**, 241–250 (2015).
162. Broadwell, R. D. & Brightman, M. W. Entry of peroxidase into neurons of the central and peripheral nervous systems from extracerebral and cerebral blood. *J. Comp. Neurol.* **166**, 257–283 (1976).
163. Geller, S. *et al.* Tanycytes Regulate Lipid Homeostasis by Sensing Free Fatty Acids and Signaling to Key Hypothalamic Neuronal Populations via FGF21 Secretion. *Cell Metab.* **30**, 833-844.e7 (2019).
164. Straub, L. & Wolfrum, C. FGF21, energy expenditure and weight loss – How much brown fat do you need? *Mol. Metab.* **4**, 605–609 (2015).
165. Barrett, P. *et al.* Short Photoperiod-Induced Decrease of Histamine H3 Receptors Facilitates Activation of Hypothalamic Neurons in the Siberian Hamster. *Endocrinology* **150**, 3655–3663 (2009).
166. Song, C. K. & Bartness, T. J. CNS sympathetic outflow neurons to white fat that express MEL receptors may mediate seasonal adiposity. *Am. J. Physiol. - Regul. Integr. Comp. Physiol.* **281**, (2001).
167. Kaminskis, B. *et al.* Characterisation of endogenous players in fibroblast growth factor-regulated functions of hypothalamic tanycytes and energy-balance nuclei. *J. Neuroendocrinol.* **31**, (2019).
168. Bentsen, M. A. *et al.* Transcriptomic analysis links diverse hypothalamic cell types to fibroblast growth factor 1-induced sustained diabetes remission. *Nat. Commun.* **2020 111 11**, 1–16 (2020).
169. Hanai, K. *et al.* Central action of acidic fibroblast growth factor in feeding regulation. <https://doi.org/10.1152/ajpregu.1989.256.1.R217> **256**, (1989).
170. Oomura, Y. *et al.* A new brain glucosensor and its physiological significance. *Am. J. Clin. Nutr.* **55**, 278S-282S (1992).
171. Scarlett, J. M. *et al.* Central injection of fibroblast growth factor 1 induces sustained remission of diabetic hyperglycemia in rodents. *Nat. Med.* **22**, 800–806 (2016).
172. Brown, J. M. *et al.* The Hypothalamic Arcuate Nucleus–Median Eminence Is a Target for Sustained Diabetes Remission Induced by Fibroblast Growth Factor 1. *Diabetes* **68**, 1054–1061 (2019).
173. Lelliott, C. J. *et al.* Monoclonal Antibody Targeting of Fibroblast Growth Factor Receptor 1c Ameliorates Obesity and Glucose Intolerance via Central Mechanisms. *PLoS One* **9**, e112109 (2014).
174. Samms, R. J. *et al.* Antibody-Mediated Inhibition of the FGFR1c Isoform Induces a Catabolic Lean State in Siberian Hamsters. *Curr. Biol.* **25**, 2997–3003 (2015).
175. Sun, H. D. *et al.* Monoclonal antibody antagonists of hypothalamic FGFR1 cause potent but reversible hypophagia and weight loss in rodents and monkeys. *Am. J. Physiol. - Endocrinol. Metab.* **292**, 964–976 (2007).
176. Freire-Regatillo, A., Argente-Arizón, P., Argente, J., García-Segura, L. M. & Chowen, J. A. Nonneuronal cells in the hypothalamic adaptation to metabolic signals. *Front. Endocrinol. (Lausanne)*. **8**, 1–24 (2017).

177. Collden, G. *et al.* Neonatal overnutrition causes early alterations in the central response to peripheral ghrelin. *Mol. Metab.* **4**, 15–24 (2015).
178. Langlet, F., Mullier, A., Bouret, S. G., Prevot, V. & Dehouck, B. Tanycyte-like cells form a blood-cerebrospinal fluid barrier in the circumventricular organs of the mouse brain. *J. Comp. Neurol.* **521**, 3389–3405 (2013).
179. Langlet, F. *et al.* Tanycytic VEGF-A boosts blood-hypothalamus barrier plasticity and access of metabolic signals to the arcuate nucleus in response to fasting. *Cell Metab.* **17**, 607–617 (2013).
180. Coppola, A. *et al.* A Central Thermogenic-like Mechanism in Feeding Regulation: An Interplay between Arcuate Nucleus T3 and UCP2. *Cell Metab.* **5**, 21–33 (2007).
181. Langlet, F. *et al.* Tanycytic VEGF-A boosts blood-hypothalamus barrier plasticity and access of metabolic signals to the arcuate nucleus in response to fasting. *Cell Metab.* **17**, 607–617 (2013).
182. Altimus, C. M. *et al.* Rod photoreceptors drive circadian photoentrainment across a wide range of light intensities. *Nat. Neurosci.* **13**, 1107–1112 (2010).
183. Güler, A. D. *et al.* Melanopsin cells are the principal conduits for rod–cone input to non-imageforming vision. *Nat.* **453**, 102–105 (2008).
184. Hastings, M. H. *et al.* Non-photopic signalling in the suprachiasmatic nucleus. *Biol. Cell* **89**, 495–503 (1997).
185. Grippo, R. M., Purohit, A. M., Zhang, Q., Zweifel, L. S. & Güler, A. D. Direct Midbrain Dopamine Input to the Suprachiasmatic Nucleus Accelerates Circadian Entrainment. *Curr. Biol.* **27**, 2465–2475.e3 (2017).
186. Andersson, E. A. *et al.* MTNR1B G24E variant associates with BMI and fasting plasma glucose in the general population in studies of 22,142 Europeans. *Diabetes* **59**, 1539–1548 (2010).
187. Wang, Y. X. PPARs: Diverse regulators in energy metabolism and metabolic diseases. *Cell Res.* **20**, 124–137 (2010).
188. Lee, A., Ader, M., Bray, G. A. & Bergman, R. N. Diurnal Variation in Glucose Tolerance Cyclic Suppression of Insulin Action and Insulin Secretion in Normal-Weight, But Not Obese, Subjects.
189. Kalsbeek, A., Buijs, R. M., van Heerikhuize, J. J., Arts, M. & van der Woude, T. P. Vasopressin-containing neurons of the suprachiasmatic nuclei inhibit corticosterone release. *Brain Res.* **580**, 62–67 (1992).
190. Nader, N., Chrousos, G. P. & Kino, T. Circadian rhythm transcription factor CLOCK regulates the transcriptional activity of the glucocorticoid receptor by acetylating its hinge region lysine cluster: potential physiological implications. *FASEB J.* **23**, 1572–1583 (2009).
191. So, A. Y. L., Bernal, T. U., Pillsbury, M. L., Yamamoto, K. R. & Feldman, B. J. Glucocorticoid regulation of the circadian clock modulates glucose homeostasis. *Proc. Natl. Acad. Sci. U. S. A.* **106**, 17582–17587 (2009).
192. Oishi, K. *et al.* Genome-wide expression analysis reveals 100 adrenal gland-dependent circadian genes in the mouse liver. *DNA Res.* **12**, 191–202 (2005).
193. Balsalobre, A., Marcacci, L. & Schibler, U. Multiple signaling pathways elicit circadian gene expression in cultured Rat-1 fibroblasts. *Curr. Biol.* **10**, 1291–1294 (2000).

194. Balsalobre, A. *et al.* Resetting of circadian time in peripheral tissues by glucocorticoid signaling. *Science* (80-.). **289**, 2344–2347 (2000).
195. Kiessling, S., Eichele, G. & Oster, H. Adrenal glucocorticoids have a key role in circadian resynchronization in a mouse model of jet lag. *J. Clin. Invest.* **120**, 2600–2609 (2010).
196. Redman, J., Armstrong, S. & Ng, K. T. Free-running activity rhythms in the rat: Entrainment by melatonin. *Science* (80-.). **219**, 1089–1091 (1983).
197. Marcheva, B. *et al.* Disruption of the clock components CLOCK and BMAL1 leads to hypoinsulinaemia and diabetes. *Nature* **466**, 627–631 (2010).
198. Preitner, N. *et al.* The orphan nuclear receptor REV-ERB α controls circadian transcription within the positive limb of the mammalian circadian oscillator. *Cell* **110**, 251–260 (2002).
199. Rietveld, W. J., Ten Hoor, F., Kooij, M. & Flory, W. Changes in 24-hour fluctuations of feeding behavior during hypothalamic hyperphagia in rats. *Physiol. Behav.* **21**, 615–622 (1978).
200. Wiater, M. F., Li, A. J., Dinh, T. T., Jansen, H. T. & Ritter, S. Leptin-sensitive neurons in the arcuate nucleus integrate activity and temperature circadian rhythms and anticipatory responses to food restriction. *Am. J. Physiol. - Regul. Integr. Comp. Physiol.* **305**, R949 (2013).
201. Refinetti, R., Kaufman, C. M. & Menaker, M. Complete suprachiasmatic lesions eliminate circadian rhythmicity of body temperature and locomotor activity in golden hamsters. *J. Comp. Physiol. A.* **175**, 223–232 (1994).
202. Horvath, T. L. An Alternate Pathway for Visual Signal Integration into the HypothalamoPituitary Axis: Retinorecipient Intergeniculate Neurons Project to Various Regions of the Hypothalamus and Innervate Neuroendocrine Cells Including Those Producing Dopamine. *J. Neurosci.* **18**, 1546–1558 (1998).
203. Saeb-Parsy, K. *et al.* Neural connections of hypothalamic neuroendocrine nuclei in the rat. *J. Neuroendocrinol.* **12**, 635–648 (2000).
204. Gillette, M. U. & McArthur, A. J. Circadian actions of melatonin at the suprachiasmatic nucleus. *Behav. Brain Res.* **73**, 135–139 (1996).
205. Hunt, A. E., Al-Ghoul, W. M., Gillette, M. U. & Dubocovich, M. L. Activation of MT₂ melatonin receptors in rat suprachiasmatic nucleus phase advances the circadian clock. *Am. J. Physiol. - Cell Physiol.* **280**, (2001).
206. Liu, C. *et al.* Molecular Dissection of Two Distinct Actions of Melatonin on the Suprachiasmatic Circadian Clock. *Neuron* **19**, 91–102 (1997).
207. Shimomura, K. *et al.* Genetic suppression of the circadian Clock mutation by the melatonin biosynthesis pathway. *Proc. Natl. Acad. Sci. U. S. A.* **107**, 8399–8403 (2010).
208. Arendt, J. & Broadway, J. Light and melatonin as zeitgebers in man. *Chronobiol. Int.* **4**, 273–282 (1987).
209. Armstrong, S. M., Cassone, V. M., Chesworth, M. J., Redman, J. R. & Short, R. V. Synchronization of mammalian circadian rhythms by melatonin. *J. Neural Transm. Suppl.* **21**, 375–394 (1986).
210. Cassone, V. M., Chesworth, M. J. & Armstrong, S. M. Entrainment of rat circadian rhythms by daily injection of melatonin depends upon the hypothalamic suprachiasmatic nuclei. *Physiol. Behav.* **36**, 1111–1121 (1986).

211. Cassone, V. M., Chesworth, M. J. & Armstrong, S. M. Dose-Dependent Entrainment of Rat Circadian Rhythms by Daily Injection of Melatonin. *J. Biol. Rhythms* **1**, 219–229 (1986).
212. Korf, H. W., Von Gall, C. & Stehle, J. The circadian system and melatonin: Lessons from rats and mice. *Chronobiol. Int.* **20**, 697–710 (2003).
213. Skene, D. J. & Arendt, J. Circadian rhythm sleep disorders in the blind and their treatment with melatonin. *Sleep Med.* **8**, 651–655 (2007).
214. Folkard, S. Do permanent night workers show circadian adjustment? A review based on the endogenous melatonin rhythm. *Chronobiol. Int.* **25**, 215–224 (2008).
215. Zawilska, J. B., Skene, D. J. & Arendt, J. Physiology and pharmacology of melatonin in relation to biological rhythms. *Pharmacol. Reports* **61**, 383–410 (2009).
216. Lee, A., Ader, M., Bray, G. A. & Bergman, R. N. Diurnal variation in glucose tolerance. Cyclic suppression of insulin action and insulin secretion in normal-weight, but not obese, subjects. *Diabetes* **41**, 750–759 (1992).
217. Boden, G., Chen, X. & Polansky, M. Disruption of circadian insulin secretion is associated with reduced glucose uptake in first-degree relatives of patients with type 2 diabetes. *Diabetes* **48**, 2182–2188 (1999).
218. La Fleur, S. E., Kalsbeek, A., Wortel, J., Fekkes, M. L. & Buijs, R. M. A daily rhythm in glucose tolerance. A role for the suprachiasmatic nucleus in insulin-independent glucose uptake? *Diabetes* **50**, 1237–1243 (2001).
219. Qian, J., Yeh, B., Rakshit, K., Colwell, C. S. & Matveyenko, A. V. Circadian Disruption and Diet-Induced Obesity Synergize to Promote Development of β -Cell Failure and Diabetes in Male Rats. (2015) doi:10.1210/en.2015-1516.
220. Singer, M. E., Dorrance, K. A., Oxenreiter, M. M., Yan, K. R. & Close, K. L. The type 2 diabetes ‘modern preventable pandemic’ and replicable lessons from the COVID-19 crisis. *Prev. Med. Reports* **25**, 101636 (2022).
221. Boe, D. M., Yu, D. & Weber, C. R. Occludin S408 phosphorylation regulates tight junction protein interactions and barrier function. *J. Cell Biol* **193**, 565–582 (2011).
222. Van Itallie, C. M., Fanning, A. S., Bridges, A. & Anderson, J. M. ZO-1 Stabilizes the Tight Junction Solute Barrier through Coupling to the Perijunctional Cytoskeleton. *Mol. Biol. Cell* **20**, 3930–3940 (2009).
223. Rodríguez, E. M., Blázquez, J. L. & Guerra, M. The design of barriers in the hypothalamus allows the median eminence and the arcuate nucleus to enjoy private milieus: The former opens to the portal blood and the latter to the cerebrospinal fluid. *Peptides* **31**, 757–776 (2010).
224. Parkash, J. *et al.* Semaphorin7A regulates neuroglial plasticity in the adult hypothalamic median eminence. *Nat. Commun.* **6**, 1–17 (2015).
225. De Seranno, S. *et al.* Role of Estradiol in the Dynamic Control of Tanycyte Plasticity Mediated by Vascular Endothelial Cells in the Median Eminence. *Endocrinology* **151**, 1760–1772 (2010).
226. Müller-Fielitz, H. *et al.* Tanycytes control the hormonal output of the hypothalamic-pituitary-thyroid axis. *Nat. Commun.* **8**, 1–13 (2017).
227. Liu, T. *et al.* Modulating Endothelial Barrier Function by Targeting Vimentin Phosphorylation. *J. Cell. Physiol.* **229**, 1484–1493 (2014).

228. Lewis, S. A., Traub, P. & Spilker, C. M. The N-terminal domain of vimentin alters bladder permeability. *J. Urol.* **170**, 2091–2094 (2003).
229. Rajasekaran, A. K., Hojo, M., Huima, T. & Rodriguez-Boulan, E. Catenins and zonula occludens-1 form a complex during early stages in the assembly of tight junctions. *J. Cell Biol.* **132**, 451–463 (1996).
230. La Fleur, S. E., Kalsbeek, A., Wortel, J. & Buijs, R. M. A suprachiasmatic nucleus generated rhythm in basal glucose concentrations. *J. Neuroendocrinol.* **11**, 643–652 (1999).
231. Kalsbeek, A., Buijs, R. M., van Heerikhuizen, J. J., Arts, M. & van der Woude, T. P. Vasopressin-containing neurons of the suprachiasmatic nuclei inhibit corticosterone release. *Brain Res.* **580**, 62–67 (1992).
232. Parton, L. E. *et al.* Glucose sensing by POMC neurons regulates glucose homeostasis and is impaired in obesity. *Nature* **449**, 228–232 (2007).
233. Xu, J. *et al.* Genetic identification of leptin neural circuits in energy and glucose homeostases. (2018) doi:10.1038/s41586-018-0049-7.
234. Deane, R. & Segal, M. B. The transport of sugars across the perfused choroid plexus of the sheep. *J. Physiol.* **362**, 245–260 (1985).
235. Abdul Muneer, P. M., Alikunju, S., Szlachetka, A. M., Murrin, L. C. & Haorah, J. Impairment of brain endothelial glucose transporter by methamphetamine causes blood-brain barrier dysfunction. *Mol. Neurodegener.* **6**, (2011).
236. Salas, M. *et al.* Resolution of the direct interaction with and inhibition of the human GLUT1 hexose transporter by resveratrol from its effect on glucose accumulation. *Am J Physiol Cell Physiol* **305**, 90–99 (2013).
237. Ostrowski, N. L., Lolait, S. J. & Young, W. S. Cellular localization of vasopressin V1a receptor messenger ribonucleic acid in adult male rat brain, pineal, and brain vasculature. *Endocrinology* **135**, 1511–1528 (1994).
238. Dumais, K. M. & Veenema, A. H. Vasopressin and oxytocin receptor systems in the brain: Sex differences and sex-specific regulation of social behavior. *Frontiers in Neuroendocrinology* vol. 40 1–23 (2016).
239. Liu, S. *et al.* Involvement of the suprachiasmatic nucleus in body temperature modulation by food deprivation in rats. *Brain Res.* **929**, 26–36 (2002).
240. Buijs, R. M., Chun, S. J., Nijima, A., Romijn, H. J. & Nagai, K. Parasympathetic and Sympathetic Control of the Pancreas: A Role for the Suprachiasmatic Nucleus and Other Hypothalamic Centers That Are Involved in the Regulation of Food Intake. *J. Comp. Neurol* **431**, 405–423 (2001).
241. la Fleur, S. E., Kalsbeek, A., Wortel, J. & Buijs, R. M. Polysynaptic neural pathways between the hypothalamus, including the suprachiasmatic nucleus, and the liver. *Brain Res.* **871**, 50–56 (2000).
242. ANAND, B. K., CHHINA, G. S., SHARMA, K. N., DUA, S. & SINGH, B. Activity of single neurons in the hypothalamic feeding centers: effect of glucose. <https://doi.org/10.1152/ajplegacy.1964.207.5.1146> **207**, 1146–1154 (1964).
243. Oomura, Y. *et al.* Reciprocal Activities of the Ventromedial and Lateral Hypothalamic Areas of Cats. *Science (80-)*. **143**, 484–485 (1964).

244. Bentsen, M. A., Mirzadeh, Z. & Schwartz, M. W. Revisiting How the Brain Senses Glucose-And Why. *Cell Metab.* **29**, 11–17 (2019).
245. Oomura, Y., Ooyama, H., Sugimori, M., Nakamura, T. & Yamada, Y. Glucose Inhibition of the Glucose-sensitive Neurone in the Rat Lateral Hypothalamus. *Nat.* 1974 2475439 **247**, 284–286 (1974).
246. Zimmerman, C. A. *et al.* Thirst neurons anticipate the homeostatic consequences of eating and drinking. *Nature* **537**, 680–684 (2016).
247. Pasquettaz, R. *et al.* Peculiar protrusions along tanycyte processes face diverse neural and nonneural cell types in the hypothalamic parenchyma. *J. Comp. Neurol.* cne.24965 (2020) doi:10.1002/cne.24965.
248. Meek, T. H. *et al.* Functional identification of a neurocircuit regulating blood glucose. doi:10.1073/pnas.1521160113.
249. Garfield, A. S. *et al.* A parabrachial-hypothalamic cholecystokinin neurocircuit controls counterregulatory responses to hypoglycemia. *Cell Metab.* **20**, 1030–1037 (2014).
250. Üner, A. G. *et al.* Role of POMC and AgRP neuronal activities on glycaemia in mice. *Sci. Reports* 2019 91 **9**, 1–14 (2019).
251. Nurses, sleep disturbances, desynchronization of circadian rhythms, and performance: a dangerous liaison? A narrative mini-review.
252. Martínez Madrid, M., Campos, M., Madrid Pérez, J., Rol, M. & Moreno-Casbas, T. The challenge of chronodisruption assessment. The case of nursing staff shift workers. *Sleep Med.* **14**, e192–e193 (2013).
253. Salgado-Delgado, R., Ángeles-Castellanos, M., Buijs, M. R. & Escobar, C. Internal desynchronization in a model of night-work by forced activity in rats. *Neuroscience* **154**, 922–931 (2008).
254. Leng, Y., Musiek, E. S., Hu, K., Cappuccio, F. P. & Yaffe, K. Association between circadian rhythms and neurodegenerative diseases. *Lancet Neurol.* **18**, 307–318 (2019).
255. Maury, E., Ramsey, K. M. & Bass, J. Circadian Rhythms and Metabolic Syndrome. *Circ. Res.* **106**, 447–462 (2010).
256. Lee, Y., Field, J. M. & Sehgal, A. Circadian Rhythms, Disease and Chronotherapy. *J. Biol. Rhythms* **36**, 503–531 (2021).
257. Bolborea, M. & Langlet, F. What is the physiological role of hypothalamic tanycytes in metabolism? *Am. J. Physiol. - Regul. Integr. Comp. Physiol.* **320**, (2021).